1969

Lattice dynamics of YZn

Thomas Stephen Prevender
Iowa State University

LATTICE DYNAMICS OF YZn

by

Thomas Stephen Prevender

A Dissertation Submitted to the

Graduate Faculty in Partial Fulfillment of

The Requirements for the Degree of

DOCTOR OF PHILOSOPHY

Major Subject: Metallurgy

Approved:

Signature was redacted for privacy.

In Charge of Major Work

Signature was redacted for privacy.

Head of Major Department

Signature was redacted for privacy.

Dean of Graduate College

Iowa State University
of Science and Technology
Ames, Iowa

1969

TABLE OF CONTENTS

		Page
I.	INTRODUCTION	1
II.	SAMPLE DESCRIPTION	4
III.	LATTICE DYNAMICS OF THE CsCl STRUCTURE IN THE HARMONIC APPROXIMATION	10
IV.	INELASTIC NEUTRON SCATTERING	21
V.	X-RAY DIFFRACTION	51
VI.	VELOCITIES OF SOUND	75
VII.	CALCULATIONS AND SUMMARY	81
VIII.	LITERATURE CITED	99
IX.	ACKNOWLEDGMENTS	102
X.	APPENDIX A	103
XI.	APPENDIX B	106
XII.	APPENDIX C	108
XIII.	APPENDIX D	112
XIV.	APPENDIX E	116
XV.	APPENDIX F	121

I. INTRODUCTION

Within recent years there has been an increasing effort to use inelastic neutron scattering to study the lattice dynamics of alloys (1). Much of this work has involved disordered binary alloys in which a continuous range of solubility exists between the elements. A study of disordered alloys can yield information such as the frequency distribution function and the concentration dependence of the phonon dispersion curves. However the current state of the lattice dynamics of disordered alloys does not include a model that relates the dispersion curves to the interatomic force constants. An advantage of ordered vs. disordered alloys is that for a perfectly ordered alloy it is possible to derive explicit expressions for the dispersion curves in terms of the interatomic force constants. With the use of such expressions it is possible to perform a least-squares analysis of the measured dispersion curves to obtain a set of best-fit interatomic force constants. Once the force constants have been found it is possible to calculate a number of experimentally measurable quantities. To the author's knowledge the only ordered alloy that has been studied by the use of inelastic neutron scattering is β-brass (2).

This thesis describes a series of experiments and calculations involving the ordered alloy YZn. The purpose of this work was to better understand the lattice dynamics of binary alloys and also to test the effectiveness of simple models in predicting lattice dynamical properties. The primary experiment was a determination of the phonon dispersion curves of YZn along the directions $(0\ 0\ \zeta)$, $(\zeta\ \zeta\ 0)$, $(\zeta\ \zeta\ \zeta)$ and $(\frac{1}{2}\ \frac{1}{2}\ \zeta)$. The three velocities of sound in the (1 1 0) direction were also measured to find the limiting values of the slopes of the acoustic branches of the

dispersion curves.

With the aid of a non-linear least-squares computer program (3) attempts were made to find force constant models that could represent the measured dispersion curves. The model that was finally adopted was a general sixth neighbor model that utilized twenty-four force constants. In terms of this model the frequency distribution function, lattice specific heat, Debye temperature and Debye-Waller factors were calculated.

Since one of the objectives of this work was to test the effectiveness of simple force constant models, it was decided to investigate how well a model based only on the measured elastic constants would fare. To this end, the elastic constant values were used to determine the two parameters involved in a first nearest neighbor model. The frequency distribution function, lattice specific heat, Debye temperature and Debye-Waller parameters were calculated using this model and the results compared with both experiment and the sixth neighbor model.

Two additional experiments were performed on YZn. The first was an x-ray diffractometer experiment designed to measure both the degree of order possessed by the sample and the sum of the Debye-Waller factors for Y and Zn. The second experiment involved monitoring the differential magnetic susceptibility over the temperature range of 1.2 to 22°K. This second experiment was undertaken because some features of the dispersion curves suggested that YZn might be a superconductor. However, it was found that for temperatures greater than 1.2°K, YZn was not superconducting.

In the following sections will be found a description of the YZn single crystal that was used in the experiments, a discussion of the

lattice dynamics of the CsCl structure, descriptions of the experimental procedures together with a discussion of the results and calculations.

II. SAMPLE DESCRIPTION

There were several reasons why YZn was chosen for study. First of all it has the CsCl structure which offers a very high degree of symmetry (4,5). Second, both Y and Zn have very good neutron scattering properties as summarized in Table 1.

Table 1. Physical properties of Y and Zn

Atomic mass (amu)	Y 88.91	Zn 65.38
Thermal neutron cross sections (6)		
Coherent scattering (barns)	7.60 ± 0.06	4.1 ± 0.1
Incoherent scattering (barns)	0.05 ± 0.03	-
Absorption (barns)	1.28 ± 0.02	1.10 ± 0.04

Third, since β-brass also has the CsCl structure a comparison with that experiment (2) is possible. Finally, and perhaps of greatest practical importance, the phase diagram (7) of YZn shown in Fig. 1 indicated the possibility of growing a suitably large single crystal.

In Table 2 are listed the impurity levels (in ppm by weight) of the Y and Zn components. The Y was supplied by Mr. John Croat through the cooperation of Dr. F. H. Spedding. The Zn was purchased from Cominco American Inc., Spokane, Washington and was stated to be 99.999% Zn.

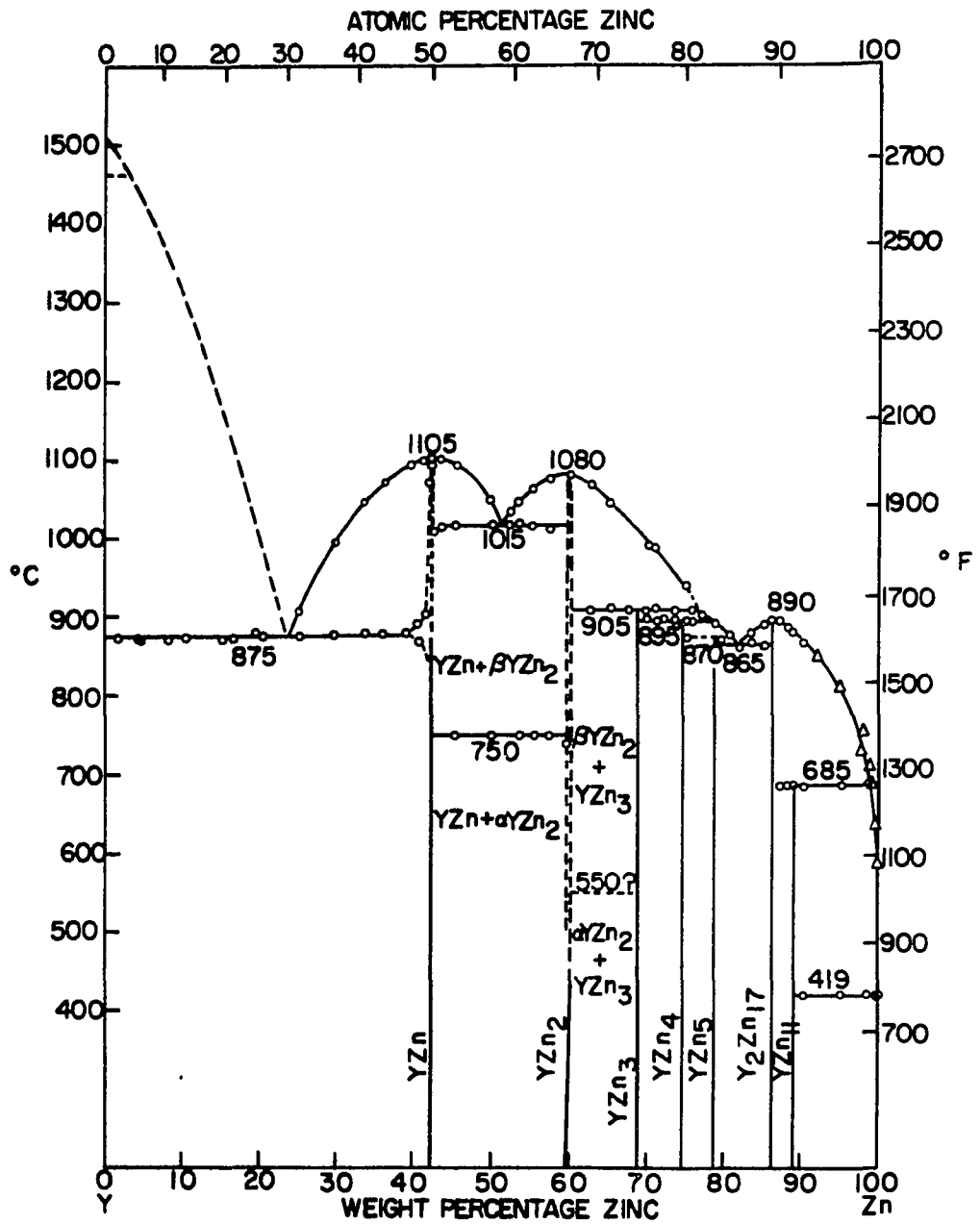

Fig. 1. The Y-Zn phase diagram under constrained vapor conditions

Table 2. Major impurities of Y and Zn in ppm by weight

Y	H = 13	Ca < 20	Sm < 200
	C = 30	Ti < 30	Gd < 100
	N = 47	Cr < 40	Tb < 200
	O = 755	Fe = 34	Dy < 100
	F = 118	Cu < 70	Ho < 60
	Mg < 30	Ta < 400	Er < 50
	Si < 80	Nd < 200	Yb < 100
Zn	Cd = .2	Fe = .2	Mg < .1
	Cu = .2	Pb = 1.0	Si < .5

Preparation of the sample involved three stages. First, equal atomic percentages of Y and Zn were carefully weighed (53.6255 ± 0.0001 gm. Y and 39.4335 ± 0.0001 gm. Zn) and then sealed in a pointed one inch diameter Ta crucible. The sealing was done in a vacuum of approximately 5×10^{-5} mm. Hg with an electron beam welder. After sealing, the Ta crucible was itself sealed inside a stainless steel cylinder. In order to homogenize the sample it was then rocked for two hours in a rocking furnace at a temperature of at least 1135°C. Upon cooling to room temperature the Ta crucible was removed from the stainless steel and installed in a Bridgman furnace where it was protected by vacuum. A schematic diagram of the Bridgman furnace is shown in Fig. 2. The furnace, of original design, was meant to maximize the temperature gradient at the solid-liquid interface, and also to provide a variable rate of descent of the sample through the maximum

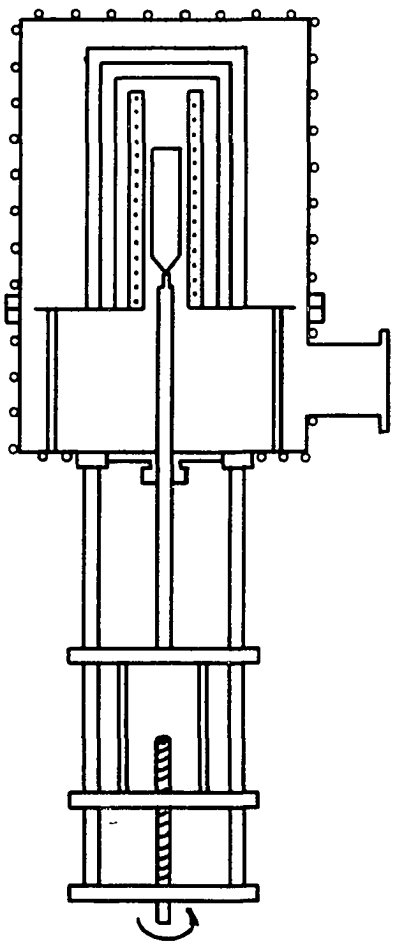

Fig. 2. Schematic Diagram of the Bridgman furnace

temperature gradient region. Temperature gradients of at least 200°C/in. were attained by quite effective insulation of the hot top part of the furnace from the relatively cool bottom. This thermal insulation was achieved with a system of radiation shields, the use of stainless steel support rods for the furnace core and, to a large extent, the vacuum of approximately $1x10^{-6}$ mm. Hg that existed inside the furnace. Vertical speeds of the sample were continuously variable from 0.08 in./hr. to 2 in./hr. through use of a Bodine NSH-12RC electric motor with a Minarik SH-14 speed control. Temperature control was accomplished by using a West stepless temperature controller whose sensing element was attached directly to the furnace heating element. The sample temperature (or rather a temperature no greater than the coolest part of the sample) was indicated by a thermocouple located at the top of the Ta sample support tube.

The sample growing technique began with the sample raised above the maximum temperature gradient region. Before the sample was lowered the vacuum was allowed to equilibrate at approximately $1x10^{-6}$ mm. Hg while the sample temperature thermocouple reached 1113°C. The sample was lowered at 0.08 in./hr. for forty five hours at which time the sample thermocouple indicated 435°C. Upon removal from the Ta crucible the sample was etched and inspected for grain boundaries. Upon finding no grain boundaries the sample was then x-rayed with the use of Laue back-reflection techniques which revealed it to be a single crystal. Subsequent chemical analysis[a] to determine the composition of the sample indicated it was made

---

[a]B. Lauerman, Ames Laboratory, Ames, Iowa. Chemical analysis. Private communication. 1969.

up of 57.71 ± 0.2 wt. % Y and 42.09 ± 0.04 wt. % Zn. This is to be compared with the equiatomic percent objective which would have given 57.63 wt. % Y and 42.37 wt. % Zn. Perhaps a more meaningful indication of the sample composition may be found by calculating the ratio of the wt. percents since this procedure eliminates the effect of impurities. The value of this ratio for the experimentally determined wt. percents was

$$\frac{42.09 \pm 0.04}{57.71 \pm 0.2} = 0.729 \pm 0.004$$

For the case of equal atomic percents the ratio was

$$\frac{42.37}{57.63} = 0.735$$

Therefore it seems that the sample was indeed very close to the desired composition. This conclusion was further substantiated by the value obtained for the long-range order parameter which will be discussed in Section V.

III. LATTICE DYNAMICS OF THE CsCl STRUCTURE IN THE HARMONIC APPROXIMATION

There are several (8, 9, 10) rigorous discussions of the Born Von Karman theory of lattice dynamics available in the literature. The treatment given here is meant to be of the nature of a review of the general theory with specialization to the CsCl case.

If one considers a crystal to be composed of N_c unit cells each containing S atoms and if the origin of a coordinate system is chosen to be one of the atoms, then the equilibrium position of the origin of the $\underline{\ell}$-th unit cell is given by

$$\underline{R}(\ell) = \ell_1 \underline{a}_1 + \ell_2 \underline{a}_2 + \ell_3 \underline{a}_3 . \tag{3.1}$$

Similarly, the position of the s-th atom in a unit cell relative to the origin of the cell is given by $\underline{R}(s)$. Therefore, the equilibrium position of the s-th atom in the ℓ-th unit cell is

$$\underline{R}(\ell,s) = \underline{R}(\ell) + \underline{R}(s). \tag{3.2}$$

As a result of thermal fluctuations each atom may be considered to have a time dependent displacement from its equilibrium position given by $\underline{u}(\ell,s)$. The total kinetic energy of the crystal due to these thermal fluctuations is

$$T = \frac{1}{2} \sum_{\substack{\ell,s \\ \alpha}} M_s \dot{u}_\alpha^2(\ell,s). \tag{3.3}$$

where M_s is the mass of the s-th kind of atom and $u_\alpha(\ell,s)$ is the α-th Cartesian component of $\underline{u}(\ell,s)$.

The total potential energy Φ of the crystal is assumed to be a

function of the instantaneous positions of the atoms. If a Taylor's expansion is performed on Φ in terms of the atomic displacements $\underline{u}(\ell,s)$ the result is

$$\Phi = \Phi_0 + \sum_{\ell,s,\alpha} \Phi_\alpha(\ell,s)\, u_\alpha(\ell,s) + \frac{1}{2}\sum_{\substack{\ell,s,\alpha \\ \ell',s',\beta}} \Phi_{\alpha\beta}(\ell\ell' ss')\, u_\alpha(\ell,s)\, u_\beta(\ell's'). \tag{3.4}$$

Since the lattice dynamics are to be considered in the harmonic approximation terms of order greater than two are dropped in the expansion. The Φ_α and $\Phi_{\alpha\beta}$ appearing in the expansion are defined as

$$\Phi_\alpha(\ell,s) = \left.\frac{\partial \Phi}{\partial u_\alpha(\ell,s)}\right|_0 \tag{3.5a}$$

$$\Phi_{\alpha\beta}(\ell,s) = \left.\frac{\partial^2 \Phi}{\partial u_\alpha(\ell,s)\partial u_\beta(\ell',s')}\right|_0 \tag{3.5b}$$

where the subscript 0 means that the expressions are to be evaluated in the equilibrium configuration. From Eq. (3.5a) it is seen that $\Phi_\alpha(\ell,s)$ is just the negative of the α-th component of the force on the atom at (ℓ,s). Since this force is evaluated at equilibrium it is zero and hence the linear terms in the expansion vanish.

$\Phi_{\alpha\beta}(\ell\ell',ss')$ is the force in the α-th direction on the atom at $\underline{R}(\ell,s)$ due to a unit displacement in the β direction of the atom at $\underline{R}(\ell's')$. The $\Phi_{\alpha\beta}(\ell s,\ell's')$ are commonly referred to as interatomic force constants.

There are three useful restrictions that may be applied to the $\Phi_{\alpha\beta}$ without specializing to a particular lattice. The first of these results

because the choice of origin in an infinite crystal is completely arbitrary. Therefore $\Phi_{\alpha\beta}(\ell\ell',ss')$ does not depend on ℓ and ℓ' individually but only on the difference $\ell - \ell'$. The second condition results from a consideration of the effect of a translation of all the atoms in the crystal by the vector $\underline{t}$. As a result of the translation the potential energy of the crystal becomes

$$\Phi = \Phi_0 + \frac{1}{2} \sum_{\substack{\ell,s,\alpha \\ \ell',s',\beta}} \Phi_{\alpha\beta}(\ell-\ell',ss')\, t_\alpha t_\beta \tag{3.6}$$

But since Φ depends only on the relative positions of the atoms which do not change as a result of the translation $\underline{t}$, then it follows that

$$\sum_{\substack{\ell,\ell' \\ s,s'}} \Phi_{\alpha\beta}(\ell-\ell',ss') = 0 \tag{3.7}$$

The third condition follows from a consideration of the behavior of the force on an atom when the lattice undergoes a rigid translation $\underline{t}$. The force on the atoms at (ℓ,s) is given by

$$F_\alpha(\ell,s) = -\frac{\partial \Phi}{\partial u_\alpha(\ell,s)} = \sum_{\ell',s',\beta} \Phi_{\alpha\beta}(\ell-\ell',ss')\, t_\beta \tag{3.8}$$

Since $F_\alpha(\ell,s)$ must be independent of the translation $\underline{t}$ then it must be true that

$$\sum_{\ell',s'} \Phi_{\alpha\beta}(\ell-\ell',ss') = 0 \tag{3.9}$$

The Hamiltonian for the crystal can be written as

$$H = \Phi_0 + \frac{1}{2} \sum_{\ell,s,\alpha} M_s \dot{u}_\alpha^2(\ell,s) + \frac{1}{2} \sum_{\substack{\ell,s,\alpha \\ \ell',s',\beta}} \Phi_{\alpha\beta}(\ell\ell',ss')$$

$$u_\alpha(\ell,s)\, u_\beta(\ell',s') \ . \tag{3.10}$$

The equations of motion for the atom at $\underline{R}(\ell,s)$ are then

$$M_s \ddot{u}_\alpha(\ell,s) = \frac{-\partial H}{\partial u_\alpha(\ell,s)} = - \sum_{\ell',s',\beta} \Phi_{\alpha\beta}(\ell\ell',ss')\, u_\beta(\ell',s') \ . \tag{3.11}$$

In order to find the atomic displacements one must solve the 3N coupled equations of motion where N is the number of atoms in the crystal. Since the Hamiltonian Eq. (3,10) is a sum of two quadratic forms it is possible to find a principal axis transformation which simultaneously diagonalizes both parts. Such a transformation is

$$u_\alpha(\ell,s) = \frac{1}{\sqrt{NM_s}} \sum_{q,j} e_\alpha(\underline{q},js)\, Q(\underline{q},j)\, e^{i\underline{q}\cdot\underline{R}(\ell,s)} e^{i\omega t} \ . \tag{3.12}$$

This transformation represents the time dependent displacement $u_\alpha(\ell,s)$ as being composed of a sum of elementary excitations (phonons). The phonons are thought of as plane waves of wave vector $\underline{q}$ and circular frequency $\omega_j(\underline{q})$. Associated with any $\underline{q}$ there are in general 3S values of $\omega_j(\underline{q})$ and a corresponding set of 3S polarization vectors, the $\underline{e}(q,j,s)$, that specify the direction of vibration of an atom due to the phonon $(\underline{q},j)$.

Combination of Eqs.(3.11) and (3.12) yields

$$\omega^2 e_\alpha(\underline{q},js) = \sum_{\beta,s'} \sum_{\ell'} \frac{\Phi_{\alpha\beta}(\ell-\ell',ss')}{\sqrt{M_s M_{s'}}}$$

$$e^{i\underline{q}\cdot[\underline{R}(\ell',s') - \underline{R}(\ell,s)]} \; e_\beta(\underline{q},js') \; . \tag{3.13}$$

$D_{\alpha\beta}(\underline{q},ss')$ may be defined as

$$D_{\alpha\beta}(\underline{q},ss') = \sum_{\ell'} \frac{\Phi_{\alpha\beta}}{\sqrt{M_s M_{s'}}} (\ell',ss') \; e^{i\underline{q}\cdot[\underline{R}(\ell',s') - \underline{R}(s)]} \; . \tag{3.14}$$

where for simplicity ℓ is taken to be zero. The matrix $\tilde{D}$, of which $D_{\alpha\beta}(\underline{q},ss')$ is an element, is known as the dynamical matrix. Eq. (3.14) may be looked at as a Fourier series expansion of $D_{\alpha\beta}(\underline{q},ss')$ where the $\Phi_{\alpha\beta}(M_s M_{s'})^{-\frac{1}{2}}$ are just the Fourier coefficients.

Eq. (3.13) may be rewritten as

$$\sum_{\beta,s'} (D_{\alpha\beta}(\underline{q},ss') - \omega^2\delta_{\alpha\beta}\delta_{ss'}) \; e_\beta(\underline{q},js') = 0 \; . \tag{3.15}$$

Eq. (3.15) will have a non-trivial solution if

$$\det \left| \; D_{\alpha\beta}(\underline{q},ss') - \omega^2\delta_{\alpha\beta}\delta_{ss'} \; \right| = 0. \tag{3.16}$$

In the case of the CsCl lattice there are two atoms per unit cell with $\underline{R}_o = (0\ 0\ 0)$ and $\underline{R}_1 = (1\ 1\ 1)\ a_o/2$. Because of the fact that there are two atoms per unit cell the dynamical matrix will be a (6x6) matrix. The six eigenvalues $\omega^2 j(\underline{q})$ of $\tilde{D}(\underline{q},ss')$ are the squares of the circular frequencies of the phonons associated with the direction $\underline{q}$ in reciprocal space.

If Eq. (3.13) is rewritten in the form

$$\omega^2_j(\underline{q}) \; e_\alpha(\underline{q},js) = \sum_{\beta,s'} D_{\alpha\beta}(\underline{q},s'j) \; e_\beta(\underline{q},s'j) \; . \tag{3.17}$$

it may be seen that for each of the $\omega^2 j(\underline{q})$ there will be an associated eigenvector $e_\alpha(\underline{q},s,j)$. The eigenvectors may be chosen to satisfy the orthonormality and closure relations.

$$\sum_{s,\alpha} e^*_\alpha(\underline{q},sj)\, e_\alpha(\underline{q},sj') = \delta_{jj'} \,. \tag{3.18a}$$

$$\sum_{j} e^*_\beta(\underline{q},s'j)\, e_\alpha(\underline{q},sj) = \delta_{\alpha\beta}\delta_{ss'} \,. \tag{3.18b}$$

There are many properties (4, 9, 11) of $\tilde{D}(ss',\underline{q})$, its eigenvectors and eigenvalues that may be deduced on quite general grounds by considering only the symmetry of the lattice. For instance, it may be shown that in the CsCl case $\tilde{D}(ss'\underline{q})$ is a real symmetric matrix. This implies that the $\omega^2 j(\underline{q})$ are real and so $\omega_j(\underline{q})$ is either real or purely imaginary. But from Eq. (3.12) an imaginary $\omega_j(\underline{q})$ would result in an exponentially increasing or decreasing atomic coordinate. Since this would result in an unstable lattice we have that $\omega_j(\underline{q})$ is real and hence $\omega^2 j(\underline{q})$ is positive. However the condition that $\omega^2{}_j(\underline{q})$ be positive implies that the principal minors of $\tilde{D}$ be positive.

To see how $\tilde{D}(ss',\underline{q})$ is obtained the force on an atom at $\underline{R}(\ell,s)$ may be considered as due to the displacement of an atom at $\underline{R}(\ell',s')$.

$$\underline{F}(\underline{\ell},\underline{s}) = \begin{pmatrix} \phi_{11} & \phi_{12} & \phi_{13} \\ \phi_{21} & \phi_{22} & \phi_{23} \\ \phi_{31} & \phi_{32} & \phi_{33} \end{pmatrix} \underline{u}(\underline{\ell}',s'). \tag{3.19}$$

or, in matrix notation

$$\underline{F}(\ell,s) = \tilde{\phi}(\ell s,\ell' s')\ \underline{u}(\ell' s') \ . \tag{3.20}$$

Note that the elements of $\tilde{\phi}(\ell s,\ell' s')$ (referred to as a force constant matrix) are just the $\phi_{\alpha\beta}(\ell s,\ell' s')$ defined in Eq. (3.5b). From Eq. (3.5b) it may be seen that $\tilde{\phi}(\ell s,\ell' s')$ is symmetric. A particular $\tilde{\phi}(\ell s,\ell' s')$ can be further simplified by considering the effect on it of the symmetry operators that transform $\underline{R}(\ell' s') - \underline{R}(\ell s)$ into itself. In general, if $\tilde{U}$ is a symmetry operation of the crystal that transforms an $\underline{R}(\ell' s')$ into itself the associated $\tilde{\phi}$ becomes

$$\tilde{U}\ \tilde{\phi}\ \tilde{U}^{-1} = \tilde{\phi} \ . \tag{3.21}$$

For example, consider the CsCl case. A nearest neighbor of an origin atom has coordinates of the form (1 1 1) $a_o/2$ where a_o is the lattice parameter. The vector $\underline{R}(\ell',s') - \underline{R}(\ell,s)$ in this case is just (1 1 1) $a_o/2$. The general form of the dynamical matrix relating these two atoms is

$$\tilde{\phi}_{111} = \begin{pmatrix} \phi_{11} & \phi_{12} & \phi_{13} \\ \phi_{12} & \phi_{22} & \phi_{23} \\ \phi_{13} & \phi_{23} & \phi_{33} \end{pmatrix} \ . \tag{3.22}$$

A symmetry operation that transforms $\underline{R}(\ell' s')$ into itself is a reflection in the plane x=y. For this operation

$$\tilde{U} = \begin{pmatrix} 0 & 1 & 0 \\ 1 & 0 & 0 \\ 0 & 0 & 1 \end{pmatrix} . \tag{3.23}$$

Combination of Eqs. (3.18), (3.19) and (3.20) yields

$$\tilde{\phi}_{111} = \begin{pmatrix} \phi_{11} & \phi_{12} & \phi_{23} \\ \phi_{12} & \phi_{11} & \phi_{23} \\ \phi_{23} & \phi_{23} & \phi_{33} \end{pmatrix} . \tag{3.24}$$

Another symmetry operation that transforms R(ℓ',s) into itself is a 120° rotation about the (1 1 1) direction; for this operation

$$\tilde{U} = \begin{pmatrix} 0 & 0 & 1 \\ 1 & 0 & 0 \\ 0 & 1 & 0 \end{pmatrix} . \tag{3.25}$$

If the $\tilde{U}$ of Eq. (3.25) is applied to the $\tilde{\phi}_{111}$ of Eq. (3.24) it may be shown that $\tilde{\phi}_{111}$ has simplified to

$$\tilde{\phi}_{111} = \begin{pmatrix} \phi_{11} & \phi_{12} & \phi_{12} \\ \phi_{12} & \phi_{11} & \phi_{12} \\ \phi_{12} & \phi_{12} & \phi_{11} \end{pmatrix} . \tag{3.26}$$

There are seven other atoms that along with the one at $\underline{R}(1\ 1\ 1)\ a_o/2$ comprise the set of first neighbor atoms. The force constant matrices for the other atoms in the set may be found by transforming $\tilde{\phi}_{111}$ by the appropriate symmetry operations. For example, the operation that takes $\underline{R}(1\ 1\ 1)$ to $\underline{R}(1\ 1\ \underline{1})$ is $\tilde{S}$ where

$$\tilde{S}\ \underline{R}(1\ 1\ 1) = \underline{R}(1\ 1\ \underline{1})\ . \tag{3.27}$$

and $\tilde{S}$ is

$$\tilde{S} = \begin{pmatrix} 1 & 0 & 0 \\ 0 & 1 & 0 \\ 0 & 0 & \underline{1} \end{pmatrix}\ . \tag{3.28}$$

In this case

$$\tilde{\phi}_{111} = \tilde{S}\ \tilde{\phi}_{111}\ \tilde{S}^{-1} \tag{3.29}$$

or, if the operations indicated in Eq. (3.29) are performed $\tilde{\phi}_{111}$ becomes

$$\tilde{\phi}_{111} = \begin{pmatrix} \phi_{11} & \phi_{12} & -\phi_{12} \\ \phi_{12} & \phi_{11} & -\phi_{12} \\ -\phi_{12} & -\phi_{12} & -\phi_{11} \end{pmatrix}\ . \tag{3.30}$$

Similarly, one may find the $\tilde{\phi}$'s corresponding to the other atoms in the set. From a knowledge of the $\tilde{\phi}$'s for the different neighbor sets (see Appendix A) one can construct $\tilde{D}(ss',\underline{q})$ as indicated in Eq. (3.14).

The matrix $\tilde{D}(ss',\underline{q})$ is of the form

$$\left(\begin{array}{c|c} Y - Y & Y - Zn \\ \hline Zn - Y & Zn - Zn \end{array}\right) \tag{3.31}$$

where each quadrant is a 3x3 matrix representing the various types of atom-atom interactions; (see Appendix B for a list of the elements of $\tilde{D}(ss',\underline{q})$. If $\underline{q}$ is taken to be along a high symmetry direction it is possible to considerably simplify the form of $\tilde{D}(ss',\underline{q})$. Let $\tilde{D}_{\sigma\sigma'}$, represent any of the quadrants of $\tilde{D}(ss',\underline{q})$ then if $\tilde{U}$ is an operator that transforms $\underline{q}$ into itself,

$$\tilde{D}_{\sigma\sigma'} = \tilde{U}\,\tilde{D}_{\sigma\sigma'}\,\tilde{U}^{-1} \quad . \tag{3.32}$$

For example, if $\underline{q}$ lies along the direction (0,0,1), $\tilde{D}(ss',\underline{q})$ becomes

$$\tilde{D}(ss',\underline{q}) = \begin{pmatrix} D^{00}_{11} & 0 & 0 & D^{01}_{11} & 0 & 0 \\ 0 & D^{00}_{11} & 0 & 0 & D^{01}_{11} & 0 \\ 0 & 0 & D^{00}_{33} & 0 & 0 & D^{01}_{33} \\ D^{01}_{11} & 0 & 0 & D^{11}_{11} & 0 & 0 \\ 0 & D^{01}_{11} & 0 & 0 & D^{11}_{11} & 0 \\ 0 & 0 & D^{01}_{33} & 0 & 0 & D^{11}_{33} \end{pmatrix} \tag{3.33}$$

Similarly $\tilde{D}(ss',\underline{q})$ simplifies for a $\underline{q}$ along (1 1 1), (1 1 0) and $(\frac{1}{2}\ \frac{1}{2}\ \zeta)$. This simplification of $\tilde{D}$ allows for the solution of Eq. (3.14)

yielding explicit expressions for $\omega^2 j(\underline{q})$. The expressions for $\omega^2 j(\underline{q})$ along the four symmetry directions for a sixth neighbor model are listed in Appendix C. In the next section it will be shown how the experimental $\omega_j(\underline{q})$ values are used to find the interatomic force constants.

IV. INELASTIC NEUTRON SCATTERING

In the last section it was shown, within the harmonic approximation, how it was possible to derive expressions for $\nu_j(\underline{q})$. Here a discussion will be given of how inelastic neutron scattering was used for the experimental measurements of $\nu_j(\underline{q})$. When a beam of monoenergetic neutrons is scattered by a crystalline sample, the incident neutrons may be scattered by elastic coherent, elastic incoherent, inelastic coherent or inelastic incoherent scattering processes. Since it is the interaction of neutrons with phonons that is of interest, elastic scattering will be disregarded. The discussion will be further restricted to a consideration of coherent scattering and will dismiss incoherent scattering as a source of background on which the coherent scattering is superimposed. Further, only one-phonon scattering will be considered as being significant. Multi-phonon scattering does not produce sharp peaks as in the one-phonon case and multi-phonon scattering will be treated as another source of background.

Several derivations (12, 13, 14) of the one-phonon inelastic coherent neutron scattering cross section have appeared in the literature. The expression for the cross section which results from these derivations is

$$\frac{d^2\sigma}{d\Omega dE}^{coh} = \frac{Nk}{4\pi k_0} \sum_{\underline{q},j} \frac{1}{\omega_j(\underline{q})} \{ \delta(\underline{Q} + \underline{q} - \underline{\tau})\, \delta(\omega - \omega_j(\underline{q}))\, (\underline{n} + 1)$$

$$+ \delta(\underline{Q} - \underline{q} - \underline{\tau})\, \delta(\omega + \omega_j(\underline{q}))\, \underline{n} \} \left| \sum_s \frac{b_s}{\sqrt{M_s}} \right.$$

$$\left. e^{-W_s}\, \underline{Q} \cdot \underline{e}_s(\underline{q},j)\, e^{i\underline{\tau} \cdot \underline{R}_s} \right|^2 . \qquad (4.1)$$

This particular form of the cross section was derived with $u_\alpha(\ell,s)$ defined as in Eq. (3.12).

The symbols in Eq. (4.1) have the following meanings:

N = the number of unit cells in the sample

$\underline{k}$ = wave vector of the scattered neutron

$\underline{k}_0$ = wave vector of the incident neutron

$\omega_j(\underline{q})$ = the frequency of a phonon with polarization j and wave vector $\underline{q}$

$\underline{Q}$ = momentum transfer vector

$\underline{\tau}$ = reciprocal lattice vector

$\hbar\omega$ = energy change of the incident neutron

$\underline{n}(\underline{q},j)$ = occupation number for the phonon state specified by $(\underline{q},j)$

$\underline{b}_s$ = the average neutron scattering length for the atom at site $\underline{R}_s$ in the unit cell

W_s = the Debye-Waller parameter for the atom at $\underline{R}_s$ where $2W_s = \langle(\underline{Q}\cdot\underline{u}_s)^2\rangle$

$\underline{e}_s(\underline{q},j)$ = the polarization vector for the atom at $\underline{R}_s$ due to a phonon with wave vector $\underline{q}_j$

M_s = mass of the atom at $\underline{R}_s$

σ_1^{coh} = the ratio of the flux of neutrons scattered by one-phonon processes to the flux of incident neutrons

$d\Omega$ = solid angle region into which neutrons may be scattered

dE = energy interval in which the scattered neutron energy lies

From Eq. (4.1) it may be seen that to have a non-zero value for the cross section two conditions imposed by the two sets of delta functions must be satisfied. The first condition is that

$$\underline{Q} \equiv \underline{k}_0 - \underline{k} = \underline{\tau} \pm \underline{q} \quad . \tag{4.2}$$

which is an expression of conservation of momentum. The second condition is that

$$\frac{\hbar^2}{2m}(\underline{k}_0^2 - \underline{k}^2) \pm \hbar\omega = \pm h\nu_j(\underline{q}) \quad . \tag{4.3}$$

which expresses the requirement of conservation of energy. In these equations the (±) refer to neutron energy ($^{\text{loss}}_{\text{gain}}$) processes. In deriving Eq. (4.1) it was assumed that only harmonic interactions existed between the atoms in the solid. If anharmonic forces are allowed, the delta functions involving ω in Eq. (4.1) should be replaced by functions that are approximately Lorentzian in character (1, 15, 16). In addition to the problem of anharmonicity broadening the δ functions in Eq. (4.1) there are instrumental effects (14) that, by themselves, give approximately Gaussian line shapes.

In the remainder of this section it will be shown how the experimentally adjustable variables in Eq. (4.1) were chosen so as to maximize the scattering cross section.

A triple-axis neutron spectrometer located at the Ames Lab Research Reactor was used to observe one-phonon scattering processes. A schematic diagram of this instrument is shown in Fig. 3. The angles shown in Fig. 3 have the following significance:

θ_M is the Bragg angle for elastic scattering of a neutron of wave vector $\underline{k}_0$.

$2\theta_{SC}$ is the scattering angle for a neutron whose wave vector was initially $\underline{k}_0$ and finally $\underline{k}$.

θ_{AN} is the Bragg angle for elastic scattering of a neutron of wave vector $\underline{k}$.

θ_{ST} is an angle that denotes the degree of rotation of the sample table from some arbitrary origin.

A detailed description of the spectrometer may be found elsewhere (17, 18) so only a brief account will be given here. Essentially the spectrometer consists of three parts: the monochromator, sample table and analyzer.

Located in the center of the monochromator drum is a Zn single crystal. The function of this crystal is to select a narrow energy band of neutrons from the Maxwellian distribution incident on the crystal and scatter them into the sample. During the course of an experiment the monochromator is stationary and hence, $\underline{k}_o$ is fixed in magnitude. However, the sample which is mounted on a support passing through the vertical axis of the sample table, can rotate with the table. Rotation of the sample about an axis perpendicular to the plane of scattering can be seen to be equivalent to rotating $\underline{k}_o$ in the reciprocal space of the crystal. Neutrons scattered from the sample may be momentum-analyzed by noting the orientation and position of the Zn analyzer crystal.

Prior to the use of the spectrometer to detect phonons a careful alignment of the sample in the neutron beam was necessary. A preliminary alignment of the sample on its goniometer had been accomplished by the use

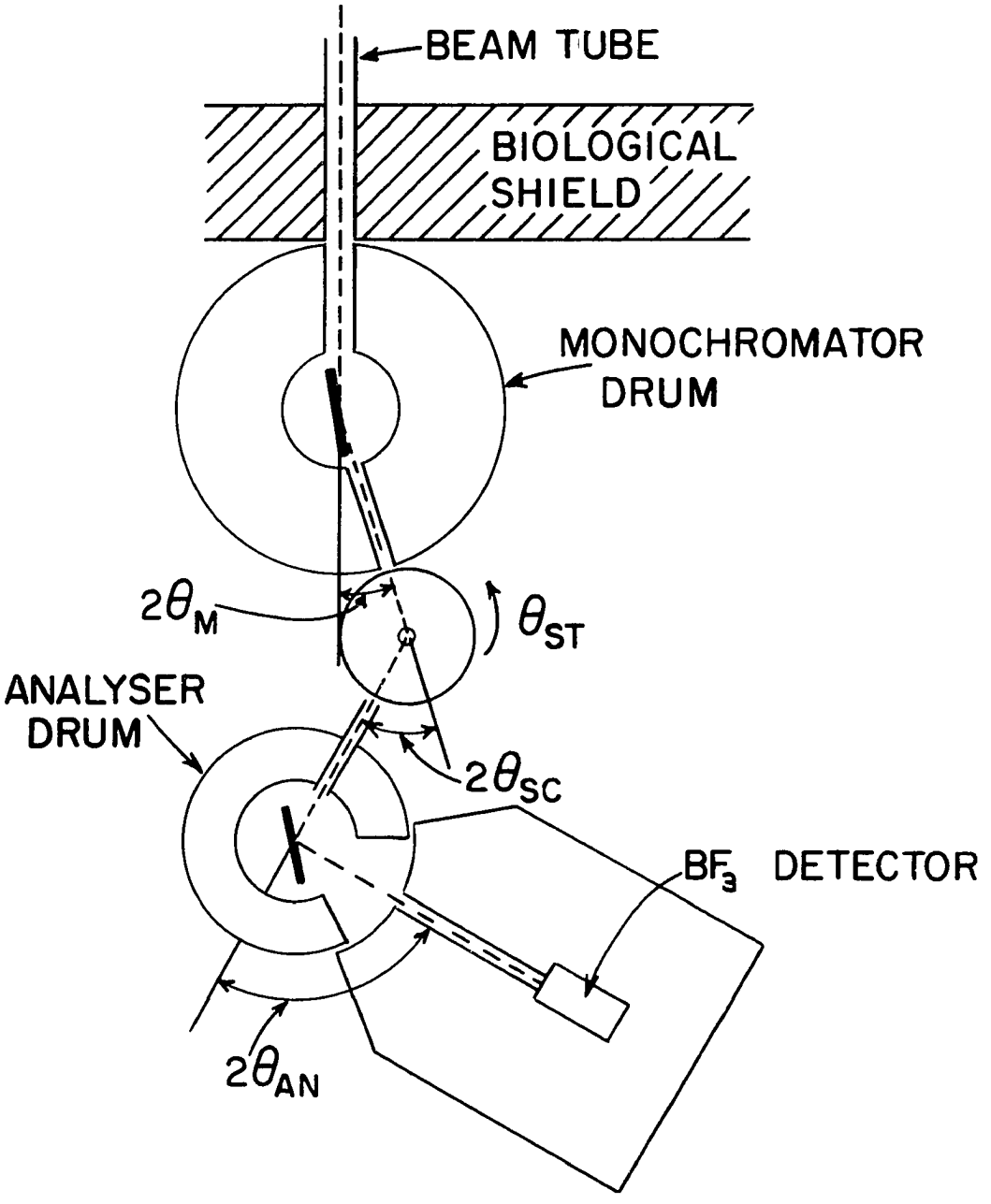

Fig. 3. Schematic diagram of the ALRR triple axis spectrometer

of Laue back-reflection techniques. In the case of YZn the lattice parameter was not accurately known prior to the neutron diffraction experiment and consequently had to be determined while the sample was on the spectrometer. Alignment was accomplished by the following procedure.

First a set of four reflection (e.g. the {0 0 2}) lying in the plane of the spectrometer were chosen for the alignment procedure. Then $2\theta_{AN}$ was set for elastic scattering. Next an assumed value of the lattice parameter was chosen so that a first approximation to $2\theta_{SC}$ could be made. The sample table and goniometer were then adjusted until a maximum in the intensity of scattered neutrons was observed. At this point it was necessary to make a scan of intensity vs. θ_{ST}. A typical scan of θ_{ST} is shown in Fig. 4. The mean value of the curve that resulted from this scan was used to determine a new value of θ_{ST}. With the new θ_{ST} a $2\theta_{SC}$ scan was made to find the new $2\theta_{SC}$ angle. The above procedure proceeded through several iterations until θ_{ST} and $2\theta_{SC}$ converged to their final values. Then the axes of the goniometer on which the sample was mounted were adjusted to further maximize the Bragg reflected intensity. These axes were adjusted by trying to roughly equalize the intensities of the four reference reflections.

There were two reasons for trying to equalize these four reflections. First, since the sample was practically transparent to the neutron beam the center of scattering and the center of mass were approximately coincident. Therefore, equalization of the four reflections would tend to locate the center of the sample in the center of the beam. Second, the equalization of the four reflections insured that the four {0 0 2} directions lay in the plane of scattering.

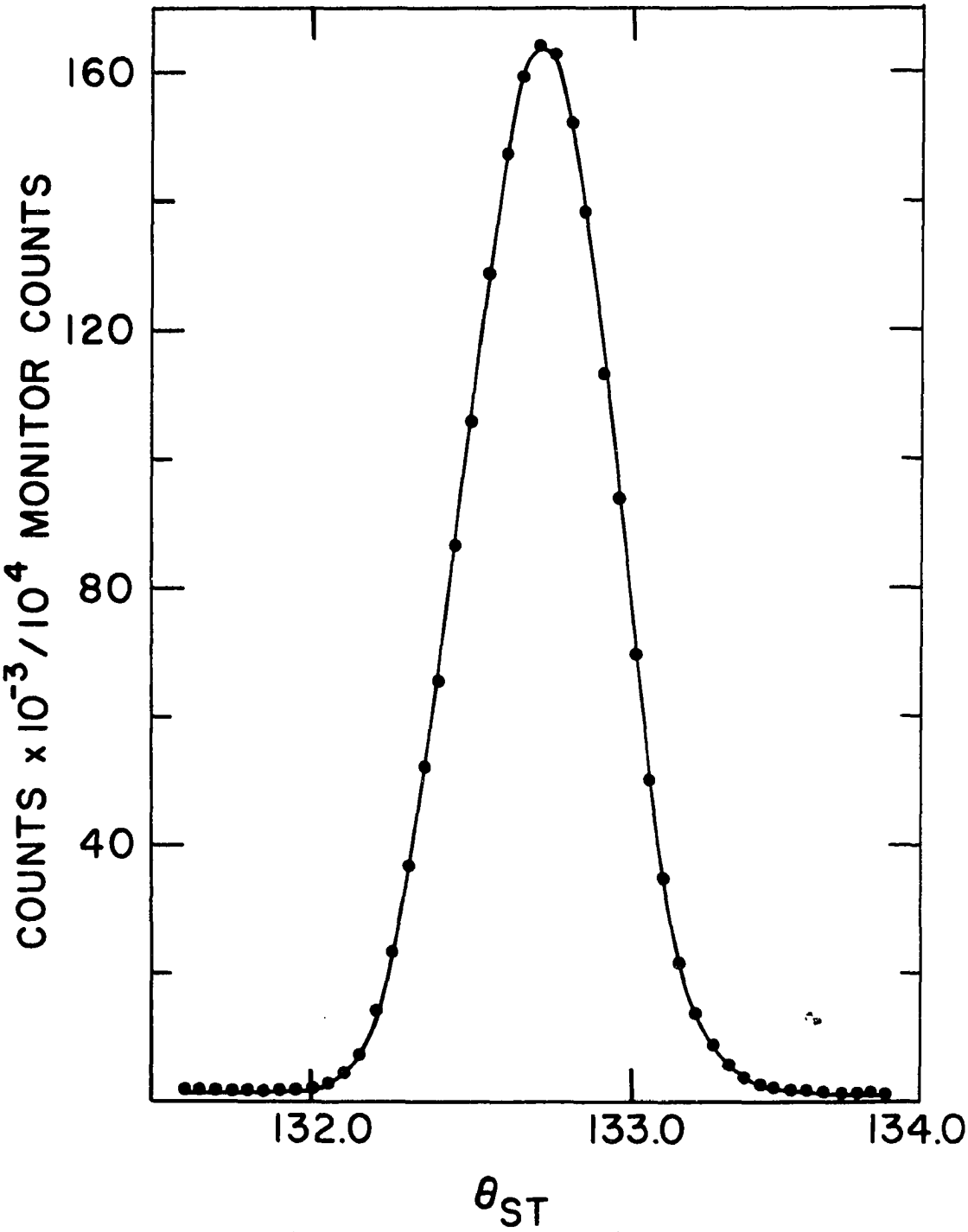

Fig. 4. Typical θ_{ST} scan of {0 0 2} reflection

The above alignment procedure was repeated several times during the course of the neutron scattering experiments. This was necessary because two sample orientations and also two values of k_o were used. The two orientations were respectively the ($\underline{1}$ 1 0) and (0 0 1) planes parallel to the plane of scattering. These two orientations were chosen because this made possible the observation of all eighteen branches of the dispersion curves for the four important symmetry directions. In addition, through the appropriate alignment of the YZn sample on its goniometer, the two orientations ($\underline{1}$ 1 0) and (0 0 1) could be interchanged by adjusting only one arc of the goniometer. Two different neutron wavelengths, $\lambda = 1.265A°$ and $\lambda = 1.6169A°$, were employed for k_o. Most of the phonons were observed with the smaller wavelength but some of the low frequency phonons were obtained with the larger value of λ.

Perhaps the most successful method for the determination of dispersion curves has been the "constant Q" technique (19) which is illustrated by the reciprocal space diagram of Fig. 5. As the name implies, the experiment is done at a fixed value of $\underline{Q}$. However, at the chosen $\underline{Q}$ the energy transfer $\hbar\omega$ is varied by changing the magnitude of $\underline{k}$, while $\underline{k}_o$ remains constant. If, as the energy transfer is varied, it becomes equal to one of the phonon energies corresponding to a phonon of wave vector $\underline{q}$ then the cross section of Eq. (4.1) becomes non-zero. As mentioned previously, the expected delta function in intensity predicted by Eq. (4.1) actually turns out to be more representative of a Gaussian function. In Fig. 6 is shown the result of the attempt to observe the T_1A type phonon characterized in Fig. 5.

An inspection of Eq. (4.1) reveals that there are a very large number

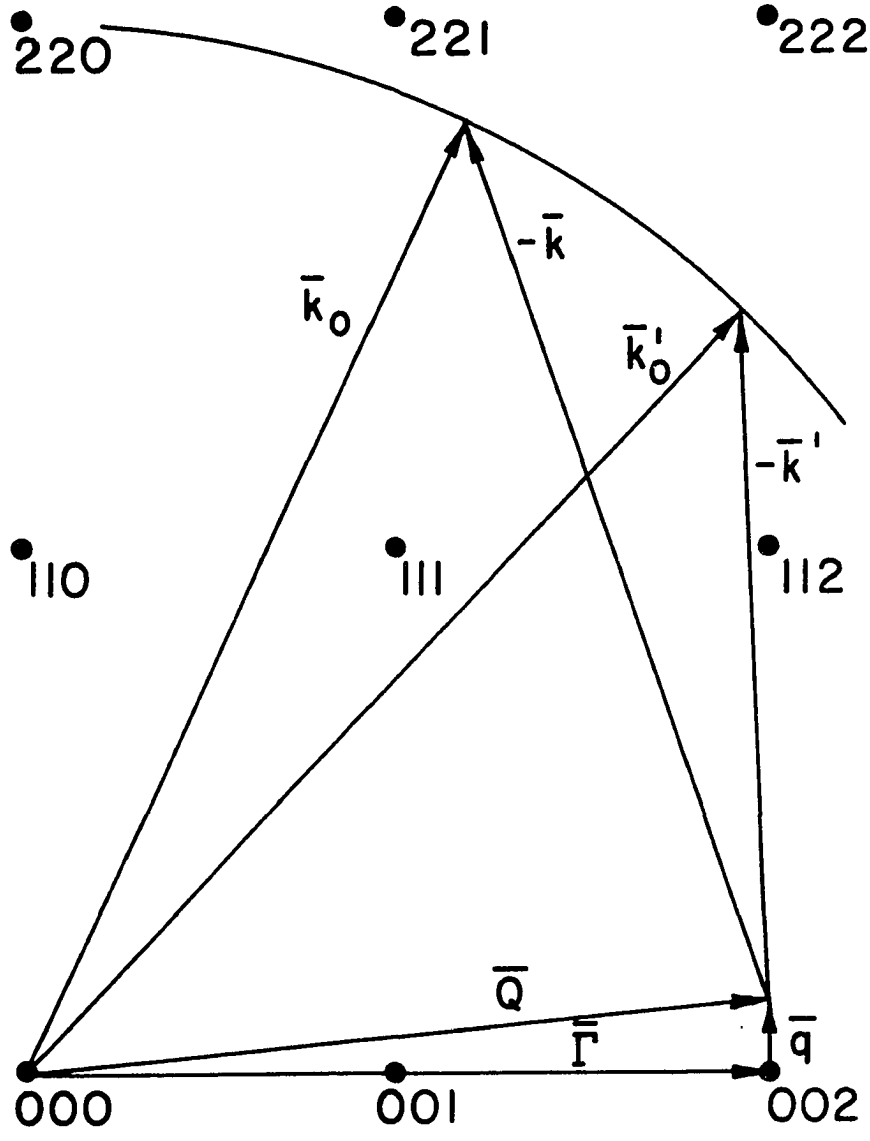

Fig. 5. Reciprocal space diagram illustrating the constant Q technique for a T_1 A phonon

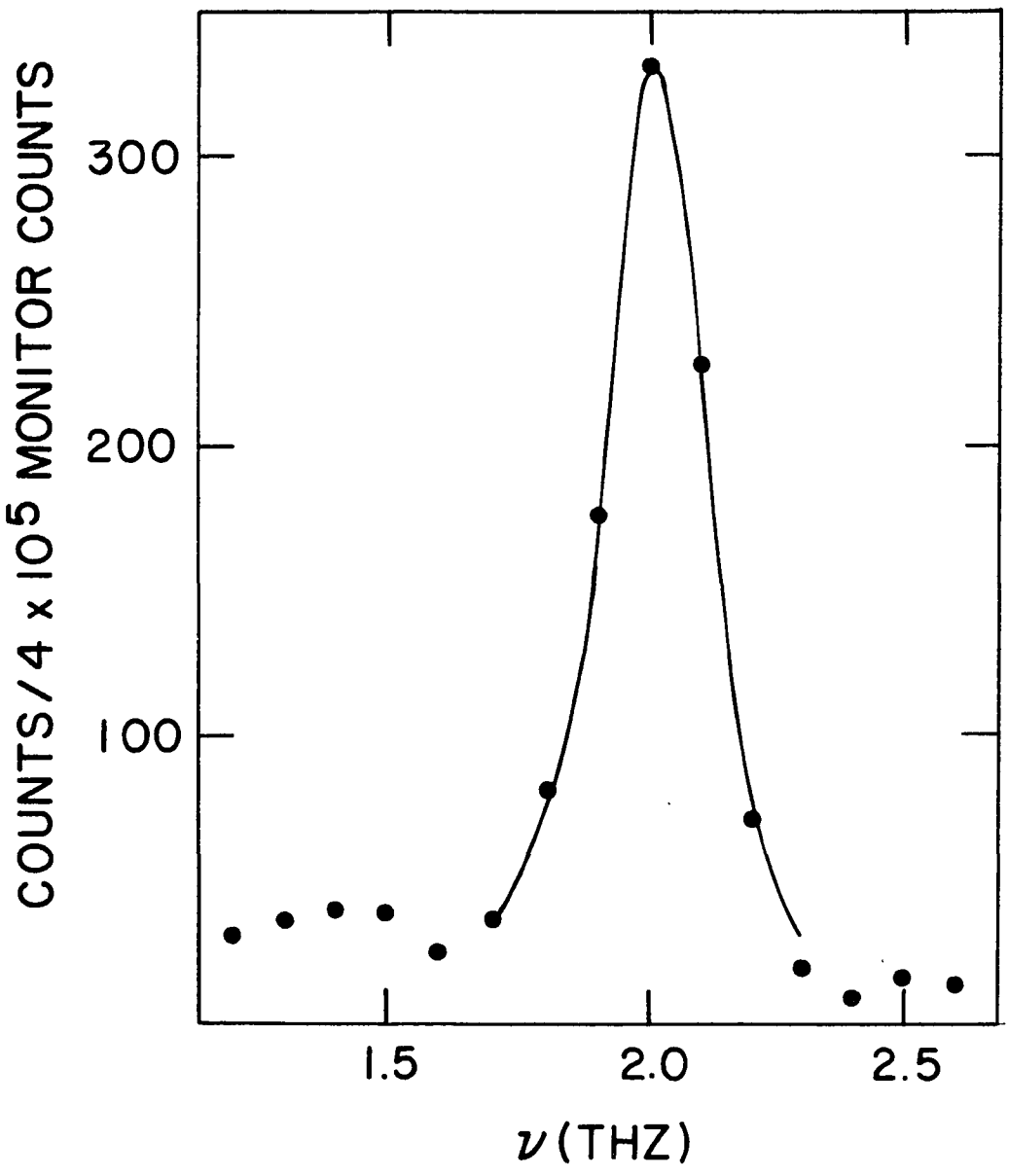

Fig. 6. Experimental result for the T_1 A phonon illustrated in Fig. 5

of ways to satisfy the delta functions involving $\underline{q}$ and $\nu_j(\underline{q})$. The question of how to choose the experimentally adjustable parameters was approached by a consideration of the effect of each parameter individually on the cross section.

1. $\underline{k_o}$

The values of k_o that were used in the experiment were selected by considering several competing effects. As stated previously, the energy spectrum of neutrons incident on the monochromater has an approximately Maxwellian distribution peaked at an energy corresponding to T = 50°C. Therefore, in order to maximize the intensity of scattered neutrons k_o should correspond to T = 50°C. However, as will be shown later, one would like k_o to be quite large so that distant reciprocal lattice points may be reached. On the other hand, the $1/k_o$ term in Eq. (4.1) makes one want a small k_o. Another very important reason for choosing k_o as small as possible was to minimize the resolution function (14, 20). In the final analysis more than one k_o was found to be necessary.

2. $\underline{k}$

$\underline{k}$ was not really chosen but rather was determined by the choice of other parameters, e.g., $\underline{k_o}$, $\underline{Q}$ and $\hbar\omega$.

3. τ

The effect of the choice of τ on the cross section was extremely important for the following reasons.

The inelastic structure factor defined as

$$\left| \sum_s \frac{b_s}{\sqrt{M_s}} e^{-W_s} \underline{Q} \cdot \underline{e}_s(\underline{q},j) \, e^{i\underline{\tau}} \cdot \underline{R}_s \right|^2 \qquad (4.4)$$

appears as a factor in the inelastic coherent cross section for one phonon scattering. For $\underline{q}$ along symmetry directions the polarization vectors $\underline{e}_s(\underline{q},j)$ are either parallel (longitudinal modes) or perpendicular (transverse modes) to $\underline{q}$. This fact allows for the arrangement of experimental conditions so as to maximize $\underline{Q} \cdot \underline{e}_s$ for one polarization while simultaneously minimizing it for another. However, the situation is complicated somewhat by the $\underline{q}$ dependence of the polarization vectors. That is, while both $\underline{e}_o$ and $\underline{e}_1$ remain either parallel or perpendicular to $\underline{q}$ their relative values change subject to the constraint imposed by Eq. (3.18).

To illustrate the behavior of the structure factor one may consider the case where $W_0 = W_1$; then, Eq. (4.4) becomes

$$Q^2 \, e^{-2Q^2\langle(\underline{u} \cdot \hat{Q})^2\rangle} \left| \sum_s \frac{b_s}{\sqrt{M_s}} \hat{Q} \cdot \underline{e}_s(\underline{q},j) \, e^{i\underline{\tau} \cdot \underline{R}_s} \right|^2 . \qquad (4.5)$$

From Eq. (4.5) it may be seen that there is a very strong $\underline{Q}$ (and hence $\underline{\tau}$) dependence of the structure factor. Since the Debye-Waller factors are relatively slowly varying, Eq. (4.5) indicates almost a Q^2 dependence of the structure factor. It is for this reason that one chooses Q to be large.

Another feature of the structure factor may be brought out if one defines the functions

$$a(\underline{q},j) = \frac{b_o}{\sqrt{M_o}} \hat{Q} \cdot \underline{e}_o(\underline{q},j)$$

$$b(\underline{q},j) = \frac{b_1}{\sqrt{M_1}} \hat{Q} \cdot \underline{e}_1(\underline{q},j) \quad . \qquad (4.6)$$

Then Eq. (4.5) becomes

$$Q^2 e^{-2Q^2\langle(\underline{u}\cdot\hat{Q})^2\rangle}(a(\underline{q},j) \pm b(\underline{q},j))^2 \quad . \tag{4.7}$$

the $(\pm)$ refer to $\binom{\text{even}}{\text{odd}}$ values of $\underline{\tau}$. Eq. (4.7) illustrates the dependence of the structure factor on whether $\underline{\tau}$ is even or odd. That is, if the structure factor for a particular polarization is large at an even reciprocal lattice point, then it will be small at an odd point.

In addition to the $\underline{\tau}$ dependence there is also a strong $\underline{q}$ dependence of the structure factor. To illustrate the $\underline{q}$ dependence, Eq. (4.4) may be simplified by the neglect of the relatively slowly varying Debye-Waller factors, the choice $\underline{\tau} = (0\ 0\ 0)$ and the substitution for $\underline{Q}$ of a unit vector $(\hat{Q})$ either parallel or perpendicular to $\underline{q}$. The normalized inelastic structure factor may then be defined as

$$|F|^2_{\text{NORM}} = \sum_s \frac{b_s}{\sqrt{M_s}} (\hat{Q}\cdot\underline{e}_s(\underline{q},j))^2 \quad . \tag{4.8}$$

In Figs. 7 and 8 are shown graphs of $|F|^2_{\text{NORM}}$ for the four symmetry directions. The $|F|^2_{\text{NORM}}$ curves were calculated (21) with the use of a sixth neighbor force constant model. The behavior of the structure factor curves is quite similar to that found for β-brass (2).

There is yet another consideration that influences the choice of $\underline{\tau}$ to be used to observe a phonon, and that is the employment of proper focusing conditions (14, 20, 22, 23). Focusing effects arise because of the imperfect collimation and finite mosaic spreads of the crystals used in a triple axis spectrometer. Because of these two factors the observed shape of a phonon peak is a function of the geometrical arrangement of the spectrometer arms. In the focused condition a phonon peak will tend to be

somewhat narrower and higher than in the defocused state. It turns out that for energy loss processes the focused condition for transverse phonons may be attained with $\underline{q}$ in a clockwise sense from a reciprocal lattice point.

Once it was decided where (i.e. which value of $\underline{Q}$) and how (energy loss or gain) to try to observe a phonon it was necessary to program the spectrometer to do the constant $\underline{Q}$ experiment. This involved instructing an on-line SDS 910 computer to calculate and punch on paper tape the instrument angles and counting procedure. The tape was then read by a Friden Tapereader and the information transmitted to the spectrometer.

A monitor counter (UF_3 fission counter) that detected the neutrons incident on the sample served as a means of normalizing the fluctuations in reactor power. That is, the BF_3 detector counted scattered neutrons for the time it took a preset number of incident neutrons to pass through the monitor counter. To eliminate spurious electrical signals that might give incorrect values for the intensity of scattered neutrons the counting was repeated for four repetitions.

4. Energy gain or loss

The option of doing an energy gain vs. energy loss experiment was almost always decided in favor of the latter. Primarily this was due to the better energy resolution of energy loss experiments. In addition, the phonon occupation numbers, $\underline{n}$, $\underline{n}$ + 1 for energy gain and loss respectively, made energy loss the better choice. The few times that energy gain was used were because the longer "reach" afforded by $k > k_0$ enabled some optical phonons to be observed.

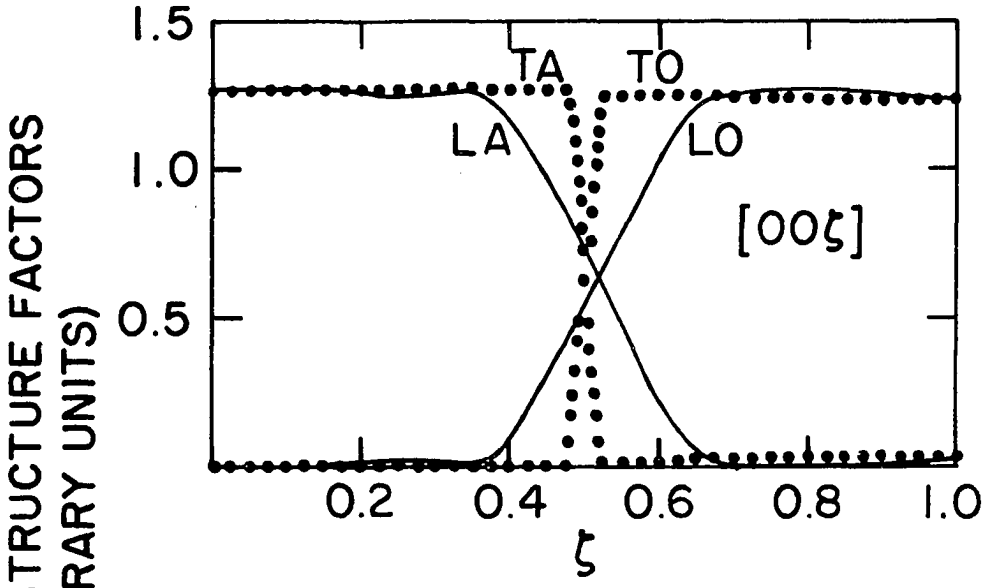

Fig. 7a. $|F|^2_{NORM}$ for [0 0 ζ] direction

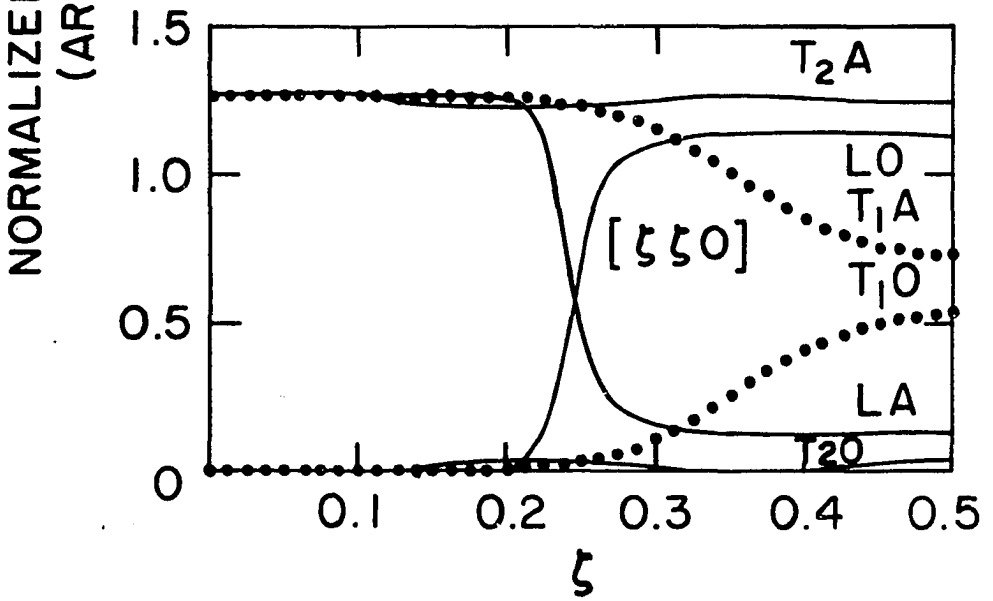

Fig. 7b. $|F|^2_{NORM}$ for [ζ ζ 0] direction

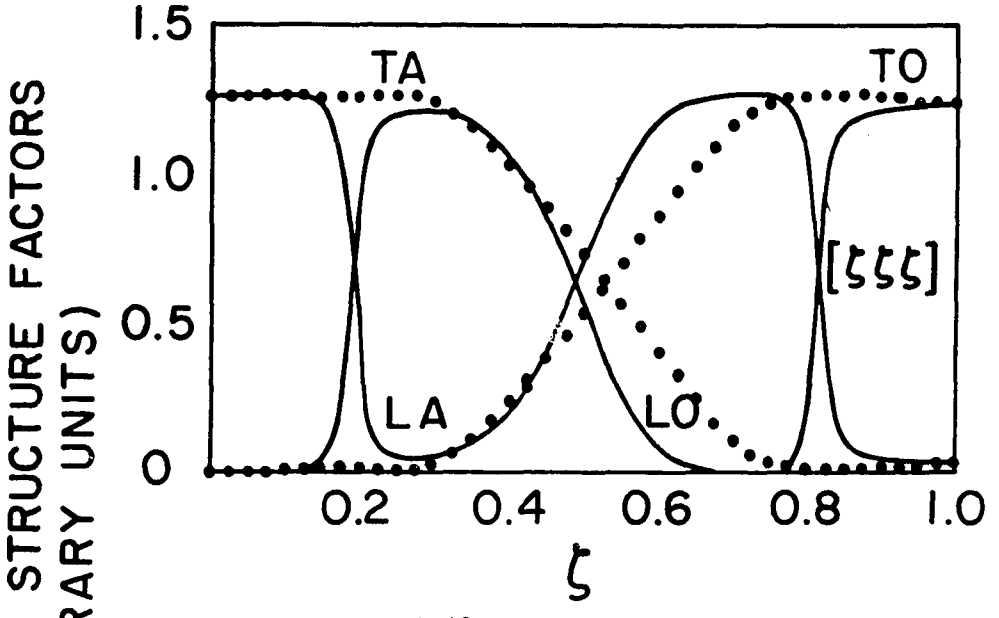

Fig. 8a. $|F|^2_{NORM}$ for [ζ ζ ζ] direction

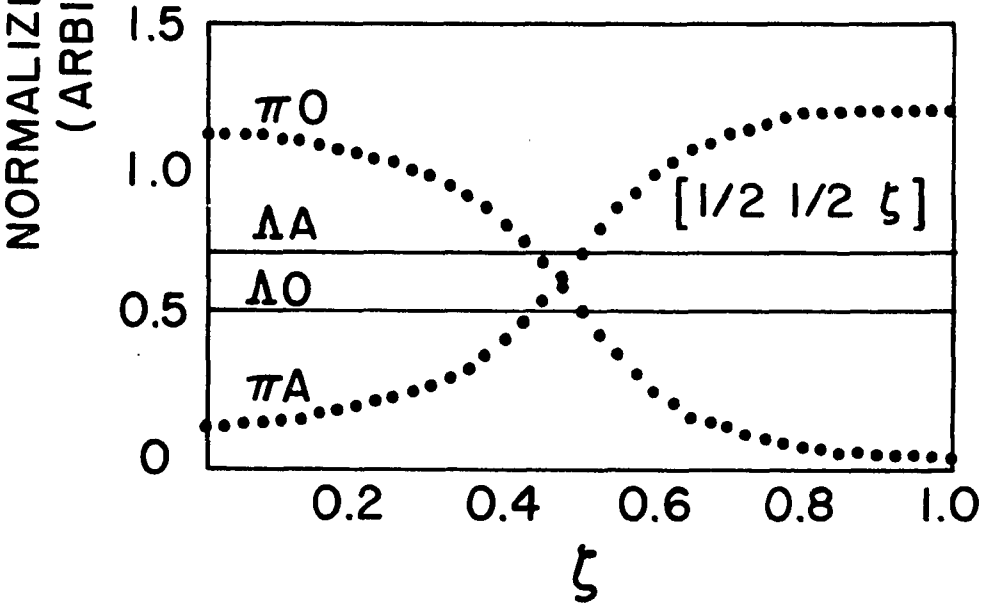

Fig. 8b. $|F|^2_{NORM}$ for $[\frac{1}{2}\ \frac{1}{2}\ \zeta]$ direction

Data Analysis:

The raw data consisted of sets of scattered neutron intensities vs. energy transfer values for specified values of $\underline{Q}$. Since the phonon frequencies were taken to be the mean values of the phonon peaks in the intensity vs. ν curves it was necessary to find these mean values. Two methods were used; the first was to simply draw a smooth curve through the experimental points and decide from the shape of the curve and the background what the phonon frequency was. The second method employed a computer program written by Mr. T.O. Brun (24) in which the phonon peak and the varying background were fitted to a sum of Gaussian functions of adjustable magnitude and position. The errors assigned to the phonons were determined by taking account of such factors as their intensity, the variation of the background around the phonon peak and the agreement between determinations of the same phonon using different values of $\underline{\tau}$. A list of the phonons retained for fitting may be found in Table 3. In addition to the 108 phonons that were determined by the use of neutron diffraction, the three phonons associated with the measured velocities of sound (Section VI) in the [1 1 0] direction are also listed in Table 3. These three phonons were also used in the non-linear least squares force constant program.

Table 3. Phonon frequencies and estimated errors (units of 10^{12} Hz.) of normal modes at 295°K

ζ	ν	$\delta\nu$	ζ	ν	$\delta\nu$
	LA [0 0 ζ]			TO [0 0 ζ]	
0.150	1.61	0.03	0.050	4.54	0.06
0.200	2.08	0.04	0.150	4.46	0.03
0.250	2.43	0.04	0.250	4.33	0.05
0.300	2.64	0.04	0.350	4.07	0.05
0.350	2.93	0.06	0.450	3.73	0.05
0.400	3.04	0.05	0.500	3.48	0.05
0.450	3.15	0.06		LA [ζ ζ 0]	
0.500	3.20	0.04	0.010	0.18	0.01
	LO [0 0 ζ]		0.200	3.24	0.05
0.150	4.48	0.05	0.304	3.12	0.03
0.250	4.38	0.03	0.354	2.68	0.03
0.300	4.29	0.03	0.400	2.16	0.04
0.400	4.30	0.06	0.450	1.96	0.03
0.500	4.28	0.10	0.500	1.86	0.05
	TA [0 0 ζ]			LO [ζ ζ 0]	
0.250	1.92	0.04	0.080	4.44	0.03
0.300	2.30	0.02	0.160	4.20	0.03
0.350	2.61	0.04	0.250	3.99	0.08
0.400	2.92	0.03	0.300	4.25	0.04
0.450	3.19	0.03	0.350	4.58	0.04
0.500	3.48	0.05	0.425	4.98	0.04
			0.500	5.27	0.05

Table 3. Continued

ζ	ν	δν	ζ	ν	δν
	T_1^A [ζ ζ 0]		0.400	1.86	0.03
0.010	0.11	0.01	0.450	1.75	0.08
0.148	1.58	0.03		T_2^Q [ζ ζ 0]	
0.198	1.99	0.03	0.0	4.48	0.07
0.248	2.28	0.03	0.102	4.51	0.05
0.298	2.29	0.03	0.202	4.60	0.10
0.347	2.29	0.03	0.302	4.80	0.10
0.398	2.17	0.03	0.402	4.87	0.05
0.447	1.96	0.03		LA [ζ ζ ζ]	
0.500	1.82	0.03	0.098	2.08	0.03
	T_1^Q [ζ ζ 0]		0.123	2.55	0.03
0.050	4.47	0.03	0.148	2.95	0.03
0.150	4.27	0.03	0.250	2.79	0.08
0.250	3.96	0.04	0.300	2.58	0.05
0.350	3.81	0.06	0.350	2.65	0.05
0.425	3.71	0.06	0.400	2.89	0.05
0.500	3.78	0.05	0.450	3.17	0.05
	T_2^A [ζ ζ 0]		0.500	3.31	0.07
0.005	0.04	0.01			
0.200	1.34	0.04			
0.250	1.61	0.04			
0.300	1.80	0.04			
0.350	1.85	0.04			

Table 3. Continued

ζ	ν	$\delta\nu$	ζ	ν	$\delta\nu$
	LO [ζ ζ ζ]			TO [ζ ζ ζ]	
0.000	4.48	0.05	0.000	4.69	0.03
0.050	4.48	0.05	0.100	4.63	0.03
0.100	4.24	0.05	0.200	4.62	0.05
0.150	3.98	0.03	0.300	4.74	0.04
0.250	3.97	0.06	0.400	4.86	0.05
0.300	4.37	0.07	0.500	4.90	0.05
0.350	4.69	0.08		πA [$\frac{1}{2}$ $\frac{1}{2}$ ζ]	
0.400	4.76	0.06	0.100	1.90	0.08
0.450	4.74	0.05	0.200	2.25	0.05
	TA [ζ ζ ζ]		0.300	2.75	0.05
0.100	1.09	0.03	0.400	3.20	0.04
0.150	1.64	0.03		πO [$\frac{1}{2}$ $\frac{1}{2}$ ζ]	
0.200	2.12	0.04	0.200	5.04	0.08
0.250	2.63	0.04	0.300	5.00	0.05
0.300	3.04	0.07	0.400	4.85	0.05
0.350	3.20	0.05		ΛA [$\frac{1}{2}$ $\frac{1}{2}$ ζ]	
0.400	3.25	0.05	0.100	2.40	0.07
0.450	3.33	0.06	0.300	3.65	0.10
0.500	3.37	0.07	0.400	3.40	0.10
				ΛO [$\frac{1}{2}$ $\frac{1}{2}$ ζ]	
			0.100	3.75	0.15
			0.400	4.60	0.10

Analysis of the dispersion curves in terms of force constant models began with attempts to determine the range of the interatomic forces. For all the measured dispersion curves, with the exception of the ΛA, ΛO branches in the $[\frac{1}{2}\ \frac{1}{2}\ \zeta]$ direction, the following relation holds;

$$\frac{M_0M_1}{2}\{\omega_A^2(\underline{q},j) + \omega_0^2(\underline{q},j)\} = \sum_{n=0}^{N} A_n \cos 2\pi n\zeta \quad . \tag{4.9}$$

In the above equation, the subscripts A,O refer to the acoustic and optic branches respectively. The variable ζ is defined as

$$\zeta = q/q\ \text{max} \quad . \tag{4.10}$$

For the ΛA and ΛO branches (which correspond to independent vibrations of the Y and Zn species) the equation analagous to Eq. (4.9) is

$$\frac{M_0M_1}{2}\omega_{A,O}^2 = \sum_{n=o}^{N} A_n \cos 2\pi n\zeta \quad . \tag{4.11}$$

The Fourier coefficients in these two equations may be thought of (25) as interplanar force constants acting between planes normal to $\underline{q}$. For the CsCl structure the $A_1 \cdots A_N$ represent the interplanar force constants between planes of like atoms. The contribution of the force constants acting between planes of unlike atoms is contained in A_o. A list of the A_n may be found in Appendix D.

The Fourier analysis involved finding the minimum number of coefficients needed to adequately describe a pair of branches of the dispersion curves. The lowest neighbor set number appearing in the highest Fourier coefficient gave the range of the force interactions. From such an analysis it became obvious that the dispersion curves could be fit fairly well

by a fifth neighbor model for all branches except ΛA and ΛO in the $(\frac{1}{2}\ \frac{1}{2}\ \zeta)$ direction. But for these two branches a sixth neighbor model was found to be necessary.

The computer program that was used to find the Fourier coefficients was a least squares program that minimized the function

$$\sum_{i} \frac{(\nu^2_{\text{OPTIC}}(i) + \nu^2_{\text{ACOUSTIC}}(i))_{\text{OBSERVED}} - (\nu^2_{\text{OPTIC}}(i) + \nu^2_{\text{ACOUSTIC}}(i))}{[\nu(i)\ \delta\nu(i)]^2_{\text{OPTIC}} + [\nu(i)\ \delta\nu(i)]^2_{\text{ACOUSTIC}}} . \tag{4.12}$$

A list of the Fourier coefficients and their estimated uncertainties is contained in Table 4.

Table 4. Coefficients of Fourier analysis

Dispersion Curve(s)	A_n (10^7dy/cm)	δA_n (10^6dy/cm)
LA, LO [0 0 ζ]	$A_0 = .46659$	$\delta A_0 = .00288$
	$A_1 = -.07474$	$\delta A_1 = .00449$
	$A_2 = -.00589$	$\delta A_2 = .00373$
TA, TO [0 0 ζ]	$A_0 = .42669$	$\delta A_0 = .00049$
	$A_1 = -.03377$	$\delta A_1 = .00074$
	$A_2 = .00062$	$\delta A_2 = .00073$

Table 4. Continued

Dispersion Curve(s)	A_n (10^7dy/cm)	δA_n (10^6dy/cm)
LA, LO [ζ ζ 0]	$A_0 = .50226$	$\delta A_0 = .00700$
	$A_1 = -.08793$	$\delta A_1 = .00945$
	$A_2 = -.02063$	$\delta A_2 = .01023$
T_1A, T_1O [ζ ζ 0]	$A_0 = .37836$	$\delta A_0 = .00082$
	$A_1 = .02317$	$\delta A_1 = .00117$
	$A_2 = -.01770$	$\delta A_2 = .00111$
T_2A, T_2O [ζ ζ 0]	$A_0 = .46572$	$\delta A_0 = .00662$
	$A_1 = -.09010$	$\delta A_1 = .00884$
	$A_2 = .01287$	$\delta A_2 = .00860$
LA, LO [ζ ζ ζ]	$A_0 = .50153$	$\delta A_0 = .00612$
	$A_1 = -.10209$	$\delta A_1 = .00779$
	$A_2 = .02425$	$\delta A_2 = .00911$
	$A_3 = -.02980$	$\delta A_3 = .00828$
TA, TO [ζ ζ ζ]	$A_0 = .54245$	$\delta A_0 = .00233$
	$A_1 = -.13943$	$\delta A_1 = .00325$
	$A_2 = -.00567$	$\delta A_2 = .00346$
	$A_3 = .00578$	$\delta A_3 = .00356$

Table 4. Continued

Dispersion Curve(s)	A_n (10^7dy/cm)	δA_n (10^6dy/cm)
$\pi A \quad \pi O \ [\frac{1}{2} \ \frac{1}{2} \ \zeta]$	$A_0 = .61351$	$\delta A_0 = .00335$
	$A_1 = -.03612$	$\delta A_1 = .00414$
	$A_2 = .01464$	$\delta A_2 = .00431$
$\Lambda A \ [\frac{1}{2} \ \frac{1}{2} \ \zeta]$	$A_0 = .42341$	$\delta A_0 = .00008$
	$A_1 = -.00157$	$\delta A_1 = .00009$
	$A_2 = -.00128$	$\delta A_2 = .00011$

A non-linear least-squares computer program (3) was developed to fit the twenty-four atomic force constants that appear in a sixth neighbor model. The general form of this program was suggested by Boyter and McMurry (26). The program finds a set of force constants by minimizing the variance ratio defined as

$$\text{variance ratio} = \frac{1}{N_D - N_P} \sum_{i=1}^{N_D} \frac{(\nu_i(c) - \nu_i(0))^2}{(\delta\nu_i(0))^2} \tag{4.13}$$

where

N_D = number of data points

N_P = number of adjustable parameters

$\nu_i(c)$ = calculated value of the i-th data point

$\nu_i(0)$ = observed value of the i-th data point

$\delta\nu_i(0)$ = error in the value of the i-th data point

Table 5 contains a list of the best-fit force constants for both the fifth and sixth neighbor models along with the variance ratios for the two models. The force constant notation that is used in Table 5 is that of Squires (27) and Gilat and Dolling (2). An explanation of the notation may be found in Appendix A. Figs. 9 through 12 show the experimental data for the symmetry directions along with the dispersion curves calculated using the sixth neighbor model. In addition, the experimental velocities of sound which will be discussed in Section VI are also represented in Figs. 9 through 12. A discussion of some features of the dispersion curves will be presented in Section VII.

Table 5. Interatomic force constants (units of dy/cm) for fifth and sixth neighbor force constant models

	5th Neighbor	6th Neighbor		5th Neighbor	6th Neighbor
α^1_1	5788	6199	β^3_{31}	-1134	- 600
β^1_1	6723	6271	α^4_1	645	96
α^2_{10}	5242	615	α^4_2	- 36	5
α^2_{11}	6244	8829	β^4_1	0	20
α^2_{20}	-1042	-1261	β^4_0	- 244	143
α^2_{21}	1719	2214	α^5_{10}	546	1471
α^3_{10}	-1366	-1249	α^5_{11}	620	- 168
α^3_{11}	- 271	- 479	β^5_{10}	1223	11
α^3_{30}	2641	1243	β^5_{11}	450	1236
α^3_{31}	-1409	- 202	α^6_{10}		5538
β^3_{30}	430	- 851	α^6_{11}		-2631

Table 5. Continued

	5th Neighbor	6th Neighbor
α^6_{20}		- 723
α^6_{21}		520

Variance Ratio 5th neighbor model = 6.83

Variance Ratio 6th neighbor model = 2.24

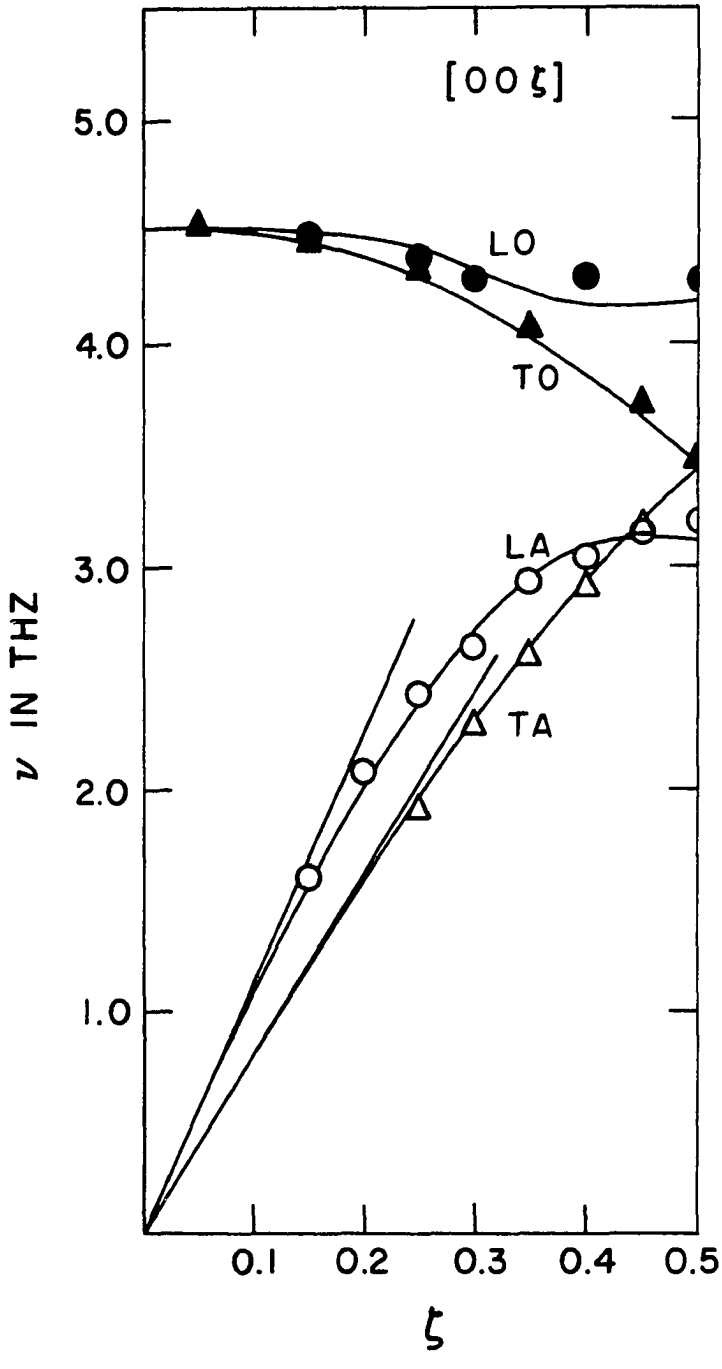

Fig. 9. Dispersion curve for [0 0 ζ] direction

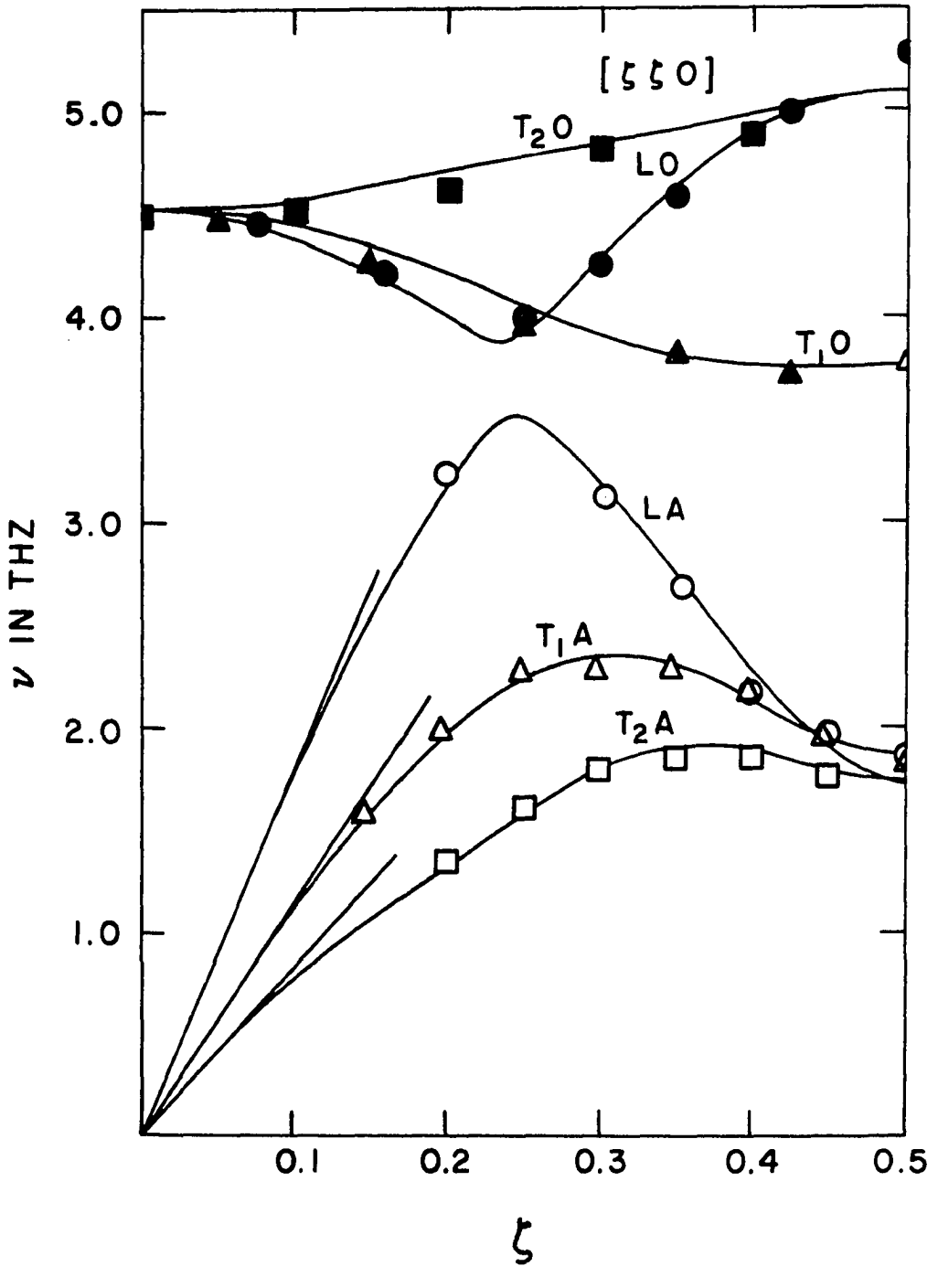

Fig. 10. Dispersion curve for [ζ ζ 0] direction

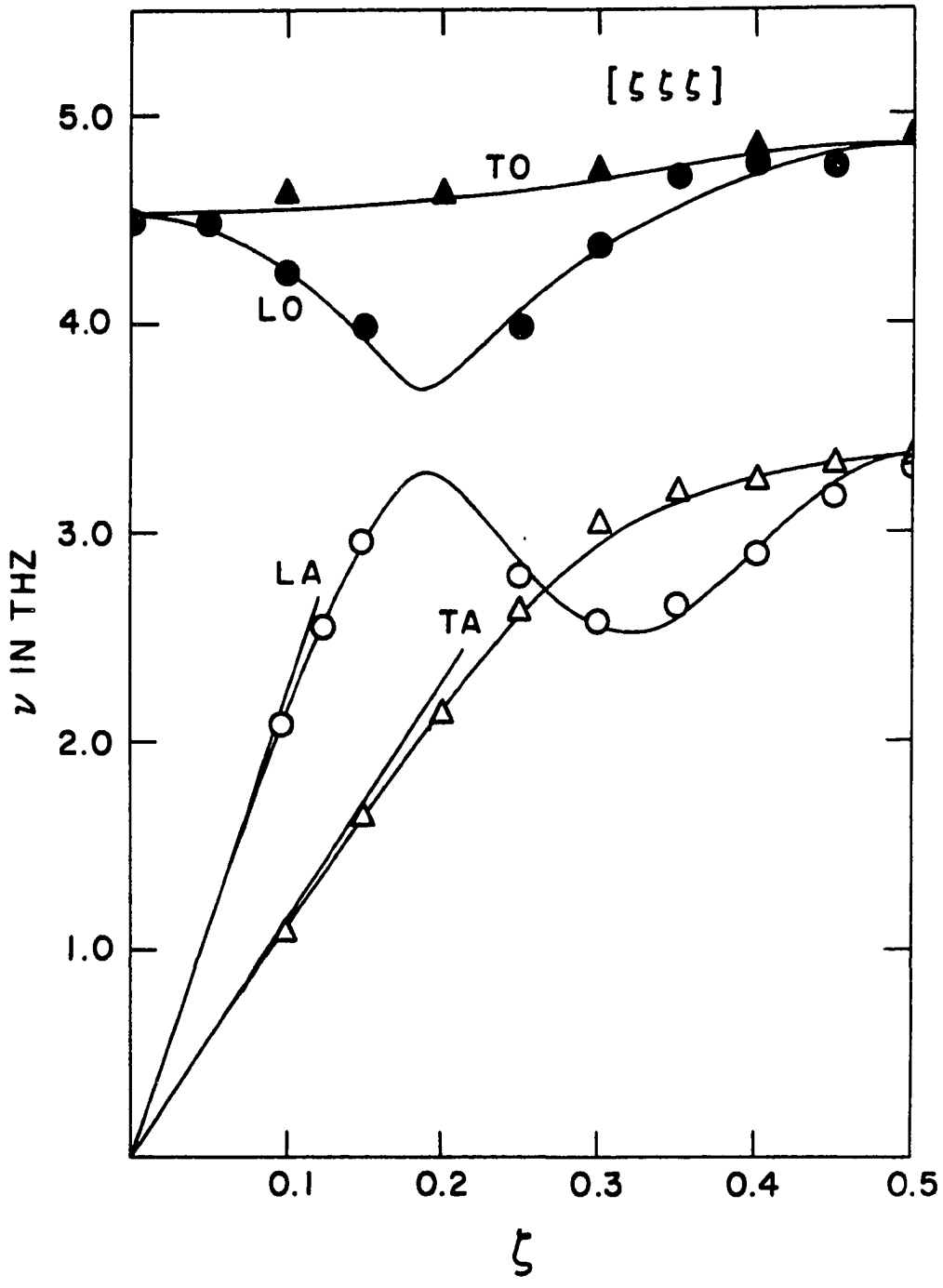

Fig. 11. Dispersion curve for [ζ ζ ζ] direction

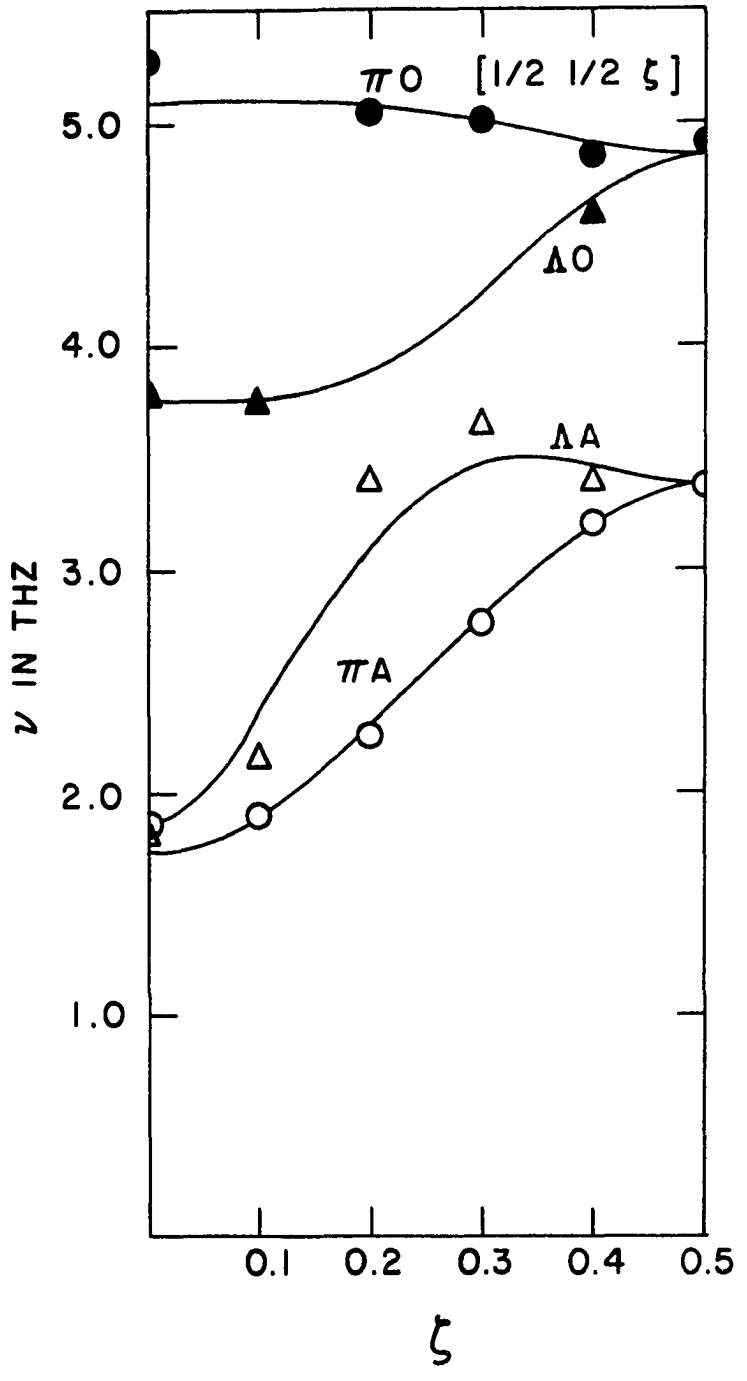

Fig. 12. Dispersion curve for $[\frac{1}{2}\ \frac{1}{2}\ \zeta]$ direction

V. X-RAY DIFFRACTION

In this section an x-ray diffraction experiment, and its interpretation, will be considered. The purpose of the experiment was to investigate the validity of an assumption that was made in Section III concerning the derivation of the $\nu_j(\underline{q})$ relations for YZn. This assumption was that the neutron diffraction sample was perfectly ordered. In order to investigate the validity of this assumption a method of plotting the x-ray diffraction results was devised that explicitly displays the degree of order possessed by the sample. In addition, the method provides an approximate value for the sum of the Debye-Waller factors of Y and Zn.

This section consists of three parts. The first part is a discussion of the experimental aspects of the x-ray diffraction experiment. The second part consists of a derivation of the method of interpretation of the x-ray data. The third part is a discussion of the effect of temperature diffuse scattering on the results of the experiment.

1. Experimental considerations

The experiment that was chosen for this investigation was a measurement of the integrated intensities of a series of {0 0 ℓ} Bragg reflections. The YZn sample which was employed in the experiment was spark-cut from the neutron diffraction sample so that its face was perpendicular to a (0 0 1) direction. After spark-cutting, the face of the sample was lightly mechanically polished and then electropolished to remove any cold-worked material present.

A General Electric XRD-6 single crystal orienter (SCO) was the instrument on which the experiment was performed. The instrument was operated in the θ-2θ scan mode. A schematic diagram of the experimental arrangement is

shown in Fig. 13. Ag radiation was employed using a 2.5 millimeter thick β-filter of Pd. The source collimator was a 0.40 MR and the detector collimator was a 0.2° HR. Because of the large size of the sample (approximately 3 cm^2 surface area) some modifications to the SCO were made to accommodate a special goniometer that held the sample. The integrated intensities were found with the use of a step-scan technique where the step increment was 0.02°. A typical scan is shown in Fig. 14. A straight-line background was drawn under the peaks and the integrated intensities were found by summing the differences between the observed peaks and their associated backgrounds.

As shown in Fig. 14 there were actually two peaks associated with each reflection. These were, of course, due to the $K\alpha_1$ and $K\alpha_2$ components of the Ag radiation. Because there were two peaks there was some ambiguity in the choice of the 2θ value to associate with a given reflection. This problem was resolved in the following way.

The 2θ values corresponding to the positions of the peaks for the $K\alpha_1$ and $K\alpha_2$ wavelengths were defined to be $2\theta_I$ and $2\theta_{II}$ respectively. Since the $K\alpha_1$ component of radiation was twice as intense as the $K\alpha_2$, the following method was used to find $2\theta_{AVERAGE}$.

$$2\theta_{AV.} = \frac{1}{3}[2(2\theta_I) + 2\theta_{II}] \quad . \tag{5.1}$$

Similarly, the average value of λ was

$$\lambda_{AV.} = \frac{1}{3}(2\lambda_I + \lambda_{II}) \quad . \tag{5.2}$$

These average values were then used to find the Lorentz polarization factors and the values of $(\sin\theta/\lambda)^2$. A summary of the experimental data

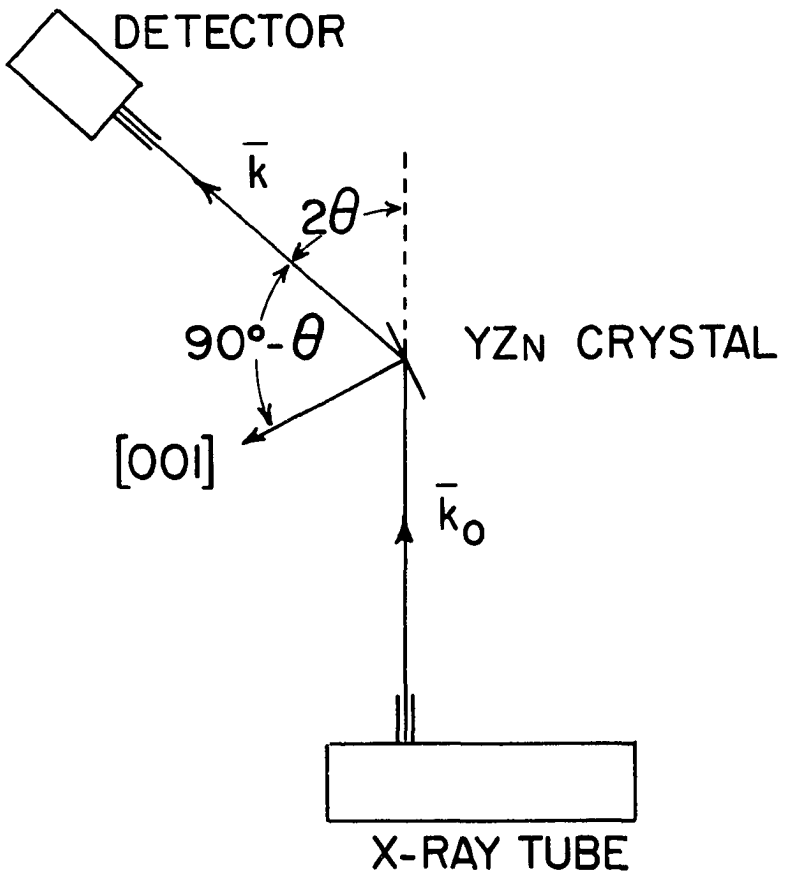

Fig. 13. Schematic diagram of the x-ray diffraction experiment

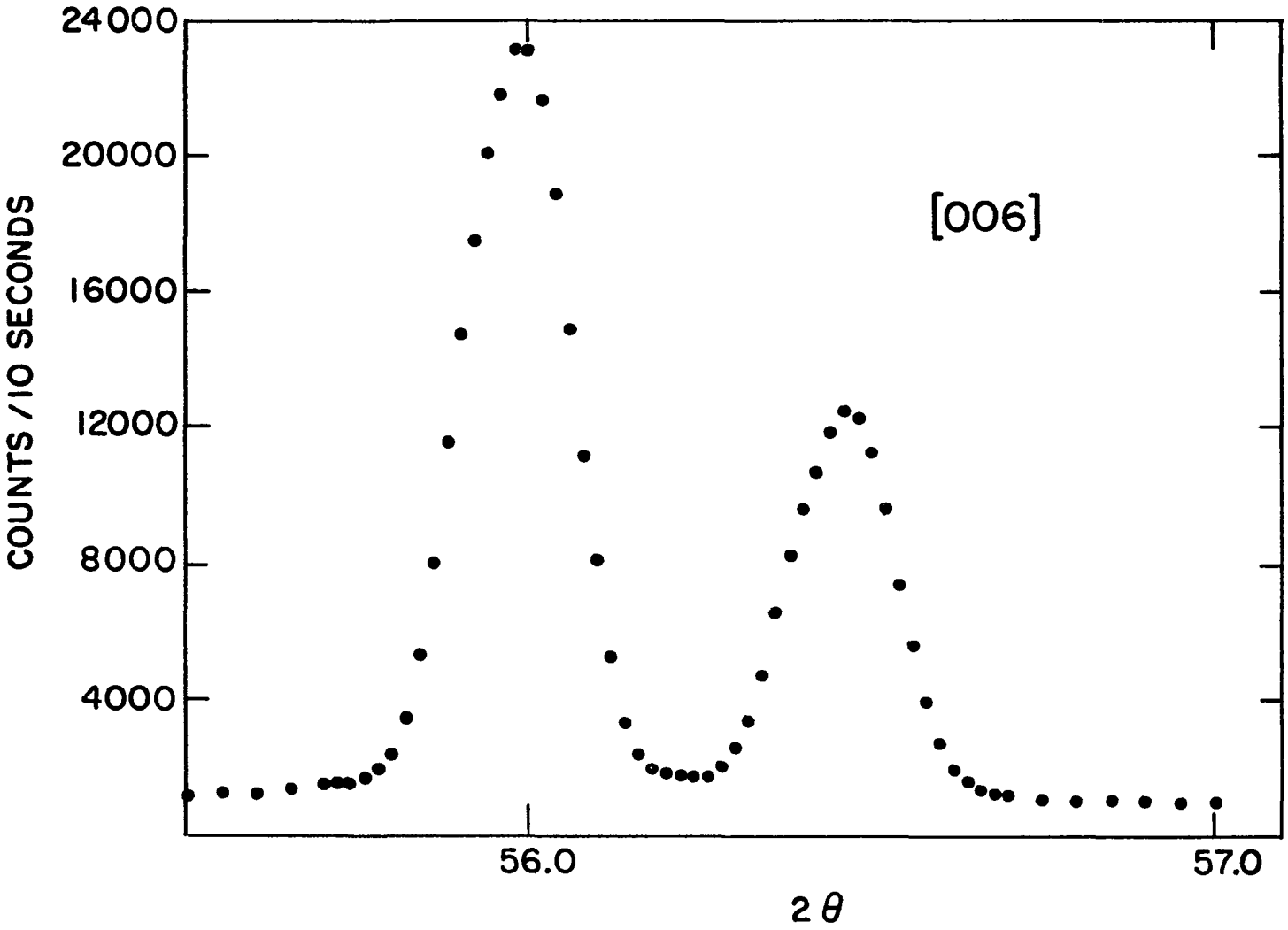

Fig. 14. Scan of the $K_{\alpha 1}$ and $K_{\alpha 2}$ components of the {0 0 6} reflection

is contained in Table 6. The quantity $K_{E,0}$ that is listed in Table 6 will be defined in the next part of this section.

Table 6. Data of x-ray diffractometer experiment

Reflection No.	I_{OBS} (Counts/10 sec.)	θ Avg.	$\frac{\sin^2\theta}{\lambda^2}$	$K_{E,0}$
002	14,183,880	9.03	0.0783	0.114
003	141,700	13.61	0.1761	7.39
004	2,007,310	18.29	0.3132	0.164
005	63,690	23.09	0.4890	5.00
006	330,780	28.08	0.7043	0.195
007	12,540	33.30	0.9584	4.88
008	50,100	38.86	1.2517	0.175
009	2,258	44.89	1.5282	3.36
0010	8,775	51.64	1.9550	0.125
0012	1,125	70.19	2.8143	0.114

2. Interpretation of x-ray experiment

Before the results of the particular experiment involving YZn are considered, perhaps a brief review of some x-ray scattering theory is in order. The results of this review will be used later in this section when a derivation of the scheme that was used to interpret the x-ray experiment will be given.

By analogy with the neutron scattering case the wave vectors of the incident and scattered x-rays are taken to be $\underline{k}_o$ and $\underline{k}$, respectively,

where $k_o = 2\pi/\lambda$. Because it is possible for an incident x-ray to create or destroy phonons, the magnitudes of k and k_o are not exactly the same. However, since the energy of an x-ray photon is approximately 10^4ev compared to phonon energies of approximately 10^{-2}ev it is an extremely good approximation to take $k_o = k$. The scattering vector $\underline{Q}$ will be defined as

$$\underline{Q} = \underline{k}_o - \underline{k} \quad . \tag{5.3}$$

For the case of a static lattice it can be shown (9, 28) that the differential scattering cross section is

$$\frac{d\sigma}{d\Omega} = N^2 V_z \left| \sum_s f_s(\underline{Q}) e^{i\underline{Q}\cdot\underline{R}_s} \right|^2 \delta(\underline{Q} - \underline{\tau}) \quad . \tag{5.4}$$

where

N = number of unit cells

V_z = volume of Brillouin Zone

$\underline{\tau}$ = reciprocal lattice vector

σ = the ratio of scattered x-ray flux to the incident flux

$d\Omega$ = the solid angle region into which x-rays may be scattered

$\underline{R}_s$ = a unit cell vector

The f_s in the preceding equation are the complex scattering factors of the form

$$f_s = f_{s_0} + f_{s_1} + i\, f_{s_2} \quad . \tag{5.5}$$

f_{s_0} is the normal scattering factor and f_{s_1} and f_{s_2} are the real and imaginary components of the anomalous dispersion corrections. The unit

of intensity in this equation is that associated with the scattering by a single electron under the same conditions; this unit is

$$\frac{e^4}{r^2 m^2 c^4} \frac{(1 + \cos^2 2\theta)}{2} \quad . \tag{5.6}$$

Here e and m are, respectively, the charge and mass of the electron, c is the velocity of light, r is the distance from the electron to the point of observation and 2θ is the scattering angle. The effect of thermal vibrations may be taken into account by the addition of a time-dependent displacement $\underline{u}_s(t)$ to $\underline{R}_s$. As in Eq. (3.12) $\underline{u}_s$ is defined as

$$\underline{u}_s = \sum_{q,j} \underline{e}_{sj}(\underline{q})\, Q(\underline{q},j)\, e^{i\underline{q}\cdot(\underline{R}_\ell + \underline{R}_s)}\, e^{i\omega t} \quad . \tag{5.7}$$

It may be shown (9, 28, 29) that with the addition of $\underline{u}_s(t)$ to $\underline{R}_s$ the differential scattering cross section then becomes

$$\frac{d\sigma}{d\Omega} = \left(\frac{d\sigma}{d\Omega}\right)_0 + \left(\frac{d\sigma}{d\Omega}\right)_1 + \cdots . \tag{5.8}$$

The first term in this series is the Bragg scattering term

$$\left(\frac{d\sigma}{d\Omega}\right)_0 = N^2 V_z \left| \sum_s f_s\, e^{-w_s}\, e^{i\underline{Q}\cdot\underline{R}_s} \right|^2 \delta(\underline{Q} - \underline{\tau}) \quad . \tag{5.9}$$

The e^{-w_s} terms are the Debye-Waller factors. w_s is defined as

$$w_s = 8\pi^2 \langle u_s^2 \rangle \frac{\sin^2\theta}{\lambda^2} \quad . \tag{5.10}$$

where $\langle u_s^2 \rangle$ is the mean square displacement of a type s lattice point in a direction perpendicular to the reflecting planes. The second term, corresponding to one-phonon processes. is

$$\left(\frac{d\sigma}{d\Omega}\right)_1 = N \sum_{q,j} \frac{\coth \frac{h\nu_j(\underline{q})}{2kt}}{2\omega_j(\underline{q})} \left| \sum_s f_s e^{-W_s} \frac{[\underline{Q}\cdot\underline{e}_s(\underline{q},j)]}{\sqrt{M_s}} e^{i\underline{\tau}\cdot\underline{R}_s} \right|^2 . \tag{5.11}$$

It might be pointed out that Eq. (5.11) is the x-ray analog of the one-phonon neutron scattering cross section that results from an energy integration of Eq. (4.1). In fact, the term

$$\left| \sum_s f_s e^{-W_s} \frac{[\underline{Q}\cdot\underline{e}_s(\underline{q},j)]}{\sqrt{M_s}} e^{i\underline{\tau}\cdot\underline{R}_s} \right|^2 . \tag{5.12}$$

might be thought of as the structure factor for inelastic one-phonon x-ray scattering. There are higher order terms in Eq. (5.8) corresponding to 2, 3, 4 etc. phonon processes, but they will be neglected here. The x-ray scattering caused by 1, 2 etc. phonon processes is referred to as temperature diffuse scattering (TDS).

An inspection of Eq. (5.11) shows that, although the one-phonon scattering occurs at all values of $\underline{q}$ in the Brillouin Zone, the largest effects occur near the reciprocal lattice points. The reason for this behavior is that the acoustic mode frequencies approach zero at these points. Consequently, if one tries to measure the integrated intensity of a Bragg peak he will really be measuring the intensity of the Bragg peak plus the intensity due to temperature diffuse scattering. Recently, several papers (30, 31, 32) have appeared in which the observation of scattering due to phonon processes is discussed. These papers show that the effects of the TDS are not negligible for higher order scattering (i.e. large Q). In the experiment considered here, TDS corrections were not made for reasons that will be presented later.

For the YZn experiment, it may be seen from Eq. (5.6) and Eq. (5.9) that the observed intensity of Bragg scattered x-rays is proportional to

$$\left| \sum_s f_s \, e^{-w_s} \, e^{i\underline{\tau}\cdot\underline{R}_s} \right|^2 (1 + \cos^2 2\theta) \quad . \tag{5.13}$$

Actually the intensity is also proportional to two other factors. One is the Lorentz factor, which, for the geometry of this experiment is equal to $(\sin 2\theta)^{-1}$ (33). The other term is the absorption factor which was a constant for the YZn experiment (33). If all these factors are combined, the resulting expression for the observed intensity of Bragg scattered x-rays is

$$I_{OBS.} = C \left| F_{E,O} \right|^2 \left(\frac{1 + \cos^2 2\theta}{\sin 2\theta} \right) \quad . \tag{5.14}$$

C is a proportionality constant and $F_{E,O}$ represents the structure factors for the cases of even and odd values of $\underline{\tau}$ respectively. F_E and F_O are defined (for the CsCl structure) (33) as,

$$F_E = (f_o \, e^{-w_o} + f_1 \, e^{-w_1}) \quad . \tag{5.15}$$

$$F_O = (f_o \, e^{-w_o} - f_1 \, e^{-w_1}) \, S \quad . \tag{5.16}$$

S is the long-range order parameter that is defined as

$$S = \frac{R_A - X_A}{1 - X_A} \quad . \tag{5.17}$$

and, where

R_A = fraction of A atoms on A sites

X_A = fraction of A atoms in the alloy

From the definition of S it may be seen that when there is perfect order i.e. when $R_A = 1$, then $S = 1$. When there is only a random arrangement of A atoms on A sites $R_A = X_A$, and $S = 0$.

The term $(\frac{1 + \cos^2 2\theta}{\sin 2\theta})$ in Eq. (5.14) is known as the Lorentz Polarization factor and will be referred to here as LP.

To summarize the development up to this point, an expression for the observed integrated intensity of Bragg scattered x-rays has been developed. This equation,

$$\frac{I_{OBS.}}{LP} = C \left|F_{E,O}\right|^2 \tag{5.18}$$

forms the starting point of a derivation of a method for displaying the x-ray data of the YZn experiment. The result of this derivation will be an equation expressing the value of the function

$$\ell n \quad \frac{I_{OBS.}}{(LP) \left|\Sigma f_s e^{i\underline{\tau}\cdot\underline{R}_s}\right|^2} \tag{5.19}$$

in terms of the long-range order parameter, the mean square displacements of Y and Zn and $(\sin \theta/\lambda)^2$. The derivation begins with the expansion of the right hand side of Eq. (5.18).

$$C\left|F_{E,O}\right|^2 = C\{\left|f_o\right|^2 e^{-2w_o} + \left|f_1\right|^2 e^{-2w_1} + 2\mathrm{Re}(f_o f_1^*) e^{-(w_1 - w_o)}\} S^2 \tag{5.20}$$

The (±) refer to ($^{\text{even}}_{\text{odd}}$) reflections. It may be noted that S^2 is contained as a factor for both even and odd reflections in Eq. (5.20). In order to write Eq. (5.20) in this form the following convention was adopted. For even reflections the symbol S is to be interpreted as 1: for odd reflections, the symbol S is defined as the long-range order parameter of Eq. (5.17). The reason for this possibly confusing notation is to eliminate the writing of unnecessary equations, and also, to allow the treatment of the even and odd cases in a unified manner. If e^{-2w_o} is factored from Eq. (5.20) the result is

$$C|F_{E,O}|^2 = C\{|f_0|^2 + |f_1|^2 e^{-2(w_1-w_0)} \pm 2\mathrm{Re}(f_0 f_1^*) e^{-(w_1-w_0)}\} e^{-2w_o} S^2 \quad . \tag{5.21}$$

It will turn out to be of advantage to expand the exponentials involving $(w_1 - w_0)$ in a Taylor series and keep only the leading terms. The justification for keeping only the leading term may be seen by considering what $(w_1 - w_0)$ is. By definition, (Eq. (5.10))

$$w_1 - w_0 = 8\pi^2(\langle u^2_{1z}\rangle - \langle u^2_{0z}\rangle)\frac{\sin^2\theta}{\lambda^2} \quad . \tag{5.22}$$

The subscript z on the u^2 indicates a mean square displacement normal to the {0 0 ℓ} planes. For cubic materials $\langle u^2\rangle$ is isotropic, and so the projection of $\langle u^2\rangle$ along a [0 0 ℓ] direction is $\langle u^2\rangle/3$. The reason that only the first term in the expansion of $(w_1 - w_0)$ need be retained is that, experimentally (34), the values of $\langle u^2\rangle$ for metals at room temperature are found to lie in the range $(0.01 - 0.1)(\text{Å}^\circ)$. In

addition, it has also been found that for crystals composed of more than one kind of atom, the differences in their $\langle u^2 \rangle$ values is small at room temperature (34). In any event, since $(w_1 - w_0)$ is proportional to $(\sin \theta/\lambda)^2$ there will be a range of $(\sin \theta/\lambda)^2$ for which the approximation is valid.

If the expansion of the exponentials is carried out, Eq. (5.18) yields

$$\frac{I_{OBS}}{LP} = C\{[|f_0|^2 + |f_1|^2 \pm 2Re(f_0 f_1^*)] - (w_1 - w_0)\,[2|f_1|^2 \pm 2Re(f_0 f_1^*)]\}\, S^2 e^{-2w_0} \quad . \tag{5.23}$$

In order to put Eq. (5.23) in a more useful form, both sides of the equation will be divided by the quantity

$$|\Sigma f_s e^{i\underline{\tau}\cdot\underline{R}_s}|^2 = |f_0|^2 + |f_1|^2 \pm 2Re(f_0 f_1^*) \quad . \tag{5.24}$$

In this case Eq. (5.23) becomes

$$\frac{I_{OBS}}{LP\,|\Sigma f_s e^{i\underline{\tau}\cdot\underline{R}_s}|^2} = \{1 - (w_1 - w_0)\,[\frac{2|f_1|^2 \pm 2Re(f_0 f_1^*)}{|\Sigma f_s e^{i\underline{\tau}\cdot\underline{R}_s}|^2}]\}\, S^2 e^{-2w_0}\, C \quad . \tag{5.25}$$

But

$$2|f_1|^2 \pm 2Re(f_0 f_1^*) = |\Sigma f_s e^{i\underline{\tau}\cdot\underline{R}_s}|^2 - |f_0|^2 + |f_1|^2 \quad . \tag{5.26}$$

Therefore, the right hand side of Eq. (5.25) may be expressed as

$$\left\{1 - (w_1 - w_0)\left[1 - \left\{\frac{|f_0|^2 - |f_1|^2}{|\Sigma f_s e^{i\underline{\tau}\cdot\underline{R}_s}|^2}\right\}\right]\right\} S^2 e^{-2w_o} C \quad . \tag{5.27}$$

It is convenient to make the definition

$$\frac{|f_0|^2 - |f_1|^2}{|f_0|^2 + |f_1|^2 \pm 2\mathrm{Re}(f_0 f_1^*)} = K_{E,O} \quad . \tag{5.28}$$

where, as usual, the E,O refers to even and odd reflections respectively. It may be noted that a table of values of $K_{E,O}$ for the YZn experiment are contained in Table 6.

The values of $K_{E,O}$ in Table 6 were calculated with the use of normal scattering factors (35) and anomalous dispersion corrections (36) which were computed on the basis of relativistic Dirac-Slater wave functions.

In addition, the $K_{E,O}$ were calculated with the assumption that an Y atom was at the position (0 0 0)$a_0/2$ and a Zn atom at the position (1 1 1)$a_0/2$. This assumption, of course, is arbitrary. If the opposite convention had been used the values of $K_{E,O}$ in Table 6 would have to be replaced by their negatives.

The x-ray data will be plotted in the form of the natural logarithm of the left hand side of Eq. (5.25) vs. $(\sin\theta/\lambda)^2$. The logarithm of the right hand side is

$$\ell n[1 - (w_1 - w_0)(1 - K_{E,O})] - 2w_0 + 2\ell n\, S + \ell n\, C \quad . \tag{5.29}$$

For the range where $(w_1 - w_0)\cdot(1 - K_{E,O})$ is small, the ℓn in

Eq. (5.29) may be expanded in a Taylor expansion. If the logarithm is expanded, and Eq. (5.27) simplified, the right hand side becomes

$$- [(w_0 - w_1) + (w_0 - w_1) K_{E,O}] - \tfrac{1}{2}[(w_0 - w_1)$$

$$(1 - K_{E,O})]^2 + 2\ell n\ S + \ell n\ C \quad . \tag{5.30}$$

In order to explicitly bring out the $(\sin \theta/\lambda)^2$ dependence, the quantity B_{iz} will be defined as

$$B_{iz} = \frac{8\pi^2}{3} \langle u_i^2 \rangle = w_i \left(\frac{\lambda^2}{\sin^2\theta}\right) . \tag{5.31}$$

With this definition, the final result of this derivation may be written as

$$\ell n \frac{I_{OBS}}{(LP)\left|\Sigma f_s e^{i\underline{\tau}\cdot\underline{R}_s}\right|^2} = - [(B_0 + B_1) + (B_0 - B_1)K_{E,O}]\frac{\sin^2\theta}{\lambda^2}$$

$$- \tfrac{1}{2}[(B_0 - B_1)(1 - K_{E,O})]^2 \left(\frac{\sin^2\theta}{\lambda^2}\right)^2 + 2\ell n\ S + \ell n\ C \quad . \tag{5.32}$$

Eq. (5.32) is the expression that will be used to interpret the experimental data of the YZn experiment.

The qualitative behavior of Eq. (5.32) may be easily seen if it is written in the form

$$y = mx + nx^2 + b \tag{5.33}$$

where

$$y = \ell n \left\{ \frac{I_{OBS}}{(LP)\left|\Sigma f_s e^{i\underline{\tau}\,\underline{R}_s}\right|^2} \right\}$$

$$m = -\left[(B_0 + B_1) - (B_1 - B_0)\, K_{E,O}\right]$$

$$n = -\tfrac{1}{2}\left[(B_0 - B_1)(1 - K_{E,O})\right]^2$$

$$b = 2\ \ell n\ S + C$$

$$x = \left(\frac{\sin^2\theta}{\lambda^2}\right) \quad . \tag{5.34}$$

Two important features are illustrated by Eq. (5.34). First, for small values of $(\sin\theta/\lambda)^2$ the slope of y(x) is determined by m. Since K_E and K_O have very different magnitudes (Table 6) m will also be quite different for even and odd reflections. This fact will allow for the identification of the species possessing the larger B_i. The second point is that the difference in the y(0) values for the odd and even curves will identify the value of the long-range order parameter.

There are two cases to consider; the first is $B_0 > B_1$, and the second is $B_0 < B_1$. The qualitative behavior of y(x) for both of these cases is illustrated in Fig. 15. If $B_0 > B_1$ then, since $K_O > K_E$, the initial slope of the curve of odd reflections will be greater (more negative) than the slope of the even curve. Alternatively, if $B_0 < B_1$, the initial slope of the odd curve will be smaller (less negative) than the slope of the even curve. Also, at x = 0, the difference of the intercepts of the even and odd curves is just twice the logarithm of the long-range order parameter.

Therefore, within the framework of the approximations that have been made in this derivation, it seems that a plot of the type shown in Fig. 15 will yield not only the value of the long-range order parameter, but will also identify the species possessing the larger Debye-Waller factor.

Fig. 16 is a plot of the YZn data treated in the above manner. Two facts appear to be obvious from an inspection of Fig. 16. First, B_1 seems to be larger than B_0. Second, the curves representing the even and odd numbered reflections appear to have a common intercept. This second point required further investigation since it seemed possible that instead of the two curves having a common intercept, the situation might have been as shown in Fig. 17. That is, $y_{ODD}(o)$ might have been considerably less than $y_{EVEN}(o)$ which would have indicated that the long-range order parameter was less than one.

To investigate this possibility, the function $y_{ODD}(x) - y_{ODD}(o)$ was plotted for a series of values of $(B_1 - B_0)$. $y_{ODD}(x) - y_{ODD}(o)$ is given by

$$y_{ODD}(x) - y_{ODD}(o) = -[(B_0 + B_1) - (B_1 - B_0)K_o]x$$

$$- \tfrac{1}{2}[(B_0 - B_1)(1 - K_o)]^2x^2 \quad . \tag{5.35}$$

The quantity $(B_0 + B_1)$ that was needed for these graphs was obtained from a measurement of the slope of the even curve and the assumption that the nx^2 term was negligible for $x < 1$. Since $K_E \approx 0.2$, this assumption seemed to be warranted. From a measurement of the slope of the even curve it was found that

$$[(B_0 + B_1) - (B_1 - B_0)K_E] \approx 1.45 \pm 0.05 \quad . \tag{5.36}$$

Or, since $K_E \simeq 0.2$ and, in all likelihood, $(B_1 - B_0) \lesssim 0.5$ it follows that

$$0 \lesssim (B_1 - B_0)K_E \lesssim 0.1 \quad . \tag{5.37}$$

Therefore, it is possible to put the following limits on $(B_0 + B_1)$.

$$1.40 \lesssim (B_0 + B_1) \lesssim 1.60 \tag{5.38}$$

With the approximate value of $(B_0 + B_1)$ from Eq. (5.38) a series of $y_{ODD}(x) - y_{ODD}(o)$ curves were plotted. Since B_0 and B_1 were not known, several sets of B_0 and B_1 values were chosen (consistent with Eq. (5.38)) and a series of $y_{ODD}(x) - y_{ODD}(o)$ curves were plotted. The maximum value of $y_{ODD}(x) - y_{ODD}(o)$ from among the curves that were plotted was 0.12. Since the ordinate of the (0 0 3) reflection, y(0 0 3), must be less than or at most equal to the maximum value of $y_{ODD}(x)$, it follows that

$$y_{ODD}(o) \gtrsim y(0\ 0\ 3) - 0.12 \quad . \tag{5.39}$$

From Fig. 16 it may be seen that y(0 0 3) - 0.12 differs from the intercept of the even curve by approximately 0.03. Therefore, twice the logarithm of the long-range order parameter can at most be 0.03 or, consequently, the long-range order parameter is indeed very close to 1.0.

3. Temperature diffuse scattering effects

At the beginning of this chapter, mention was made of TDS and its effect on measured integrated intensities. Also, it was stated that no

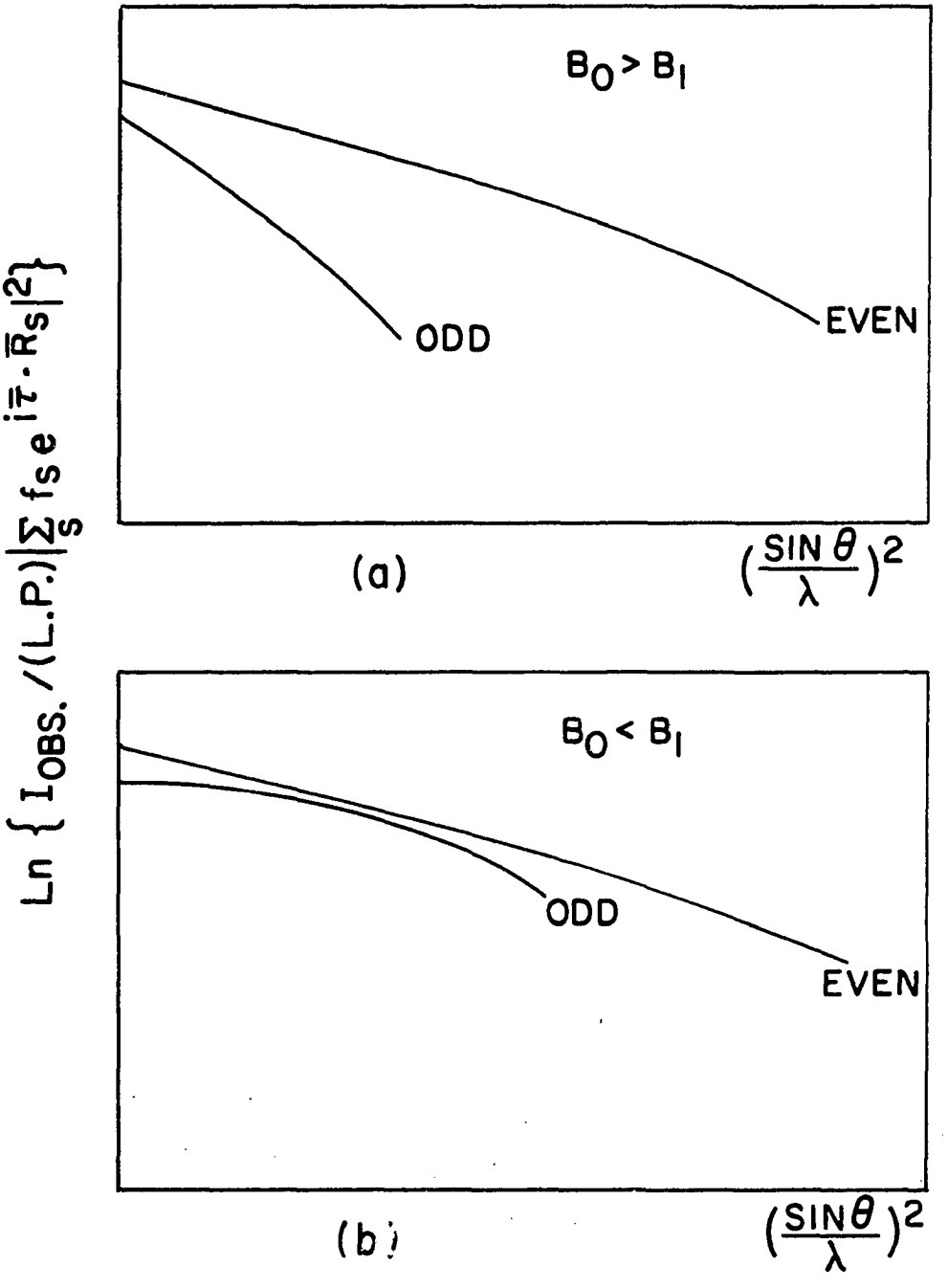

Fig. 15. Qualitative behavior of y(x) for (a) $B_0 > B_1$ and (b) $B_0 < B_1$

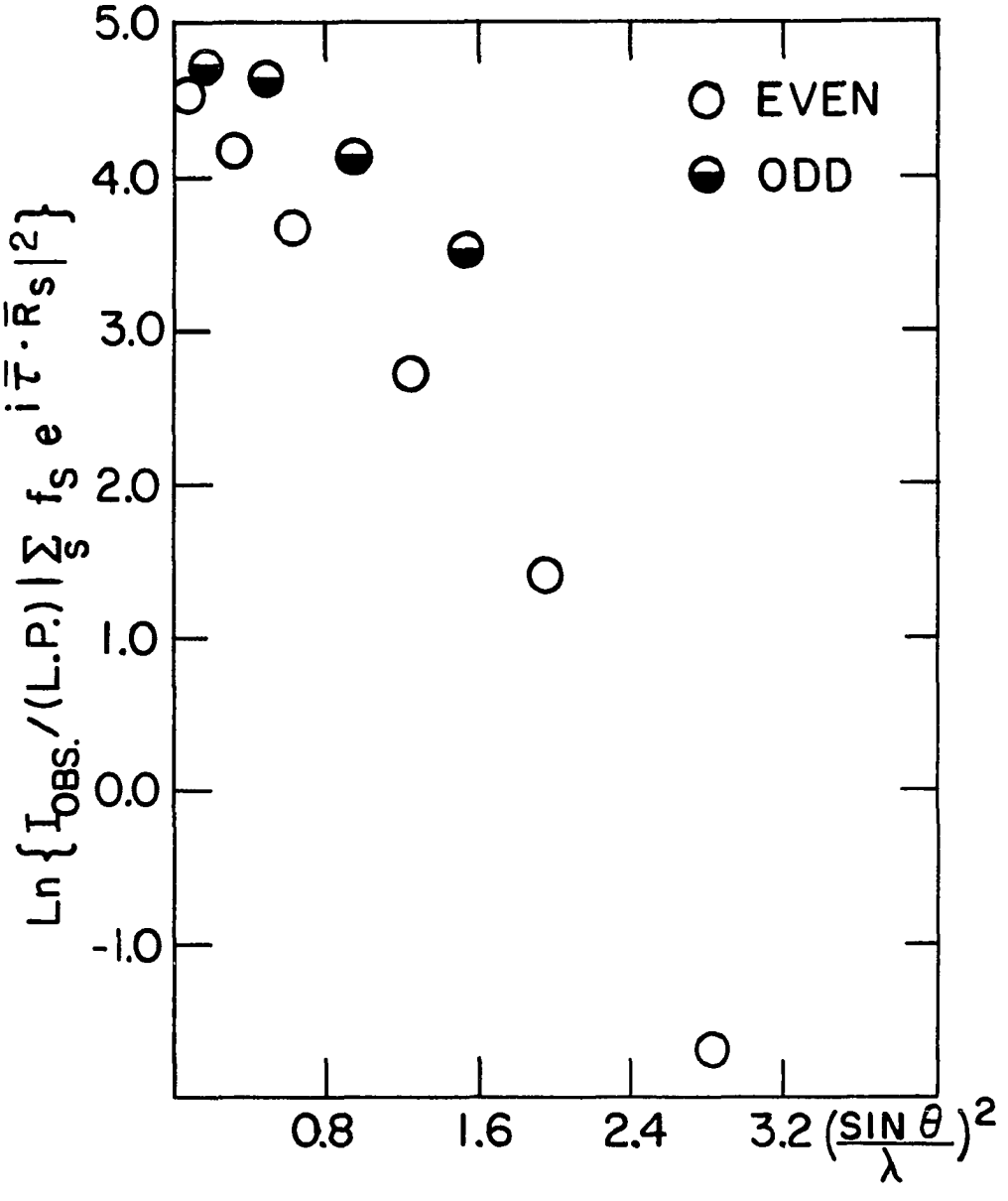

Fig. 16. X-ray diffraction data of YZn

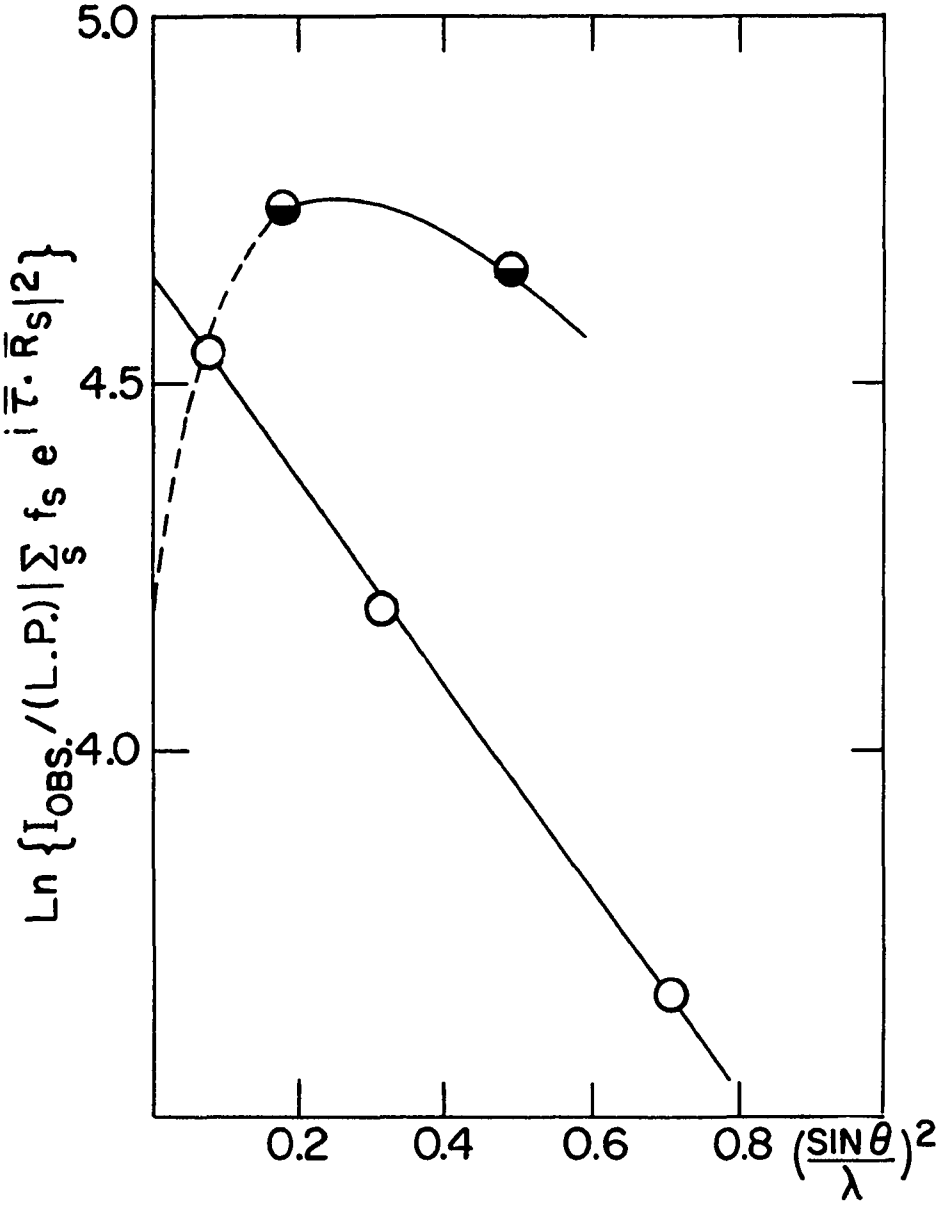

Fig. 17. Possible behavior (dotted line) of y(x) for small x

corrections for TDS were made to the YZn data. There were two main reasons for not trying to correct the measured integrated intensities for TDS effects. First, the analysis given above to determine the long-range order parameter by plotting the function

$$\ell n \quad \frac{I_{OBS}}{(LP)\left|\sum_s f_s e^{i\underline{\tau}\cdot\underline{R}_s}\right|^2} \quad . \tag{5.40}$$

vs. $(\frac{\sin\theta}{\lambda})^2$ was dependent on only the reflections up to (0 0 6). Since the TDS increases with the reflection number the errors introduced by using only these lower order reflections were assumed to be small. Second, there seemed to be no realistic way of assessing the magnitude of the TDS effects for the experiment described here. This is so because a monochromatic well-collimated x-ray beam was not used for the experiment.

In the case of a monochromatic, well-collimated incident beam, it is possible to calculate the first order TDS by performing the sum indicated in Eq. (5.11) over the effective volume in reciprocal space (31, 32, 37). By "effective volume in reciprocal space" is meant the locus of points defined by the $\underline{Q}$ vectors that not only satisfy Eq. (4.2) and Eq. (4.3) but also have associated sin θ values that correspond to the 2θ of the x-ray detector. However, for the experiment described here the effective volume received a spectrum of wavelengths of unknown distribution, thus making the integration impossible.

However, it is possible to investigate in a qualitative way what effect the inclusion of TDS might have. Here only one-phonon scattering, which is expected to be the largest part of the TDS will be considered. From Eq. (5.11) it may be seen that the integrated intensity due to one-

phonon scattering will be of the form

$$I_{(1)} = NQ^2 \int \sum_j \frac{\coth\left(\frac{h\nu_j(\underline{q})}{2kT}\right)}{2\omega_j(\underline{q})} \left| \sum_s \frac{f_s e^{-W_s}}{\sqrt{M_s}} \right.$$

$$\left. e^2_{3s}(\underline{q},j)\, e^{i\underline{\tau}\cdot\underline{R}_s} \right|^2 d^3q \quad . \tag{5.41}$$

where the integral is over the effective volume of reciprocal space. It is true that the effective volume is a function of the reflection number, but the largest contribution to the integral comes from the very small q region which is common to each reflection. Therefore the integral will be taken to be a constant. The ratio of the TDS intensity to the Bragg intensity is then (Appendix E)

$$\frac{I_{(1)}}{I_{BRAGG}} = a'Q^2 = a\,\frac{\sin^2\theta}{\lambda^2} \quad . \tag{5.42}$$

where a is presumably much less than one. By definition

$$I_{OBS} = I_{BRAGG} + I_{TDS} \ , \tag{5.43}$$

or

$$I_{OBS} = I_{BRAGG}\,(1 + a\,\frac{\sin^2\theta}{\lambda^2}) \quad . \tag{5.44}$$

Since a is very small it is a good approximation to take

$$I_{OBS} = I_{BRAGG}\, e^{a\,\frac{\sin^2\theta}{\lambda^2}} \quad . \tag{5.45}$$

If Eq. (5.34) is rewritten to include the TDS term, it then becomes

$$y = m'x + nx^2 + b \tag{5.46}$$

where

$$m' = -\left[(B_0 + B_1) - (B_1 - B_0)\, K_{E,O} - a\right] \quad . \tag{5.47}$$

As before, $m' = 1.45 \pm 0.05$. If Eq. (5.30) is rewritten to include a, then,

$$1.40 + a \leq (B_0 + B_1) \leq 1.60 + a \quad . \tag{5.48}$$

that is, the effect of a is to increase the value of $(B_0 + B_1)$ over its uncorrected value. This result is consistent with those of Buyers and Smith (38) and Nilsson (39) who also found that taking account of TDS increased their apparent B_i values.

The primary reason for doing the x-ray experiment described above was to determine the value of the long-range order parameter. However, as a by-product, the experiment also yielded the approximate value of $(B_0 + B_1)$. It was decided to try to calculate B_0 and B_1 from first principles and compare them with the experimental result. The calculation, which utilized a result of Maradudin, Montroll and Weiss (9) consisted of evaluating the expression

$$\langle u^2_{\alpha s} \rangle = \frac{\hbar}{2NM_s} \sum_{q,j} \frac{e^2_\alpha(q,j)}{\omega_j(q)} \coth \frac{h\nu_j(q)}{2kT} \quad . \tag{5.49}$$

In this situation $\langle u^2_{\alpha s} \rangle$ is the mean square displacement of an S-th type atom in the α-th direction. The polarization vectors and eigenfrequencies were calculated using the twenty-four force constant model described in

Section III. Because of the symmetry of the CsCl structure the sum in Eq. (5.49) which is over all phonon wave vectors in the Brillouin Zone can be reduced to a sum over vectors in the irreducible 1/48 Brillouin Zone. When the calculation was performed for 4960 wave vectors in the irreducible zone it yielded

$$\langle u^2_{0z} \rangle = .0311 \ (A°)$$

$$\langle u^2_{1z} \rangle = .0301 \ (A°) \tag{5.50}$$

or

$$B_{Y} = B_{o} = .819 \ (A°)$$

$$B_{Zn} = B_{1} = .793 \ (A°) \quad . \tag{5.51}$$

It is interesting to note that the calculated value of $(B_0 + B_1)$ is in good agreement with the experimental result. However, the relative magnitudes of B_0 and B_1 are in disagreement. The source of this disagreement is not known but may be due to anharmonic effects which were neglected in deriving Eq. (5.49).

VI. VELOCITIES OF SOUND

One of the experiments which was a part of this thesis was the measurement of the velocities of sound waves in YZn. There were four reasons for doing this experiment. First, a measurement of the velocities of sound (together with a knowledge of the lattice parameter) made possible a calculation of the elastic constants of YZn. This calculation is discussed below. Second, from a knowledge of the elastic constants it is possible to calculate a value for the Debye temperature at 0°K. The calculated value of $\theta_D(0°K)$ is presented below. The third objective was to find the limiting values (as $\underline{q} \rightarrow 0$) of the slopes of the acoustic branches of the dispersion curves. The reason for finding these slopes was to refine the fifth and sixth neighbor force constant models that were discussed in Section IV. That is, the measured velocities of sound were treated in such a way (which is discussed below) that they were able to be used in the non-linear least-squares fitting program of Section IV. The inclusion of the velocities of sound data in the fitting program insured that the fifth and sixth neighbor force constant models accurately described the important small q region of the dispersion curves. The fourth reason for measuring the velocities of sound was that a simple, first neighbor, force constant model was devised that used the measured velocities of sound. It is to be emphasized that this model (which will be referred to as the elastic constant model) is completely independent of any other experimental measurements. The derivation of the elastic constant model will be given in this section. Several lattice properties were calculated on the basis of the elastic constant model. They will be discussed in Section VII.

Three independent velocities of sound were determined by measuring transit times of pulses of ultrasonic waves along a [1 1 0] direction in a sample of known dimension. Specifically, the pulse superposition technique (40, 41, 42), was used to measure the transit times. This technique consists of exciting a quartz transducer to oscillate at its resonant frequency (approximately 10 MHZ) for a time t_1 after which it is passive for a time $t_2 > t_1$. The excitation of the transducer produces a pulse which transverses the sample, is reflected at the opposite face and returns to the transducer at a time t_3. During t_3 other pulses are emitted by the transducer with frequency $1/t_2$. If t_2 is adjusted so that $t_2 = nt_3$, where n is an integer, then resonance will exist in the sense that echoes from successive pulses will arrive at the transducer at the same time. If the applied voltage to the transducer is switched off for a time, the echoes incident on the transducer will produce a signal that may be amplified and displayed on an oscilloscope screen. In fact, t_2 is found by observing the oscilloscope screen and maximizing the amplitude of the echoes.

The ultrasonic measurements were made on a sample which was cut from the same crystal that was used in the neutron diffraction experiment. The crystal was spark-cut to have two parallel faces normal to a [1 1 0] direction. After spark-cutting, the sample was mechanically polished to provide a suitable surface for bonding to the transducer. Two types of bonding agents were employed, Nonaq stopcock grease and Salol (phenyl salicycate), for the longitudinal and transverse polarizations respectively.

The transit times at room temperature were (in μ seconds) $T_L = 6.626 \pm 0.03$, $T_1 = 10.376 \pm 0.04$, $T_2 = 14.493 \pm 0.06$. The subscripts L, 1 and 2 refer to atom vibrations in the [1 1 0], [0 0 1] and [$\bar{1}$ 1 0] directions

respectively. Values of the velocities of sound were found by dividing twice the sample thickness (2.9890 cm) by the transit times. With the use of the relations (43)

$$\rho v_L^2 = \tfrac{1}{2}(C_{11} + C_{12} + 2C_{44})$$

$$\rho v_1^2 = C_{44}$$

$$\rho v_2^2 = \tfrac{1}{2}(C_{11} - C_{12}) \quad . \tag{6.1}$$

where ρ is the density, the elastic constants were found to be (in units of 10^{11} dynes/cm^2) $C_{11} = 9.154$, $C_{12} = 4.378$ and $C_{44} = 4.658$. Numerical evaluation of the density was based on a value of $a_0 = 3.573$ A° for the lattice parameter.

From a knowledge of the velocities of sound it is possible to calculate a value for the Debye temperature at 0°K. This calculation involved the use of the extensive tables of Overton and Schuch (44). From these tables it was found that $\theta_D(0°K) = 291.1°K$.

The velocities of sound were also used to refine the fifth and sixth neighbor force constant models mentioned in Section IV. It was necessary to use the velocities of sound because, as may be seen from Figs. 9 - 12 there were no measured phonons below a frequency of 1.0 THZ.

The reason that lower frequency phonons were not measured by inelastic neutron scattering was that the energy resolution of the triple axis spectrometer made it impossible to do so. That is, attempts to observe low frequency phonons were hampered by the effects of the elastic Bragg peaks centered at the reciprocal lattice points. However, the low temperature lattice properties of a material are strongly dependent on this

low frequency portion of the dispersion curves. Therefore, in order to be able to make a meaningful calculation of the low temperature specific heat and Debye temperature, it was necessary to determine the slopes of the dispersion curves in the limit $\underline{q} \to 0$. In the limit $\underline{q} \to 0$ the slope of an acoustic branch of a dispersion curve is proportional to the corresponding velocity of sound. The mathematical statement of the linearity of the $\nu_j(\underline{q})$ relations for small q is

$$\nu_j = v_j q/2\pi \quad . \tag{6.2}$$

In Eq. (6.2) the quantity v_j is the velocity associated with a phonon of frequency $\nu_j(\underline{q})$ and polarization index j. If Eq. (6.2) is written in terms of the dimensionless variable ζ (which was defined in Eq. (4.10)) the equation becomes, for $\underline{q}$ in the [1 1 0] direction

$$\nu_j(\zeta) = \frac{\sqrt{2}\, v_j}{a_0} \quad . \tag{6.3}$$

The above equation was used to calculate $\nu_j(\zeta = 0.005)$ for the three polarizations. These three values of $\nu_j(\zeta)$ were then used as input data for the non-linear least-squares computer program of Section IV.

One final use was made of the velocities of sound. As stated previously one of the objectives of this thesis was to test the effectiveness of simple, easily obtained force constant models in predicting lattice dynamical properties. A common experiment for which a large quantity of results exist in the literature is the measurement of the velocities of sound. It was decided to devise a force constant model for YZn based entirely on the measured velocities of sound.

Since the velocities of sound experiment yields three independent velocities, the force constant model derived from these velocities could have no more than three parameters. For the CsCl structure a general first neighbor model contains two interatomic force constants; a general second neighbor model contains six. Therefore, the model that was chosen to describe YZn was a first neighbor model. This model will be referred to as the elastic constant model.

The two force constants that are involved in a first neighbor model were found by first linearizing the three acoustic $\nu_j(\zeta)$ relations for the [1 1 0] direction (see Appendix F) in the limit $\zeta \to 0$, and then linearly least-squares fitting these three expressions to find the two force constants. The linear least-squares fitting was done because the two force constants were over-determined by the three velocities of sound. If the linearized expressions in Appendix F are simplified to include only the first neighbor force constants the expressions become

$$\frac{\nu_1^2}{\zeta^2}(M_0 + M_1) = 4(\alpha_1^1 + B_1^1)$$

$$\frac{\nu_1^2}{\zeta^2}(M_0 + M_1) = 4\alpha^1$$

$$\frac{\nu_2^2}{\zeta^2}(M_0 + M_1) = 4\alpha_1^1 - 4\beta_1^1 \quad . \tag{6.4}$$

But from Eq. (6.3)

$$\frac{\nu_j^2}{\zeta^2} = \frac{2v_j^2}{a_0^2} \quad . \tag{6.5}$$

Therefore, the three equations become

$$\frac{v_L^2}{2a_o^2}(M_0 + M_1) = \alpha_1^1 + \beta_1^1$$

$$\frac{v_1^2}{2a_o^2}(M_0 + M_1) = \alpha_1^1$$

$$\frac{v_2^2}{2a_o^2}(M_0 + M_1) = \alpha_1^1 - \beta_1^1 \quad . \tag{6.6}$$

The best-fit values of the two parameters were found to be $\alpha_1^1 = 8075$, $\beta_1^1 = 3980$.

In the next section a number of lattice properties that were calculated on the basis of the elastic constant model will be discussed and compared with experiments and similar calculations for the fifth and sixth neighbor models.

VII. CALCULATIONS AND SUMMARY

In the previous sections the theory and experiments concerning some lattice properties of YZn have been described. Here, the results of a series of calculations of additional properties will be presented.

1. Phonon dispersion curves

Two distinct force constant models have been used to calculate the phonon dispersion curves of YZn. They were the sixth neighbor and the elastic constant models. The sixth neighbor model was explained in Section IV and the dispersion curves appropriate to that model are shown in Figs. 9 - 12. In Section VI the elastic constant model was derived and it was stated that a number of lattice properties were calculated on the basis of this model. The first of these properties that will be discussed are the phonon dispersion curves. In Fig. 18 are shown the dispersion curves that were calculated from the elastic constant model. A comparison of the experimentally determined dispersion curves with those of the elastic constant model suggests the following conclusions. The qualitative aspects of the dispersion curves are reproduced quite well by the simple model. However, for frequencies greater than 1.5 THZ the quantitative agreement is not very good. In particular, the optical branches predicted by the model are quite different from those that were found experimentally. A consequence of the simplicity of the elastic constant model is that it introduces degeneracies into the dispersion curves. An example of this degeneracy is the fact that the longitudinal and transverse branches of the dispersion curves for the [0 0 ζ] direction are degenerate for this model.

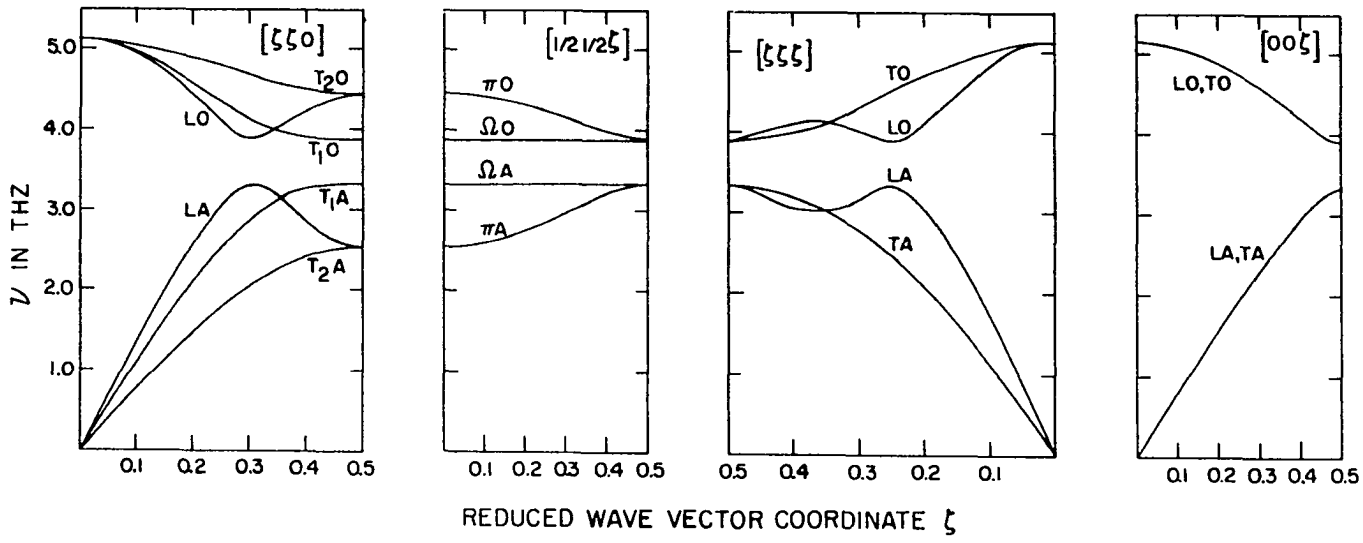

Fig. 18. Dispersion curves calculated from the elastic constant model

2. Frequency distribution function

The frequency distribution function $g(\nu)$ was calculated with the use of the extrapolation method that was originated by Raubenheimer and Gilat (45, 46). This method involves the diagonalization of the dynamical matrix on an evenly spaced mesh of points in the irreducible section of the Brillouin Zone. The eigenfrequencies for any point inside the cube surrounding a mesh point are found by linear extrapolation. For a particular cube, the number of phonons having a frequency between ν and $\nu + \delta\nu$ is found by calculating the volume between the two corresponding constant frequency planes. The frequency distribution for the solid is obtained by summing the contributions from all the cubes in the irreducible zone. In order to use the computer program of Raubenheimer and Gilat it was necessary to modify it to include sixth neighbor interactions.

In Fig. 19 is shown the frequency distribution function that was calculated at 5167 points in the irreducible zone of YZn using the twenty four force constant model described in Section IV.

All of the Van Hove singularities (47) that were expected from the measured dispersion curves appear in $g(\nu)$ and are listed below.

a. Zone boundary $T_2A(0.5, 0.5, 0)$

b. T_2A branch at $\zeta \approx 0.36$

c. T_1A branch at $\zeta \approx 0.31$

d. $LA(\zeta\ \zeta\ \zeta)$ branch at $\zeta \approx 0.31$

e. $LA(\zeta\ \zeta\ \zeta)$ branch at $\zeta \approx 0.19$

f. Zone boundary TA(0,0,0.5)

g. Zone boundary $T_1O[0.5,0.5,0]$

h. $LO[\zeta\ \zeta\ 0]$ branch at $\zeta \approx 0.24$

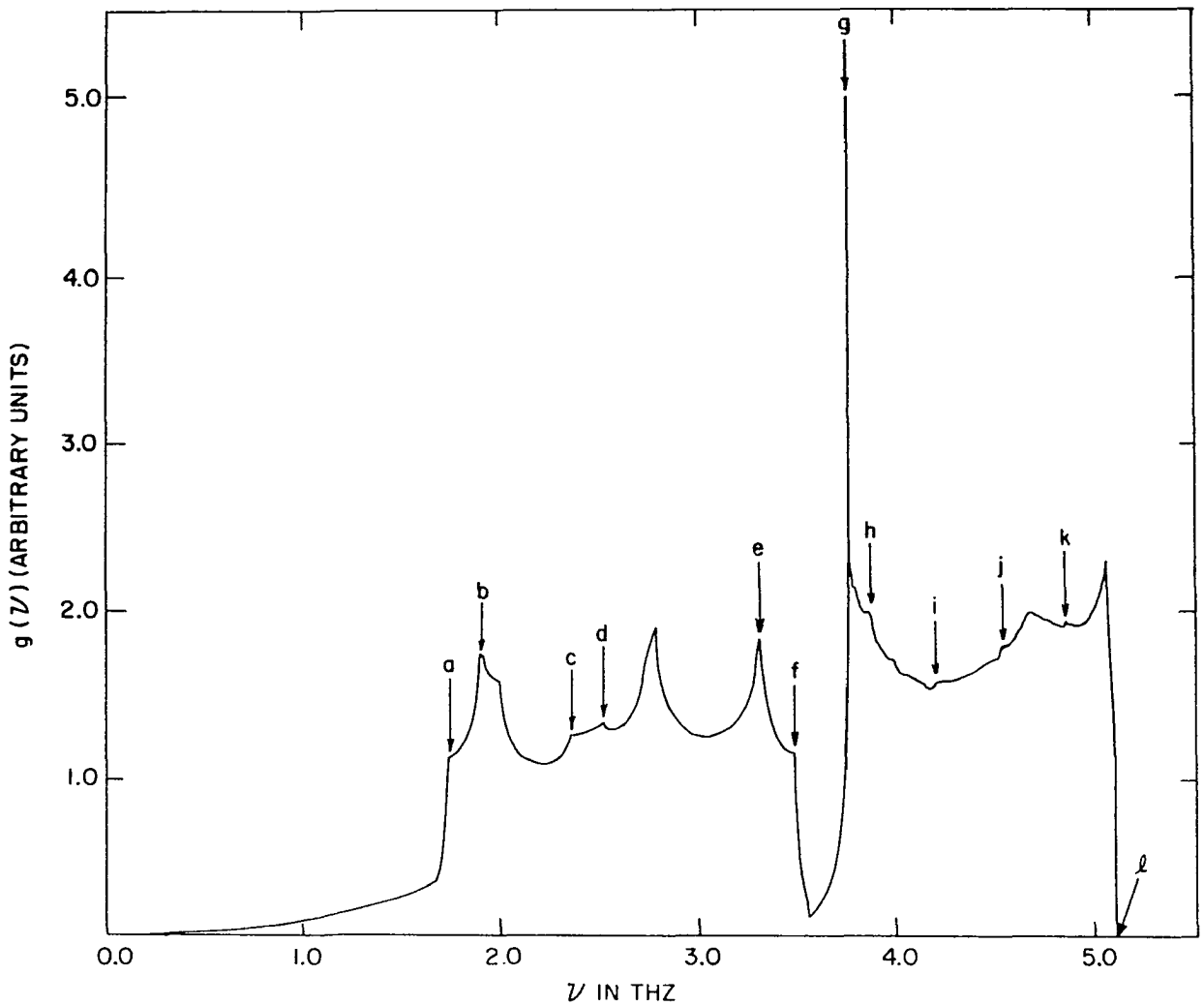

Fig. 19. Frequency distribution function calculated from the sixth neighbor model

i. Zone boundary LO[0, 0, 0.5]

j. Origin

k. Zone boundary LO, TO[0.5, 0.5, 0.5]

l. Zone boundary LO, T_2O[0.5, 0.5, 0]

Fig. 20 shows a plot of $g(\nu)$ for the first neighbor elastic constant model that was described in the previous section. The primary reason for presenting this figure is to contrast it with Fig. 19. However, as will presently be shown, these very different $g(\nu)$ functions predict very similar specific heat curves. The Van Hove singularities for the first neighbor model are also identified below.

a. Zone boundary LA, T_2A[0.5, 0.5, 0]

b. LA branch [ζ ζ 0] $\zeta \approx 0.37$

c. Zone boundary, all acoustic modes

d. Zone boundary, all

e. LO[ζ ζ ζ] $\zeta \approx 0.37$

f. Zone boundary LO, T_2O[.5, .5, 0]

g. Origin

3. Specific heat

The specific heat at constant volume was calculated from the expression

$$C_v(T) = 6Nk \int_0^\infty \frac{\left(\frac{h\nu}{kT}\right)^2 e^{h\nu/kT} g(\nu)\,d\nu}{\left(e^{\frac{h\nu}{kT}} - 1\right)^2} \qquad (7.1)$$

Fig. 21 shows a plot of $C_v(T)$ for both the elastic constant and sixth neighbor models. The similarity of the two $C_v(T)$ curves that were obtained

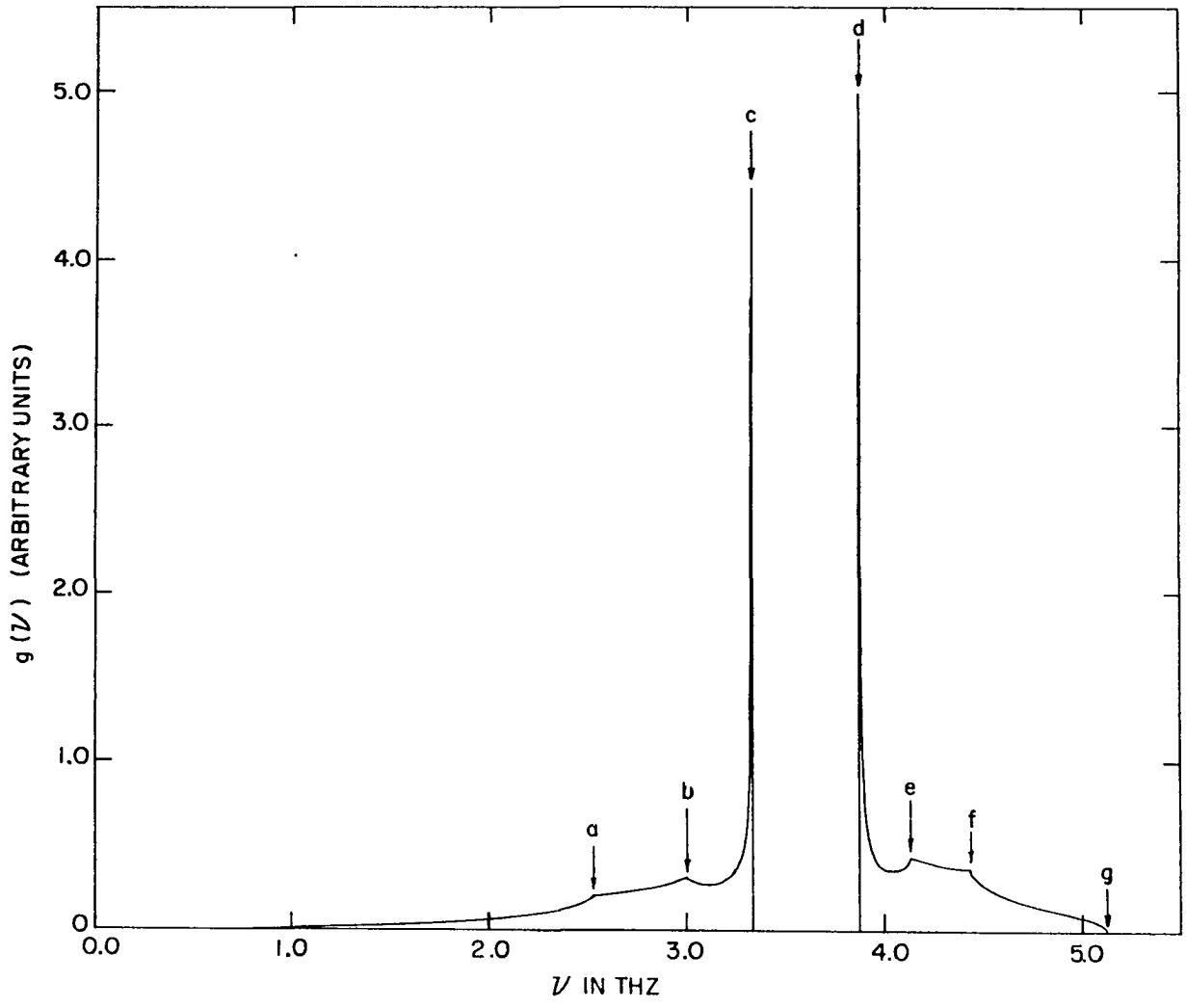

Fig. 20. Frequency distribution function calculated from the elastic constant model

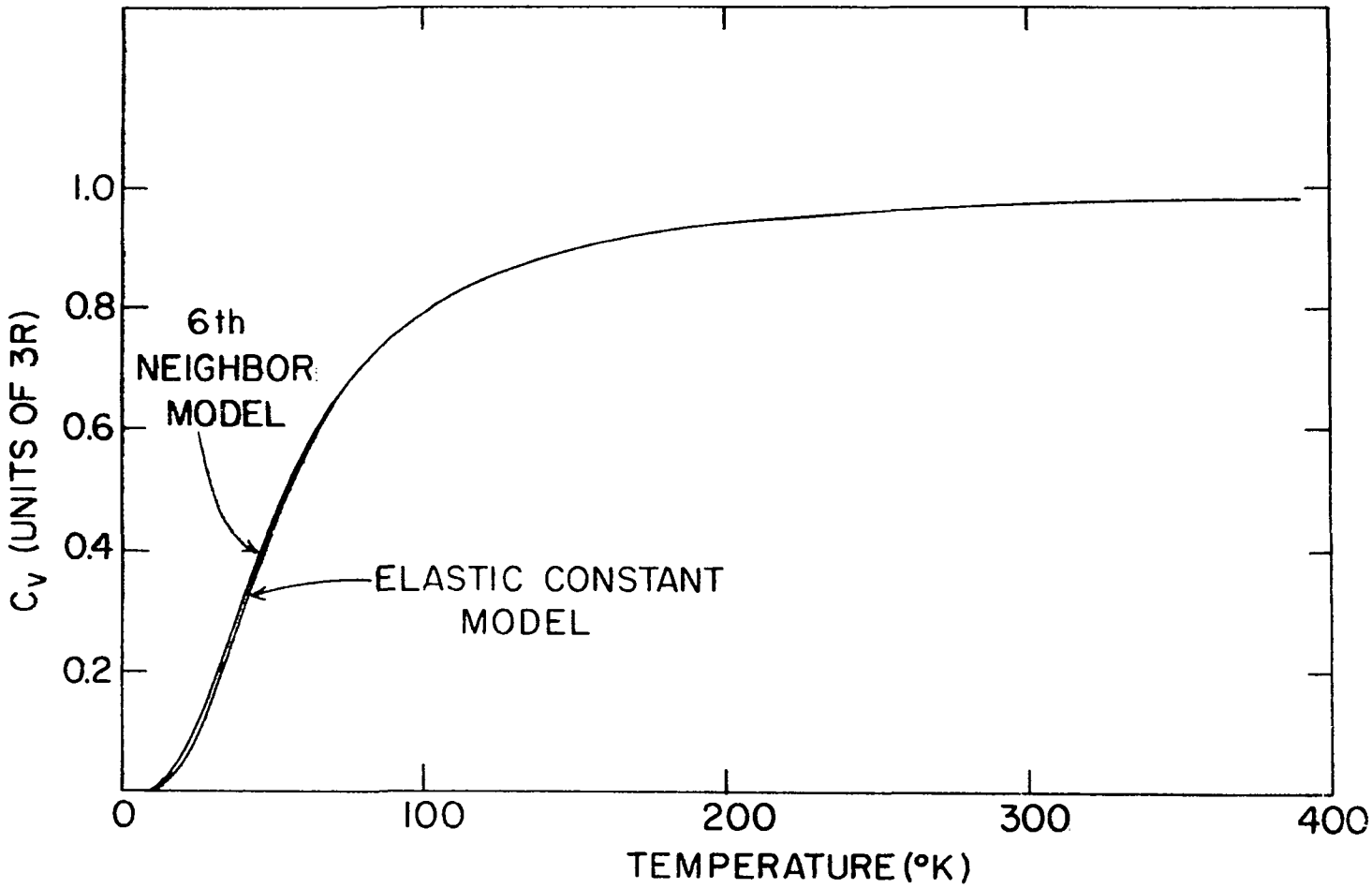

Fig. 21. Lattice specific heat calculated from the sixth neighbor and the elastic constant models

from the very different $g(\nu)$ functions provides an indication of the insensitivity of $C_v(T)$ to the $g(\nu)$ that is used.

3. Debye temperature

The Debye temperatures that were calculated on the basis of the elastic constant and sixth neighbor models are shown plotted in Fig. 22. The calculation of the Debye temperatures involved the use of a computer program (24) that fitted the calculated specific heat of Eq. (7.1) to the function

$$C_v = 6Nk \left(\frac{T}{\theta_D}\right)^3 \int_0^{\frac{\theta_D}{T}} \frac{x^4 e^x}{(e^x - 1)^2} dx \qquad (7.2)$$

At 0°K the calculated Debye temperatures for the first and sixth neighbor models were, respectively, 273.0 and 290.6 °K. It may be recalled that the value of $\theta_D(0°K)$ that was calculated from the velocities of sound was 291.1°K.

An interesting feature of Fig. 22 is that, although the low temperature behavior of $\theta_D(T)$ is quite different for the two models, for temperatures greater than 100°K, $\theta_D(T)$ is essentially the same for both. A temperature of 100°K corresponds to a frequency of only 2.08×10^{12} Hz which is well below the large peaks in the $g(\nu)$ functions.

4. Mean square displacements

In Section V, mention was made of the calculated values of the mean square displacements of the Y and Zn atoms. A feature of the mean square displacement calculation that was not mentioned in Section V was that it was possible to separate the mean square displacement of an atom into its

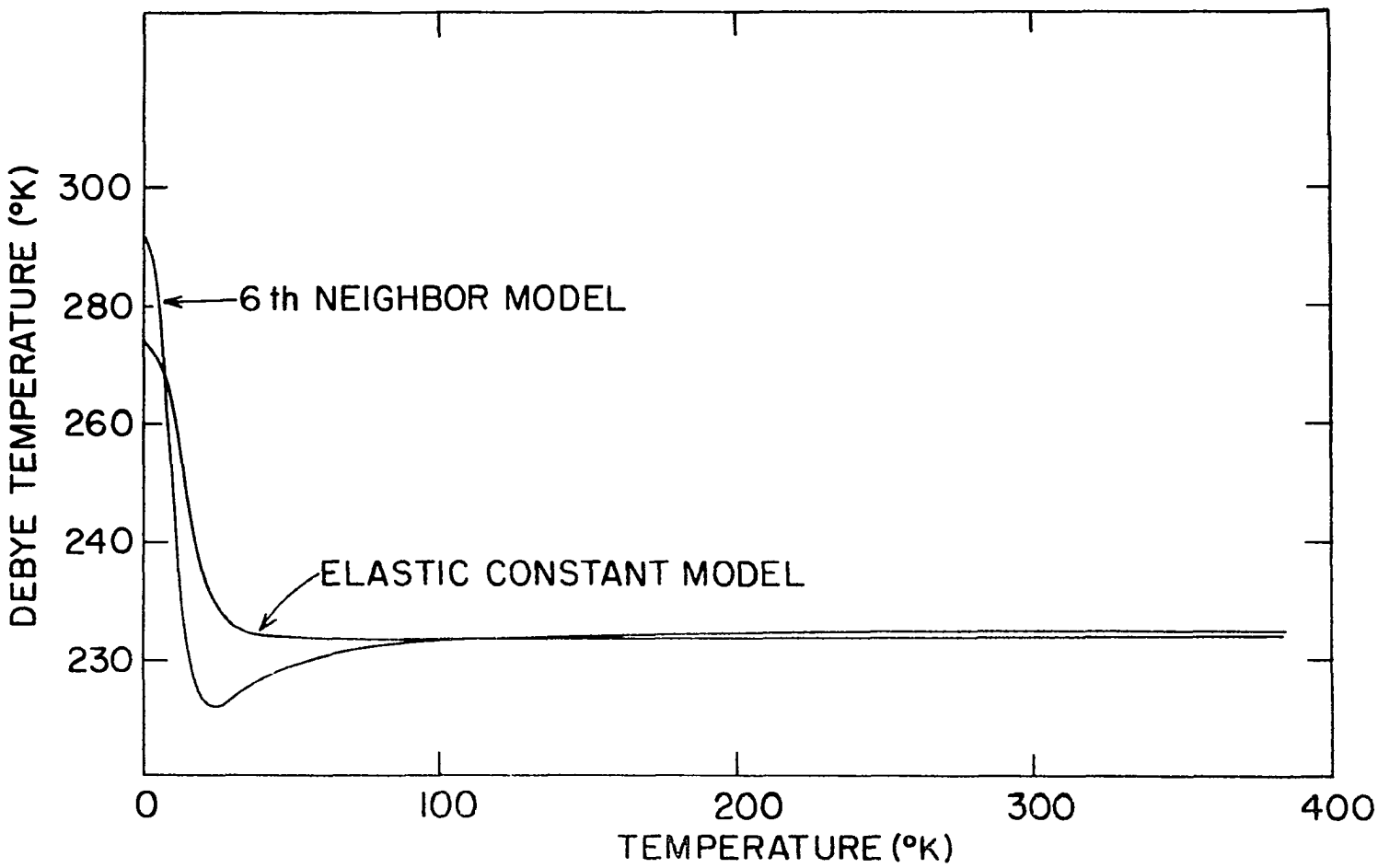

Fig. 22. Debye temperatures calculated from the sixth neighbor and the elastic constant models

acoustic and optic contributions. That is, since the mean square displacements are caused by both acoustic and optic phonons, it is possible to perform this sum for each type of phonon individually. In the case of the elastic constant model there is a definite gap between the acoustic and optic branches of the dispersion curves. This can easily be seen by an inspection of Fig. 19. For the sixth neighbor model, however, there is no gap between the acoustic and optic branches but rather $g(\nu)$ becomes very small at about $\nu = 3.55 \times 10^{12}$ Hz. The lack of a gap for the sixth neighbor model has the effect of introducing a small error into the calculation of the relative magnitudes of the acoustic and optic contributions to $\langle u^2 \rangle$. However, the sum of the two contributions is independent of the absence of a gap.

A series of calculations of the mean square displacements of Y and Zn were made with the use of the sixth neighbor model. The calculations were performed for different numbers of points in the irreducible zone. Table 7 contains the results of these calculations.

Table 7. Mean square displacements of Y and Zn in units of 10^{-18} cm^2 in the (0 0 1) direction using the sixth neighbor model

# of points in reduced zone	$\langle u^2 \rangle_{Y\ ACOUSTIC}$	$\langle u^2 \rangle_{Y\ OPTIC}$	$\langle u^2 \rangle_{Y\ TOTAL}$
35	0.603	0.062	0.665
84	0.696	0.070	0.767
220	0.781	0.078	0.859
680	0.857	0.085	0.942
1540	0.899	0.089	0.988
2925	0.925	0.092	1.017
4960	0.944	0.093	1.037
	$\langle u^2 \rangle_{Zn\ ACOUSTIC}$	$\langle u^2 \rangle_{Zn\ OPTIC}$	$\langle u^2 \rangle_{Zn\ TOTAL}$
35	0.403	0.241	0.644
84	0.467	0.276	0.743
220	0.524	0.307	0.832
680	0.577	0.335	0.913
1540	0.606	0.351	0.957
2925	0.624	0.361	0.985
4960	0.636	0.367	1.004

Two features of this table seem to be significant. First, the relative magnitudes of the acoustic and optic contributions to the mean square displacement are quite different for Y and Zn. While (to the author's knowledge) there is no basis for predicting these quantities, it does seem reasonable that

$$\langle u_Y^2 \rangle_{OPTIC} < \langle u_{Zn}^2 \rangle_{OPTIC} \tag{7.3}$$

from a consideration of atomic masses. Second, the rate of convergence of the calculated displacements was rather slow. This fact seems to add doubt as to the validity of the Debye-Waller Factor calculations of Buyers and Smith (38). In their paper, Buyers and Smith attempted to calculate the mean square displacements of Na and Cl for only 1000 points in the entire Brillouin Zone. Using 1000 points for the entire Brillouin Zone in the case of the CsCl structure would result in only about twenty points in the irreducible zone. As can be seen from Table 7 this would have resulted in mean square displacements that were much too small.

Mean square displacements were also calculated using the elastic constant model. For a mesh of 4960 points in the reduced zone the results were (in units of 10^{-18} cm^2)

$\langle u_Y^2 \rangle_{ACOUSTIC} = 0.837$ $\qquad$ $\langle u_{Zn}^2 \rangle_{ACOUSTIC} = 0.539$

$\langle u_Y^2 \rangle_{OPTIC} = 0.091$ $\qquad$ $\langle u_{Zn}^2 \rangle_{OPTIC} = 0.393$

$\langle u_Y^2 \rangle_{TOTAL} = 0.928$ $\qquad$ $\langle u_{Zn}^2 \rangle_{TOTAL} = 0.932$

It is interesting that the same qualitative behavior of the acoustic and optic components is exhibited even by this simple model, although the magnitudes of the displacements are about 10% smaller than were found with the sixth neighbor model. The same slow convergence of the displacements with respect to mesh size was also observed for this simple model.

5. Elastic constants

Although the elastic constants of YZn were measured as described in Section VI, an attempt was also made to calculate them using a sixth neighbor model. The force constants for this model were obtained from the non-linear least-squares fitting program of Section IV. Input data for the program consisted of the 108 phonon frequencies and wave vectors listed in Table 3. The variance ratio for this set of data was 2.22. In order to express the elastic constants in terms of the force constants it was necessary to solve Eqs. (6.1) and (E. 9, 10, 11) for the elastic constants. The results were

$$C_{11} = \frac{1}{2a_0}\{4\alpha^1_1 + \alpha^2_{10} + \alpha^2_{11} + 2\alpha^2_{20} + 2\alpha^2_{21} + 8\alpha^3_{10} + 8\alpha^3_{11} + 4\alpha^3_{30} + 4\alpha^3_{31}$$

$$+ 22\alpha^4_1 + 44\alpha^4_2 + 12\alpha^5_{10} + 12\alpha^5_{11} + 4\alpha^6_{10} + 4\alpha^6_{11} + 8\alpha^6_{20} + 8\alpha^6_{21}\}$$

$$C_{12} = \frac{1}{a_0}\{-2\alpha^1_1 + 4\beta^1_1 - \alpha^2_{20} - \alpha^2_{21} - 2\alpha^3_{10} - 2\alpha^3_{11} - 2\alpha^3_{30} - 2\alpha^3_{31} + 4\beta^3_{30}$$

$$+ 4\beta^3_{31} - 2\alpha^4_1 - 20\alpha^4_2 + 4\beta^4_1 + 24\beta^4_2 - 4\alpha^5_{10} - 4\alpha^5_{11} + 8\beta^5_{10}$$

$$+ 8\beta^5_{11} - 4\alpha^6_{20} - 4\alpha^6_{21}\}$$

$$C_{44} = \frac{1}{2a_0}\{4\alpha^1_1 + 4\beta^1_1 + \alpha^2_{10} + \alpha^2_{11} + \alpha^2_{20} + \alpha^2_{21} + 6\alpha^3_{10} + 6\alpha^3_{11} + 2\alpha^3_{30}$$

$$+ 2\alpha^3_{31} + 4\beta^3_{30} + 4\beta^3_{31} + 20\alpha^4_1 + 24\alpha^4_2 + 4\beta^4_1 + 24\beta^4_2 + 8\alpha^5_{10}$$

$$+ 8\alpha^5_{11} + 8\beta^5_{10} + 8\beta^1_{11} + 4\alpha^6_{10} + 4\alpha^6_{11} + 4\alpha^6_{20} + 4\alpha^6_{21}\} \qquad (7.4)$$

Upon substituting the force constants and evaluating these expressions the elastic constants were found to be (in units of 10^{11} dy/cm):

$$C_{11} = 9.831$$

$$C_{12} = 4.255$$

$$C_{44} = 4.665$$

This is to be compared with the measured values of $C_{11} = 9.154$, $C_{12} = 4.378$ and $C_{44} = 4.658$. It is felt that the calculated and measured values of the elastic constants are in fairly good agreement considering that no phonons were measured below $\nu = 1.0 \times 10^{12}$ Hz.

6. Restoring force

In the previous sections, three force constant models have been considered. They were the elastic constant, fifth neighbor and sixth neighbor models. These three models were found to have a common characteristic that was thought to be of some interest and so will be discussed here. This characteristic follows from a consideration of the restoring force experienced by an atom when it is displaced from its equilibrium position. From Eq. (3.11) the general expression for the force on the S-th atom in the

ℓ-th unit cell is

$$F^{\ell}_{s\alpha} = -\sum_{\ell',s',\beta} \phi_{\alpha\beta}(\ell\ell',ss')u_{\beta}(\ell',s') \tag{7.5}$$

The restoring force on the (ℓ,s) atom that results from its displacement a distance $\underline{t}$ is the same as the force the atom experiences when the surrounding lattice is displaced by $-\underline{t}$. Of course, within the framework of a given force constant model, the lattice surrounding an atom is represented by only those neighboring atoms that are treated in the model. Therefore the force on the (ℓ,s) atom due to a displacement $\hat{x}$ is

$$F^{\ell}_{sx} = \sum_{\ell',s',\beta} \phi_{\alpha\beta}(\ell\ell',ss')(1 - \delta_{ss'}\delta_{\ell\ell'}) \tag{7.6}$$

For a sixth neighbor model the force is

$$F^{\ell}_{sx} = 2\{4(\alpha^1_1 + \alpha^4_1 + 2\alpha^4_2) + (\alpha^2_{1\sigma} + 2\alpha^2_{2\sigma}) + 2(2\alpha^3_{1\sigma} + \alpha^3_{3\sigma}) + 4\alpha^5_{1\sigma} + (\alpha^6_{1\sigma} + 2\alpha^6_{2\sigma}) \tag{7.7}$$

The index s has been replaced by σ in Eq. (7.7) to be consistent with the force constant notation of Appendix A. As before, $\sigma = 0; 1$ corresponds to an Y or Zn atom, respectively.

The calculated values of F_{0x} and F_{1x} for the three force constant models are listed in Table 8.

Table 8. F_{0x} and F_{1x} for three force constant models

	Elastic Constant Model	Fifth Neighbor Model	Sixth Neighbor Model
F_{0x}	64,600	61,208	61,558
F_{1x}	64,600	67,408	67,788
$(F_{0x} + F_{1x})$	129,200	128,616	129,346

There are several interesting features of this table. First F_{0x} and F_{1x} have very similar respective values for both the fifth and sixth neighbor models. This fact is particularly remarkable in view of the rather different values of the individual force constants appropriate to the two models. That is, even though the individual interatomic force constants are very different for the fifth and sixth neighbor models (Table 5) the particular linear combination of interatomic force constants of Eq. (7.6) is essentially constant.

The fact that $F_{0x} = F_{1x}$ for the elastic constant model is a consequence of the simplicity of the model which requires the forces on each atom to be the same.

The relative values of F_{0x} and F_{1x} are consistent with the mean square displacement calculations. For the elastic constant model $F_{0x} = F_{1x}$ and the mean square displacements were also essentially the same. For the sixth neighbor model $F_{0x} < F_{1x}$ and, consistent with this fact, it was shown earlier in this section that $\langle u_Y^2 \rangle > \langle u_{Z_n}^2 \rangle$.

Perhaps the most unexpected result of these calculations was the fact that $(F_{0x} + F_{1x})$ was quite constant for the three models. A theoretical reason for this result was sought for but was not found.

One additional observation concerning force constants may be made from a consideration of Eq. (7.7). It is possible, from Eq. (7.7) to make a quantitative estimate of the importance of the first neighbor interactions in determining the force on an atom. For example, in the sixth neighbor model, the contribution of the first neighbor term to F_{0x} is approximately 80% of the total. The contribution of the first neighbor term to F_{1x} is approximately 73%. Therefore it would seem that even though some of the force constants associated with distant neighbors are quite large (eg. α^6_{10} = 5538 dyne/cm) the linear combinations of Eq. (7.7) are dominated by the first neighbor interaction.

7. Summary

A review of the results of the experiments that were performed on YZn suggests the following conclusions. The neutron diffraction and velocities of sound experiments indicated that a sixth neighbor model employing twenty-four force constants was needed to satisfactorily describe the phonon dispersion curves. However, the large magnitude of the sixth neighbor force constants coupled with a Fourier analysis of the sums of the squares of the phonon frequencies along symmetry directions indicated even longer range forces were present. It was thought that these long-range forces that were needed within the framework of the Born von Karman theory, might indicate that YZn was a superconductor. The experiment chosen to test this hypothesis was a measurement of the differential magnetic suscep-

tibility as a function of temperature. This experiment demonstrated that there was no evidence of a superconducting transition in tests to temperatures as low as 1.2°K.

In the Born von Karman theory derivation of the $\nu_j(\underline{q})$ expressions it was assumed that the sample was perfectly ordered in the CsCl structure. This assumption was verified by a measurement of the long-range order parameter S by means of an x-ray diffraction experiment. In addition, this experiment provided an approximate value for the sum of the Debye-Waller parameters of Y and Zn.

The question of the efficaciousness of the elastic constant model in describing the lattice properties of YZn has been considered and has led to the following conclusions. The lattice specific heat is described very well and $\theta_D(T)$ and the mean square displacements fairly well by this simple model. Qualitative features of the dispersion curves are contained in this model but quantitative features, especially for the optical branches are in some disagreement with the experiment. However, it will be recalled that this model is based only on the three measured velocities of sound, that is the two parameters α_1^1 and β_1^1 were fit to a linearized version of a general first neighbor model. In light of the crudeness of the model it seems to do a rather good job of predicting lattice properties.

Finally, an expression for the restoring force on an atom that is displaced from equilibrium was derived. This expression indicated that even for a general sixth neighbor force constant model the first neighbor interactions accounted for approximately 75% of the calculated restoring force.

VIII. LITERATURE CITED

1. G. Dolling and A.D.B. Woods, in Thermal Neutron Scattering, edited by P.A. Egelstaff (Academic Press, New York, 1965). p. 201.

2. G. Gilat and G. Dolling, Phys. Rev. 138, A1053 (1965).

3. T.S. Prevender, U.S. Atomic Energy Commission Rept. IS-2185, Iowa State University, Ames, Iowa Institute for Atomic Research (1969).

4. J.L. Warren, Rev. Mod. Phys. 40, 38 (1968).

5. N.F.M. Henry and K. Lonsdale, International Tables for X-ray Crystallography, Vol. 1. (Kynoch Press, Birmingham, England, 1952).

6. D.J. Hughes and R.B. Schwartz, Neutron Cross Sections, 2nd Ed. BNL-325 (U.S. Gov. Printing Office, Washington, 1958).

7. P. Chiotti, J.T. Mason and K.J. Gill, Trans. Met. Soc. AIME, 221, 573 (1961).

8. M. Born and K. Huang, Dynamical Theory of Crystal Lattices (Oxford University Press, Oxford, England, 1954).

9. A.A. Maradudin, E.W. Montroll and G.H. Weiss, Theory of Lattice Dynamics in the Harmonic Approximation (Academic Press, New York, 1963).

10. J.M. Ziman, Electrons and Phonons, (Oxford University Press, Oxford, England, 1960).

11. A.A. Maradudin and S.H. Vosko, Rev. Mod. Phys. 40, 1 (1968).

12. L. Van Hove, Phys. Rev. 95, 249 (1954).

13. W.M. Lomer and G.G. Low, in Thermal Neutron Scattering, edited by P.A. Egelstaff (Academic Press, New York, 1965), p. 1.

14. B.N. Brockhouse, in Phonons in Perfect Lattices and in Lattices with Point Imperfections, edited by R.W.H. Stevenson (Plenum Press, New York, 1966).

15. A.A. Maradudin and A.E. Fein, Phys. Rev. 128, 2589 (1962).

16. R.A. Cowley, Advanc. Phys. 12, 421 (1963).

17. S.K. Sinha, T.O. Brun, L.D. Muhlestein and J Sakurai, Phys. Rev. (To be published).

18. N. Wakabayashi, Lattice Dynamics of Scandium. Unpublished Ph.D. thesis. Ames, Iowa, Library, Iowa State University of Science and Technology. (1969).

19. B.N. Brockhouse, Bull. Amer. Phys. Soc. II, 5, 462 (1960).

20. M.J. Cooper and R. Nathans, Acta Cryst. 23, 357 (1967).

21. T.S. Prevender, U.S. Atomic Energy Commission Rept. IS-2186, Iowa State University, Ames, Iowa Institute for Atomic Research (1969).

22. M.F. Collins, Brit. J. Appl. Phys. 14, 805 (1963).

23. G. Peckham, U.K. Atomic Energy Authority Research Group Rept. AERE-R4380, Atomic Energy Research Establishment, Harwell, Berkshire, England. (1964).

24. T.O. Brun and S.K. Sinha, unpublished computer program. Ames, Iowa, Ames Laboratory Solid State Physics Group XV, Iowa State University of Science and Technology. (1969).

25. A.J.E. Foreman and W.M. Lomer, Proc. Phys. Soc. B70, 1143 (1957).

26. J.K. Boyter and H.L. McMurry, U.S. Atomic Energy Commission Research and Development Rept. IN-1148, Idaho Nuclear Corporation, Idaho Falls, Idaho. (1967).

27. G.L. Squires, in Inelastic Scattering of Neutrons in Solids and Liquids, (International Atomic Energy Agency, Vienna, 1963), Vol. II, p. 125.

28. W. Cochran, in Phonons in Perfect Lattices and in Lattices with Point Imperfections, edited by R.W.H. Stevenson (Plenum Press, New York, 1966).

29. R.W. James, The Optical Principles of the Diffraction of X-Rays (Cornell University Press, Ithaca, New York, 1962).

30. W.M. Lomer, Proc. Phys. Soc. 89, 135 (1966).

31. J.E. Eldridge and W.M. Lomer, Proc. Phys. Soc. 91, 459 (1967).

32. W.J.L. Buyers and T. Smith, Phys. Rev. 150, 758 (1966).

33. B.D. Cullity, Elements of X-Ray Diffraction (Addison-Wesley Publishing Company, Inc., Reading, Mass., 1956).

34. K. Lonsdale, Acta Cryst. 1, 142 (1948).

35. D.T. Cromer and J.T. Waber, Acta Cryst. 18, 104 (1965).

36. D.T. Cromer, Acta Cryst. 18, 17 (1965).

37. K.D. Rouse and M.J. Cooper, U.K. Atomic Energy Authority Research Group rept. AERE-R5725, Atomic Energy Research Establishment, Harwell, Berkshire, England. (1968).

38. W.J.L. Buyers and T. Smith, Phys. Chem. Solids 25, 483 (1964).

39. N. Nilsson, Arkiv för Fysik 12, 247 (1957).

40. H.J. McSkimin, J. Acoust. Soc. Am. 33, 12 (1961).

41. H.J. McSkimin and P. Andreatch, J. Acoust. Soc. Am. 34, 609 (1962).

42. H.J. McSkimin, J. Acoust. Soc. Am. 37, 864 (1965).

43. C. Kittel, Introduction to Solid State Physics (John Wiley and Sons, New York, 1966).

44. W.C. Overton and A.F. Schuch, U.S. Atomic Energy Commission Rept. LA-3615-MS, Los Alamos Scientific Laboratory, Los Alamos, New Mexico. (1966).

45. G. Gilat and L.J. Raubenheimer, Phys. Rev. 144, 390 (1966).

46. L.J. Raubenheimer and G. Gilat, U.S. Atomic Energy Commission Rept. ORNL-TM-1425, Oak Ridge National Laboratory, Oak Ridge, Tennessee. (1966).

47. L. Van Hove, Phys. Rev. 89, 1189 (1952).

IX. ACKNOWLEDGMENTS

I would like to thank my major professor, Dr. J.F. Smith, for initially suggesting the general topic of this thesis and for his continued interest. I particularly wish to thank Drs. S.K. Sinha and N. Wakabayashi for their invaluable assistance and many helpful discussions concerning the experimental and theoretical aspects of neutron diffraction. I am indebted to Messrs. J. Crenshaw and T.O. Brun for their cooperation with respect to some of the computer programs that were used in this thesis. I would like to express my gratitude to Messrs. D. Bailey, J. Ostenson and B. Cullen for their assistance with the x-ray diffraction, magnetic susceptibility and velocities of sound experiments respectively.

Last, but by no means least, I would like to thank my wife, not only for typing this thesis, but also for her continued encouragment and understanding during my long years of graduate study.

X. APPENDIX A

In this appendix the force constant matrices relating the force on an origin atom due to the displacement of another atom will be presented. The atoms surrounding the origin may be divided into neighbor sets where the common characteristic of the atoms in the set is their distance from the origin. A particular neighbor set is identified by the index n. An atom in a set is further specified by an index p. For the CsCl structure the origin atom may be one of two possible types and it is labeled by the index σ. In the case of YZn σ = 0; 1 corresponded to a Y or Zn atom respectively at the origin. The notation used here is essentially that of Squires (27) and Gilat and Dolling (2).

The force on an origin atom of type σ due to the displacement of the p-th atom in the n-th neighbor set is given by

$$\underline{F}^{p}_{n\sigma} = \tilde{\phi}^{p}_{n\sigma}\,\underline{u}^{p}_{n\sigma}$$

where the $\tilde{\phi}^{p}_{n\sigma}$ are listed below. The force constant matrices may represent any of three types of interactions; namely, Y-Y, Zn-Zn or Y-Zn. For the case of Y-Zn interactions the index σ will be dropped. The force constant matrices listed below are in their simplest form; i.e., all symmetry operations appropriate to the particular interaction have been utilized to simplify the form of the matrix.

Table 9. Force constant matrices for the CsCl structure

$\underline{R}(\ell,s)$	Neighbor Set #	# Of Atoms In Set	Force Constant Matrix
(1,1,1) $a_o/2$	1	8	$\begin{pmatrix} \alpha^1_1 & \beta^1_1 & \beta^1_1 \\ \beta^1_1 & \alpha^1_1 & \beta^1_1 \\ \beta^1_1 & \beta^1_1 & \alpha^1_1 \end{pmatrix}$
(2,0,0) $a_o/2$	2	6	$\begin{pmatrix} \alpha^2_{1\sigma} & 0 & 0 \\ 0 & \alpha^2_{2\sigma} & 0 \\ 0 & 0 & \alpha^2_{2\sigma} \end{pmatrix}$
(2,2,0) $a_o/2$	3	12	$\begin{pmatrix} \alpha^3_{1\sigma} & \beta^3_{3\sigma} & 0 \\ \beta^3_{3\sigma} & \alpha^3_{1\sigma} & 0 \\ 0 & 0 & \alpha^3_{3\sigma} \end{pmatrix}$
(3,1,1) $a_o/2$	4	24	$\begin{pmatrix} \alpha^4_1 & \beta^4_2 & \beta^4_2 \\ \beta^4_2 & \alpha^4_2 & \beta^4_1 \\ \beta^4_2 & \beta^4_1 & \alpha^4_2 \end{pmatrix}$

Table 9. Continued

$\underline{R}(\ell,s)$	Neighbor Set #	# Of Atoms In Set	Force Constant Matrix
(2,2,2) $a_0/2$	5	8	$\begin{pmatrix} \alpha^5_{1\sigma} & \beta^5_{1\sigma} & \beta^5_{1\sigma} \\ \beta^5_{1\sigma} & \alpha^5_{1\sigma} & \beta^5_{1\sigma} \\ \beta^5_{1\sigma} & \beta^5_{1\sigma} & \alpha^5_{1\sigma} \end{pmatrix}$
(4,0,0) $a_o/2$	6	6	$\begin{pmatrix} \alpha^6_{1\sigma} & 0 & 0 \\ 0 & \alpha^6_{2\sigma} & 0 \\ 0 & 0 & \alpha^6_{2\sigma} \end{pmatrix}$

XI. APPENDIX B

Here the elements of the dynamical matrix are listed. Although there are in general thirty six elements, the fact that $\tilde{D}$ is symmetric reduces this number to twenty one. These twenty one elements can be reduced to the four general types listed below. In the following equations i can equal 1 2 or 3· if i + 1 or i + 2 exceeds 3 it is to be interpreted as i - 2 and i - 1 respectively. The dimensionless variable ζ is defined as

$$\zeta = \frac{q}{q_{MAX}}$$

$$D_{ii}^{\sigma\sigma} = \frac{1}{M\sigma}\{8(\alpha_1^1 + \alpha_1^4 + 2\alpha_2^4) + 2\sigma_{1\sigma}^2(1 - \cos 2\pi\zeta_i) + 2\alpha_{2\sigma}^2(2 - \cos 2\pi\zeta_{i+1} - \cos 2\pi\zeta_{i+2}) + 4\alpha_{1\sigma}^3[2 - \cos 2\pi\zeta_i(\cos 2\pi\zeta_{i+1} + \cos 2\pi\zeta_{i+2})] + 4\alpha_{3\sigma}^3(1 - \cos 2\pi\zeta_{i+1}\cos 2\pi\zeta_{i+2}) + 8\alpha_{1\sigma}^5(1 - \cos 2\pi\zeta_i \cos 2\pi\zeta_{i+1}\cos 2\pi\zeta_{i+2}) + 2\alpha_{1\sigma}^6(1 - \cos 4\pi\zeta_i) + 2\alpha_{2\sigma}^6(2 - \cos 4\pi\zeta_{i+1} - \cos 4\pi\zeta_{i+2})\}$$

$$D_{ii+1}^{\sigma\sigma} = \frac{1}{M\sigma}\{4\beta_{3\sigma}^3 \sin 2\pi\zeta_i \sin 2\pi\zeta_{i+1} + 8\beta_{1\sigma}^5 \sin 2\pi\zeta_i \sin 2\pi\zeta_{i+1}\cos 2\pi\zeta_{i+2}\}$$

$$D_{ii}^{\sigma\sigma'} = -\frac{8}{\sqrt{M_0 M_1}}\{\alpha_1^1 \cos\pi\zeta_i \cos\pi\zeta_{i+1}\cos\pi\zeta_{i+2} + \alpha_1^4 \cos 3\pi\zeta_i \cos\pi\zeta_{i+1}\cos\pi\zeta_{i+2} + \alpha_2^4 \cos\pi\zeta_i(\cos 3\pi\zeta_{i+1}\cos\pi\zeta_{i+2} + \cos\pi\zeta_{i+1}\cos 3\pi\zeta_{i+2})\}$$

$$D^{\sigma\sigma'}_{i\,i+1} = \frac{8}{\sqrt{M_0 M_1}}\{\beta^1_1 \sin \pi\zeta_i \sin \pi\zeta_{i+1} \cos \pi\zeta_{i+2} + \beta^4_1 \sin \pi\zeta_i$$

$$\sin \pi\zeta_{i+1} \cos 3\pi\zeta_{i+2} + \beta^4_2(\sin 3\pi\zeta_i \sin \pi\zeta_{i+1} \cos \pi\zeta_{i+2}$$

$$+ \sin \pi\zeta_i \sin 3\pi\zeta_{i+1} \cos \pi\zeta_{i+2})\}$$

XII. APPENDIX C

The following is a list of $\omega_j^2(\underline{q})$ for a sixth neighbor model with $\underline{q}$ along the symmetry directions [0 0 ζ], [ζ ζ ζ], [ζ ζ 0] and $[\frac{1}{2}\ \frac{1}{2}\ \zeta]$. For all but the ΛA and ΛO modes which are listed last $\omega_j^2(\underline{q})$ is given by

$$M_0 M_1 \omega_j^2 = M_0 A_1 + M_1 A_0 \pm \{[M_0 A_1 - M_1 A_0]^2 + 4M_0 M_1 A_\sigma^2\}^{\frac{1}{2}}$$

Values of A_0 and A_σ for the various branches of the dispersion curves are listed below.

A. $\underline{q} = [0\ 0\ \zeta]\frac{2\pi}{a_0}$

1. LA, LO modes

a. $A_\sigma = 4(\alpha_1^1 + \alpha_1^4 + 2\alpha_2^4) + (\alpha_{1\sigma}^2 + 4\alpha_{1\sigma}^3 + 4\alpha_{1\sigma}^5)(1 - \cos 2\pi\zeta)$

$+ \alpha_{1\sigma}^6(1 - \cos 4\pi\zeta)$

b. $A = (4\alpha_1^1 + 8\alpha_2^4)\cos \pi\zeta + 4\alpha_1^4 \cos 3\pi\zeta$

2. TA, TO modes

a. $A_\sigma = 4(\alpha_1^1 + \alpha_1^4 + 2\alpha_2^4) + (\alpha_{2\sigma}^2 + 2\alpha_{1\sigma}^3 + 2\alpha_{3\sigma}^3 + 4\alpha_{1\sigma}^5)$

$(1 - \cos 2\pi\zeta) + \alpha_{2\sigma}^6(1 - \cos 4\pi\zeta)$

b. $A = 4(\alpha_1^1 + \alpha_1^4 + \alpha_2^4)\cos \pi\zeta + 4\alpha_2^4 \cos 3\pi\zeta$

B. $\underline{q} = [\zeta\ \zeta\ \zeta]\frac{2\pi}{a_0}$

1. LA, LO

a. $A_\sigma = 4(\alpha_1^1 + \alpha_1^4 + 2\alpha_2^4) + (\alpha_{1\sigma}^2 + 2\alpha_{2\sigma}^2 + 3\alpha_{1\sigma}^5 - 2\beta_{1\sigma}^5)$

$$(1 - \cos 2\pi\zeta) + (2\alpha^3_{1\sigma} + \alpha^3_{3\sigma} + 2\beta^3_{3\sigma} + \alpha^6_{1\sigma} + 2\alpha^6_{2\sigma})$$

$$(1 - \cos 4\pi\zeta) + (\alpha^5_{1\sigma} + 2\beta^5_{1\sigma}) (1 - \cos 6\pi\zeta)$$

b. $A = (3\alpha^1_1 - 2\beta^1_1 + \alpha^4_1 + 2\alpha^4_2 + 2\beta^4_1 - 4\beta^4_2) \cos\pi\zeta + (\alpha^1_1 + 2\beta^1_1$

$+ 2\alpha^4_1 + 4\alpha^4_2 - 4\beta^4_1) \cos 3\pi\zeta + (\alpha^4_1 + 2\alpha^4_2 + 2\beta^4_1 + 4\beta^4_2) \cos 5\pi\zeta$

2. TA, TO

a. $A_\sigma = 4(\alpha^1_1 + \alpha^4_1 + 2\alpha^4_2) + (\alpha^2_{1\sigma} + 2\alpha^2_{2\sigma} + 3\alpha^5_{1\sigma} + \beta^5_{1\sigma})$

$(1 - \cos 2\pi\zeta) + (2\alpha^3_{1\sigma} + \alpha^3_{3\sigma} - \beta^3_{3\sigma} + \alpha^6_{1\sigma} + 2\alpha^6_{2\sigma})$

$(1 - \cos 4\pi\zeta) + (\alpha^5_{1\sigma} - \beta^5_{1\sigma}) (1 - \cos 6\pi\zeta)$

b. $A = (3\alpha^1_1 + \beta^1_1 + \alpha^4_1 + 2\alpha^4_2 - \beta^4_1 + 2\beta^4_2) \cos\pi\zeta + (\alpha^1_1 - \beta^1_1$

$+ 2\alpha^4_1 + 4\alpha^4_2 + 2\beta^4_1) \cos 3\pi\zeta + (\alpha^4_1 + 2\alpha^4_2 - \beta^4_1 - 2\beta^4_2) \cos 5\pi\zeta$

C. $\underline{q} = [\zeta\ \zeta\ 0]\frac{2\pi}{a_0}$

1. LA, LO modes

a. $A_\sigma = 4(\alpha^1_1 + \alpha^4_1 + 2\alpha^4_2) + (\alpha^2_{1\sigma} + \alpha^2_{2\sigma} + 2\alpha^3_{1\sigma} + 2\alpha^3_{3\sigma})$

$(1 - \cos 2\pi\zeta) + (\alpha^3_{1\sigma} + \beta^3_{3\sigma} + 2\alpha^5_{1\sigma} + 2\beta^5_{1\sigma} + \alpha^6_{1\sigma} + \alpha^6_{2\sigma})$

$(1 - \cos 4\pi\zeta)$

b. $A = 2(\alpha^1_1 - \beta^1_1 + \alpha^4_2 - \beta^4_1) + 2(\alpha^1_1 + \beta^1_1 + \alpha^4_1 + 2\alpha^4_2 + \beta^4_1 - 2\beta^4_2)$

$\cos 2\pi\zeta + 2(\alpha^4_1 + \alpha^4_2 + 2\beta^4_2) \cos 4\pi\zeta$

2. $T_1 A$, $T_1 O$ modes

a. $A_\sigma = 4(\alpha^1_1 + \alpha^4_1 + 2\alpha^4_2) + (2\sigma^2_{2\sigma} + 4\alpha^3_{1\sigma})\ (1 - \cos 2\pi\zeta)$

$+ (\alpha^3_{3\sigma} + 2\alpha^5_{1\sigma} + 2\alpha^6_{2\sigma})\ (1 - \cos 4\pi\zeta)$

b. $A = 2(\alpha^1_1 + \alpha^4_1) + 2(\alpha^1_1 + \alpha^4_1 + 2\alpha^4_2) \cos 2\pi\zeta + 4\alpha^4_2 \cos 4\pi\zeta$

3. $T_2 A$, $T_2 O$ modes

a. $A_\sigma = 4(\alpha^1_1 + \alpha^4_1 + 2\alpha^4_2) + (\alpha^2_{1\sigma} + \alpha^2_{2\sigma} + 2\alpha^3_{1\sigma} + 2\alpha^3_{3\sigma})$

$(1 - \cos 2\pi\zeta) + (\alpha^3_{1\sigma} - \beta^3_{3\sigma} + 2\alpha^5_{1\sigma} - 2\beta^5_{1\sigma} + \alpha^6_{1\sigma} + \alpha^6_{2\sigma})$

$(1 - \cos 4\pi\zeta)$

b. $A = 2(\alpha^1_1 + \beta^1_1 + \alpha^4_2 + \beta^4_1) + 2(\alpha^1_1 - \beta^1_1 + \alpha^4_1 + 2\alpha^4_2 - \beta^4_1$

$+ 2\beta^4_2) \cos 2\pi\zeta + 2(\alpha^4_1 + \alpha^4_2 - 2\beta^4_2) \cos 4\pi\zeta$

D. $\underline{q} = (\frac{1}{2}\ \frac{1}{2}\ \zeta)\frac{2\pi}{a_o}$

1. πA, πO modes

a. $A_\sigma = 2(2\alpha^1_1 + 2\alpha^4_1 + 4\alpha^4_2 + \alpha^2_{1\sigma} + 2\alpha^3_{1\sigma} + \alpha^2_{2\sigma} + 2\alpha^3_{3\sigma})$

$+ (\alpha^2_{2\sigma} - 2\alpha^3_{1\sigma} - 2\alpha^3_{3\sigma} + 4\alpha^5_{1\sigma})\ (1 - \cos 2\pi\zeta) + \alpha^6_{2\sigma}$

$(1 - \cos 4\pi\zeta)$

b. $A = 4(2\beta^4_2 - \beta^1_1) \cos \pi\zeta - 4\beta^4_1 \cos 3\pi\zeta$

E. $\underline{q} = (\frac{1}{2}\ \frac{1}{2}\ \zeta)\frac{2\pi}{a_o}$

1. ΛO

$$M_1 \nu^2 = 8(\alpha_1^1 + \alpha_1^4 + 2\alpha_2^4 + \alpha_{21}^2 + 2\alpha_{11}^3) + 2(\alpha_{11}^2 - 4\alpha_{11}^3 + 4\alpha_{11}^5)$$

$$(1 - \cos 2\pi\zeta) + 2\alpha_{11}^6 (1 - \cos 4\pi\zeta)$$

2. ΛA

$$M_0 \nu^2 = 8(\alpha_1^1 + \alpha_1^4 + 2\alpha_2^4 + \alpha_{20}^2 + 2\alpha_{10}^3) + 2(\alpha_{10}^2 - 4\alpha_{10}^3 + 4\alpha_{10}^5)$$

$$(1 - \cos 2\pi\zeta) + 2\alpha_{10}^6 (1 - \cos 4\pi\zeta)$$

XIII. APPENDIX D

Here the values of the Fourier coefficients discussed in Section IV are listed. The A_n were derived for force constant models up to and including a general twenty-four force constant sixth neighbor model.

A. $q = [0\ 0\ \zeta]\ 2\pi/a_o$ LA, LO

$$A_o = 4(\alpha^1_1 + \alpha^4_1 + 2\alpha^4_2)(M_0 + M_1) + M_0(\alpha^2_{11} + 4\alpha^3_{11} + 4\alpha^5_{11} + \alpha^6_{11}) + M_1(\alpha^2_{10} + 4\alpha^3_{10} + 4\alpha^5_{10} + \alpha^6_{10})$$

$$A_1 = -M_0(\alpha^2_{11} + 4\alpha^3_{11} + 4\alpha^5_{11}) - M_1(\alpha^2_{10} + 4\alpha^3_{10} + 4\alpha^5_{10})$$

$$A_2 = -M_0\alpha^6_{11} - M_1\alpha^6_{10}$$

B $q = [0\ 0\ \zeta]\ 2\pi/a_0$ TA, TO

$$A_0 = 4(M_0 + M_1)(\alpha^1_1 + \alpha^4_1 + 2\alpha^4_2) + M_0(\alpha^2_{21} + 2\alpha^3_{11} + 2\alpha^3_{31} + 4\alpha^5_{11} + \alpha^6_{21}) + M_1(\alpha^2_{20} + 2\alpha^3_{10} + 2\alpha^3_{30} + 4\alpha^5_{10} + \alpha^6_{20})$$

$$A_1 = -M_0(\alpha^2_{21} + 2\alpha^3_{11} + 2\alpha^3_{31} + 4\alpha^5_{11}) - M_1(\alpha^2_{20} + 2\alpha^3_{10} + 2\alpha^3_{30} + 4\alpha^5_{10})$$

$$A_2 = -M_0\alpha^6_{21} - M_1\alpha^6_{20}$$

C. $q = [\zeta\ \zeta\ \zeta]\ 2\pi/a_0$ LA, LO

$$A_0 = 4(M_0 + M_1)(\alpha^1_1 + \alpha^4_1 + 2\alpha^4_2) + M_0(\alpha^2_{11} + 2\alpha^2_{21} + 2\alpha^3_{11} + \alpha^3_{31} + 2\beta^3_{31} + 4\alpha^5_{11} + \alpha^6_{11} + 2\alpha^6_{21}) + M_1(\alpha^2_{10} + 2\alpha^2_{20} + 2\alpha^3_{10} + \alpha^3_{30} + 2\beta^3_{31} + 4\alpha^5_{10} + \alpha^6_{10} + 2\alpha^6_{20})$$

$$A_1 = - M_0 (\alpha^2_{11} + 2\alpha^2_{21} + 3\alpha^5_{11} - 2\beta^5_{11}) - M_1 (\alpha^2_{10} + 2\alpha^2_{20} + 3\alpha^5_{10} - 2\beta^5_{10})$$

$$A_2 = - M_0 (2\alpha^3_{11} + \alpha^3_{31} + 2\beta^3_{31} + \alpha^6_{11} + 2\alpha^6_{21}) - M_1 (2\alpha^3_{10} + \alpha^3_{30} + 2\beta^3_{30} + \alpha^6_{10} + 2\alpha^6_{20})$$

$$A_3 = - M_0 (\alpha^5_{11} + 2\beta^5_{11}) - M_1 (\alpha^5_{10} + 2\beta^5_{10})$$

D. $\underline{q} = [\zeta\ \zeta\ \zeta]\ 2\pi/a_0$ TA,TO

$$A_0 = 4(M_0 + M_1)(\alpha^1_1 + \alpha^4_1 + 2\alpha^4_2) + M_0 (\alpha^2_{11} + 2\alpha^2_{21} + 2\alpha^3_{11} + \alpha^3_{31} + 4\alpha^5_{11} - \beta^3_{31} + \alpha^6_{11} + 2\alpha^6_{21}) + M_1 (\alpha^2_{10} + 2\alpha^2_{20} + 2\alpha^3_{10} + \alpha^3_{30} - \beta^3_{30} + 4\alpha^5_{10} + \alpha^6_{10} + 2\alpha^6_{20})$$

$$A_1 = - M_0 (\alpha^2_{11} + 2\alpha^2_{21} + 3\alpha^5_{11} + \beta^5_{11}) - M_1 (\alpha^2_{10} + 2\alpha^2_{20} + 3\alpha^5_{10} + \beta^5_{10})$$

$$A_2 = - M_0 (2\alpha^3_{11} + \alpha^3_{31} - \beta^3_{31} + \alpha^6_{11} + 2\alpha^6_{21}) - M_1 (2\alpha^3_{10} + \alpha^3_{30} - \beta^3_{30} + \alpha^6_{10} + 2\alpha^6_{20})$$

$$A_3 = - M_0 (\alpha^5_{11} - \beta^5_{11}) - M_1 (\alpha^5_{10} - \beta^5_{10})$$

E. $\underline{q} = [\zeta\ \zeta\ 0]\ 2\pi/a_0$ LA,LO

$$A_0 = 4(M_0 + M_1)(\alpha^1_1 + \alpha^4_1 + 2\alpha^4_2) + M_0 (\alpha^2_{11} + \alpha^2_{21} + 3\alpha^3_{11} + 2\alpha^3_{31} + \beta^3_{31} + 2\alpha^5_{11} + 2\beta^5_{11} + \alpha^6_{11} + \alpha^6_{21}) + M_1 (\alpha^2_{10} + \alpha^2_{20}$$

$$+ 3\alpha^3_{10} + 2\alpha^3_{30} + \beta^3_{30} + 2\alpha^5_{10} + 2\beta^5_{10} + \alpha^6_{10} + \alpha^6_{20})$$

$$A_1 = -M_0(\alpha^2_{11} + \alpha^2_{21} + 2\alpha^3_{11} + 2\alpha^3_{31}) - M_1(\alpha^2_{10} + \alpha^2_{20} + 2\alpha^3_{10} + 2\alpha^3_{30})$$

$$A_2 = -M_0(\alpha^3_{11} + \beta^3_{31} + 2\alpha^5_{11} + 2\beta^5_{11} + \alpha^6_{11} + \alpha^6_{21})$$

$$- M_1(\alpha^3_{10} + \beta^3_{30} + 2\alpha^5_{10} + 2\beta^5_{10} + \alpha^6_{10} + \alpha^6_{20})$$

F. $\underline{q} = [\zeta\ \zeta\ 0]\ 2\pi/a_0 \qquad T_1A,\ T_1O$

$$A_0 = 4(M_0 + M_1)(\alpha^1_1 + \alpha^4_1 + 2\alpha^4_2) + M_0(2\alpha^2_{21} + 4\alpha^3_{11} + \alpha^3_{31} + 2\alpha^5_{11}$$

$$+ 2\alpha^6_{21}) + M_1(2\alpha^2_{20} + 4\alpha^3_{10} + \alpha^3_{30} + 2\alpha^5_{10} + 2\alpha^6_{20})$$

$$A_1 = -M_0(2\alpha^2_{21} + 4\alpha^3_{11}) - M_1(2\alpha^2_{20} + 4\alpha^3_{10})$$

$$A_2 = -M_0(\alpha^3_{31} + 2\alpha^5_{11} + 2\alpha^6_{21}) - M_1(\alpha^3_{30} + 2\alpha^5_{10} + 2\alpha^6_{20})$$

G. $\underline{q} = [\zeta\ \zeta\ 0]\ 2\pi/a_0 \qquad T_2A,\ T_2O$

$$A_0 = 4(M_0 + M_1)(\alpha^1_1 + \alpha^4_1 + 2\alpha^4_2) + M_0(\alpha^2_{11} + \alpha^2_{21} + 3\alpha^3_{11} + 2\alpha^3_{31}$$

$$- \beta^3_{31} + 2\alpha^5_{11} - 2\beta^5_{11} + \alpha^6_{11} + \alpha^6_{21}) + M_1(\alpha^2_{10} + \alpha^2_{20}$$

$$+ 3\alpha^3_{10} + 2\alpha^3_{30} - \beta^3_{30} + 2\alpha^5_{10} + \alpha^6_{10} + \alpha^6_{20} - 2\beta^5_{10})$$

$$A_1 = -M_0(\alpha^2_{11} + \alpha^2_{21} + 2\alpha^3_{11} + 2\alpha^3_{31}) - M_1(\alpha^2_{10} + \alpha^2_{20} + 2\alpha^3_{10} + 2\alpha^3_{30})$$

$$A_2 = -M_0(\alpha^3_{11} - \beta^3_{31} + 2\alpha^5_{11} - 2\beta^5_{11} + \alpha^6_{11} + \alpha^6_{21})$$

$$- M_1(\alpha^3_{10} - \beta^3_{30} + 2\alpha^5_{10} - 2\beta^5_{10} + \alpha^6_{10} + \alpha^6_{20})$$

H. $\underline{q} = [\frac{1}{2}\ \frac{1}{2}\ \zeta]\ 2\pi/a_0 \qquad \pi A,\ \pi O$

$$A_0 = 4(M_0 + M_1)(\alpha^1_1 + \alpha^4_1 + 2\alpha^4_2) + M_0(2\alpha^2_{11} + 3\alpha^2_{21} + 2\alpha^3_{11} + 2\alpha^3_{31}$$

$$+ 4\alpha_{11}^5 + \alpha_{21}^6) + M_1 (2\alpha_{10}^2 + 3\alpha_{20}^2 + 2\alpha_{10}^3 + 2\alpha_{30}^3$$

$$+ 4\alpha_{10}^5 + \alpha_{20}^6)$$

$$A_1 = - M_0 (\alpha_{21}^2 - 2\alpha_{11}^3 - 2\alpha_{31}^3 + 4\alpha_{11}^5) - M_1 (\alpha_{20}^2 - 2\alpha_{10}^3 - 2\alpha_{30}^3 + 4\alpha_{10}^5)$$

$$A_2 = - M_0 \alpha_{21}^6 - M_1 \alpha_{20}^6$$

I. $\underline{q} = [\frac{1}{2}\ \frac{1}{2}\ \zeta]\ 2\pi/a_0 \qquad \Lambda O$

$$A_0 = M_0 (4\alpha_1^1 + 4\alpha_1^4 + 8\alpha_2^4 + 4\alpha_{21}^2 + \alpha_{11}^2 + 4\alpha_{11}^3 + 4\alpha_{11}^5 + \alpha_{11}^6)$$

$$A_1 = - M_0 (\alpha_{11}^2 - 4\alpha_{11}^3 + 4\alpha_{11}^5)$$

$$A_2 = - M_0 \alpha_{11}^6$$

J. $\underline{q} = [\frac{1}{2}\ \frac{1}{2}\ \zeta]\ 2\pi/a_0 \qquad \Lambda A$

$$A_0 = M_1 (4\alpha_1^1 + 4\alpha_1^4 + 8\alpha_2^4 + 4\alpha_{20}^2 + \alpha_{10}^2 + 4\alpha_{10}^3 + 4\alpha_{10}^5 + \alpha_{10}^6)$$

$$A_1 = - M_1 (\alpha_{10}^2 - 4\alpha_{10}^3 + 4\alpha_{10}^5)$$

$$A_2 = - M_1 \alpha_{10}^6$$

XIV. APPENDIX E

In Section IV the statement was made that the ratio of the integrated intensity due to one-phonon scattering to the integrated Bragg intensity was a constant. The basis for that statement will be presented here. From Eq. (5.11) it may be seen that the ratio of the integrated intensity due to the phonons with wave vector $\underline{q}$ to the integrated Bragg intensity is

$$\frac{I_1(\underline{q})}{I_B} = \frac{N\hbar}{2I_B} \sum_j \frac{1}{\omega_j(\underline{q})} \coth \frac{h\nu_j(\underline{q})}{2kT} \left| \sum_s \frac{f_s e^{-W_s}}{\sqrt{M_s}} \underline{Q} \cdot \underline{e}_s(\underline{q},j)\, e^{i\underline{\tau}\cdot\underline{R}_s} \right|^2 . \tag{E.1}$$

It is possible to separate the sum on j into an acoustic and an optic contribution, i.e.

$$\frac{I_1(\underline{q})}{I_B} = \frac{[I_1(\underline{q})]_{AC.}}{I_B} + \frac{[I_1(\underline{q})]_{OP.}}{I_B} . \tag{E.2}$$

The acoustic contribution may be written as

$$\frac{[I_1(\underline{q})]_{AC.}}{I_B} = \frac{Q^2 N\hbar}{2I_B} \sum_{j_{AC.}} [\omega \tanh {}^{h\nu}/_{2kT}]^{-1} \left| \frac{f_0 e^{-W_0}}{\sqrt{M_0}} e_{03} \pm \frac{f_1 e^{-W_1}}{\sqrt{M_1}} e_{13} \right|^2 . \tag{E.3}$$

where the approximation

$$\underline{Q} = (q_1, q_2, \tau + q_3) \simeq (0,0,\tau) . \tag{E.4}$$

has been made. In Eq. (E.3) the (±) refer to $\binom{\text{even}}{\text{odd}}$ reflections.

From Eq. (5.7) the atomic displacements caused by a phonon of wave vector $\underline{q}$ and polarization j are

$$\underline{u}_s(\underline{q},j) = \frac{\underline{e}_s(\underline{q},j)}{\sqrt{M_s}} e^{i\underline{q}\cdot(\underline{R}_\ell + \underline{R}_s)} e^{i\omega t} Q(\underline{q},j) \quad . \tag{E.5}$$

The ratio of the z components of the displacements of the two atoms in a unit cell is

$$u_{03}/u_{13} = \frac{e_{03}/\sqrt{M_0}}{e_{13}/\sqrt{M_1}} e^{-i\underline{q}\cdot\underline{R}_1} \quad . \tag{E.6}$$

For very small q the displacements of adjacent atoms are essentially identical for acoustic modes. Therefore, for very small q

$$e_{03}/\sqrt{M_0} = e_{13}/\sqrt{M_1} = E_{3j}(\underline{q}) \quad . \tag{E.7}$$

With the use of Eq. (E.7) $\frac{[I\ (\underline{q})]_{AC.}}{I_B}$ becomes

$$\frac{[I_1(\underline{q})]_{AC}}{I_B} \cong \frac{\tau^2 N\hbar}{2I_B} \sum_{j_{AC.}} [\omega \tanh^{h\nu}/2kT]^{-1} E_{3j}^2 \left| f_0 e^{-W_0} \pm f_1 e^{-W_1} \right|^2 \quad . \tag{E.8}$$

Since

$$I_{BRAGG} = \left| \sum_s f_s e^{-W_s} e^{i\underline{\tau}\cdot\underline{R}_s} \right|^2 \quad . \tag{E.9}$$

Eq. (E.8) may also be written as

$$\frac{I_1(\underline{q})_{AC}}{I_B} = \frac{\tau^2 N\hbar}{2} \sum_{j_{AC}} [\omega \tanh\ h\nu/2kT]^{-1} E_{3j}^2 \quad . \tag{E.10}$$

Therefore, the ratio of the integrated one-phonon acoustic TDS to the integrated Bragg intensity is

$$\frac{(I_1)_{AC.}}{I_B} = \frac{\tau^2 N\hbar}{2} \int_{j_{AC.}} \Sigma \left[\omega_j(\underline{q}) \tanh \frac{h\nu_j(\underline{q})}{2kT}\right]^{-1} E_{3j}^2 \, d^3q \quad . \tag{E.11}$$

Since $\tau = 4\pi \frac{\sin\theta}{\lambda}$, Eq. (E.11) may be expressed as

$$\frac{(I_1)_{AC.}}{I_B} = a\left|\frac{\sin\theta}{\lambda}\right|^2 . \tag{E.12}$$

For the optic modes, at small q

$$\frac{u_{03}}{u_{13}} = \frac{e_{03}/\sqrt{M_0}}{e_{13}/\sqrt{M_1}} = \frac{-M_1}{M_0} \quad . \tag{E.13}$$

Therefore,

$$\frac{[I_1(\underline{q})]_{OP}}{I_B} = \frac{\tau^2 N\hbar}{2} \Sigma_{j_{OP}} \left[\omega_j(\underline{q}) \tanh \frac{h\nu_j(\underline{q})}{2kT}\right]^{-1} \frac{\frac{e^2_{03}}{M_0} \left| f_0 e^{-w_0} - \left(\frac{M_0}{M_1}\right) f_1 e^{-w_1} \right|^2}{\left| f_0 e^{-w_0} \pm f_1 e^{-w_1} \right|^2} \quad . \tag{E.14}$$

The ratio of the integrated one-phonon TDS to the integrated Bragg intensity is therefore

$$\frac{[I_i]_{OP.}}{I_B} = \frac{\tau^2 N\hbar}{2} \int \sum_{j_{OP.}} [\omega_j(\underline{q}) \tanh \frac{h\nu_j(\underline{q})}{2kT}]^{-1} \frac{e^2}{M_0} \frac{0\,3}{}$$

$$\frac{|f_0 e^{-W_0} \pm (\frac{M_0}{M_1}) f_1 e^{-W_1}|^2}{|f_0 e^{-W_0} \pm f_1 e^{-W_1}|^2} d^3q \quad . \qquad \text{(E.15)}$$

Eq. (E.15) indicates that the ratio of the integrated optical one-phonon TDS to the integrated Bragg intensity is not a constant but indeed is much larger at the odd lattice points than the even; and, in addition, is a function of $\frac{\sin\theta}{\lambda}$. However, since at small q the frequency of the optic phonons is so much greater than the acoustic phonons the factor $[\omega_j(\underline{q}) \tanh \frac{h\nu_j(\underline{q})}{2kT}]^{-1}$ makes the integrated optic one-phonon TDS negligible compared to the acoustic. Therefore, it is a good approximation to take

$$\frac{I_1}{I_B} = a(\frac{\sin\theta}{\lambda})^2 \quad . \qquad \text{(E.16)}$$

Several times in this appendix the small q limit of quantities has been used. The justification for considering only the small q limit is that the observed integrated intensities were measured over a 2θ range that corresponded to a small q range. For example, in the case of the (0 0 6) reflection the region over which the integrated intensity for the $K_{\alpha 1}$ peak was measured was $2\delta 2\theta = 0.6°$. The $\delta\zeta$ that this $\delta\theta$ corresponds to is

$$|\delta\zeta| = \frac{a_0}{\lambda} \cot\theta\ \delta\theta \simeq 0.03 \qquad \text{(E.17)}$$

Therefore, the small q limit is justified.

XV. APPENDIX F

Here it will be shown how the linearized $\nu_j(\zeta)$ relations were derived by working through the example of the $T_1A[1\ 1\ 0]$ branch. In addition, the expressions for the LA [1 1 0] and T_2A [1 1 0] cases will be given. These $\nu_j(\zeta)$ relations are appropriate to force constant models up to and including a general sixth neighbor model.

From the results of Appendix C it may be shown that

$$
\begin{aligned}
M_0 M_1 \omega_1^2 = {} & 4(M_0 + M_1)(\alpha_1^1 + \alpha_1^4 + 2\alpha_2^4) + M_0[(2\alpha_{21}^2 + 4\alpha_{11}^3) \\
& (1 - \cos 2\pi\zeta) + (\alpha_{31}^3 + 2\alpha_{11}^5 + 2\alpha_{21}^6)(1 - \cos 4\pi\zeta)] \\
& + M_1[(2\alpha_{20}^2 + 4\alpha_{10}^3)(1 - \cos 2\pi\zeta) + (\alpha_{30}^3 + 2\alpha_{10}^5 + 2\alpha_{20}^6) \\
& (1 - \cos 4\pi\zeta)] - \{[(M_0 - M_1)\, 4(\alpha_1^1 + \alpha_1^4 + 2\alpha_2^4) \\
& + M_0[(2\alpha_{21}^2 + 4\alpha_{11}^3)(1 - \cos 2\pi\zeta) + (\alpha_{31}^3 + 2\alpha_{11}^5 + 2\alpha_{21}^6) \\
& (1 - \cos 4\pi\zeta)] - M_1[(2\alpha_{20}^2 + 4\alpha_{10}^3)(1 - \cos 2\pi\zeta) \\
& + (\alpha_{30}^3 + 2\alpha_{10}^5 + 2\alpha_{20}^6)(1 - \cos 4\pi\zeta)]]^2 \\
& + 4M_0 M_1[-4(\alpha_1^1 + \alpha_1^4 + 2\alpha_2^4) + (2\alpha_1^1 + 2\alpha_1^4 + 4\alpha_2^4) \\
& (1 - \cos 2\pi\zeta) + 4\alpha_2^4(1 - \cos 4\pi\zeta)]^2\}^{1/2} \qquad \text{(F.1)}
\end{aligned}
$$

For small x

$$1 - \cos x \approx x^2/2 \qquad \text{(F.2)}$$

If this approximation is made and used to simplify Eq. (F.1), the result is the following.

$$M_0 M_1 \omega^2 = (M_0 + M_1) A + 4\pi^2\zeta^2(M_0 B + M_0 C) - \{[(M_0 - M_1) A + (M_0 B - M_1 C) 4\pi^2\zeta^2]^2 + 4M_0 M_1 [-A + D\, 4\pi^2\zeta^2]^2\}^{1/2} . \tag{F.3}$$

where

$$A = 4(\alpha^1_1 + \alpha^4_1 + 2\alpha^4_2)$$

$$B = \alpha^2_{21} + 2\alpha^3_{11} + 2\alpha^3_{31} + 4\alpha^5_{11} + 4\alpha^6_{21}$$

$$C = \alpha^2_{20} + 2\alpha^3_{10} + 2\alpha^3_{30} + 4\alpha^5_{10} + 4\alpha^6_{20}$$

$$D = \alpha^1_1 + \alpha^4_1 + 10\alpha^4_2 \quad . \tag{F.4}$$

The square root term becomes, for small ζ,

$$\{(M_0 - M_1)^2 A^2 + 8\pi^2\zeta^2(M_0 - M_1) A (M_0 B - M_1 C) + 4M_0 M_1 [A^2 - 8\pi^2\zeta^2 AD]\}^{1/2} . \tag{F.5}$$

Eq. (F.5) may be simplified to yield

$$\{(M_0 + M_1)^2 A^2 + 8\pi^2\zeta^2 A[(M_0 - M_1)(M_0 B - M_1 C) - 4M_0 M_1 D]\}^{1/2} . \tag{F.6}$$

If the expansion

$$(a + x)^{1/2} \approx a^{1/2} + x/2a^{1/2} + \cdots \quad . \tag{F.7}$$

is used, the square root becomes

$$(M_0 + M_1)A + \frac{4\pi^2\zeta^2}{(M_0 + M_1)} [(M_0 - M_1)(M_0 B - M_1 C) - 4M_0 M_1 D] \quad . \tag{F.8}$$

So then Eq. (F.3) can be simplified to yield

$$\frac{M_0 M_1 \omega^2}{4\pi^2 \zeta^2} = M_0 B + M_1 C - [(M_0 - M_1)(M_0 B - M_1 C) - 4 M_0 M_1 D]/(M_0 + M_1) \quad . \tag{F.9}$$

After some manipulation the following relationship results.

$$\frac{\nu_1^2}{\zeta^2}(M_0 + M_1) = 2(2\alpha_1^1 + \alpha_{20}^2 + \alpha_{21}^2 + 2\alpha_{30}^3 + 2\alpha_{31}^3 + 2\alpha_{10}^3 + 2\alpha_{11}^3 + 2\alpha_1^4 + 20\alpha_2^4 + 4\alpha_{10}^5 + 4\alpha_{11}^5 + 4\alpha_{20}^6 + 4\alpha_{21}^6) \quad . \tag{F.10}$$

Similarly for the T$_2$A branch the linearized expression is

$$\frac{\nu_2^2}{\zeta^2}(M_0 + M_1) = 4\alpha_1^1 - 4\beta_1^1 + \alpha_{10}^2 + \alpha_{11}^2 + \alpha_{20}^2 + \alpha_{21}^2 + 6\alpha_{10}^3 + 6\alpha_{11}^3 + 2\alpha_{30}^3 + 2\alpha_{31}^3 - 4\beta_{30}^3 - 4\beta_{31}^3 + 20\alpha_1^4 + 24\alpha_2^4 - 4\beta_1^4 - 24\beta_2^4 + 8\alpha_{10}^5 + 8\alpha_{11}^5 - 8\beta_{10}^5 - 8\beta_{11}^5 + 4\alpha_{10}^6 + 4\alpha_{11}^6 + 4\alpha_{20}^6 + 4\alpha_{21}^6 \quad . \tag{F.11}$$

For the LA branch the linearized expression may be found to be

$$\frac{\nu_L^2}{\zeta^2}(M_0 + M_1) = 4\alpha_1^1 + 4\beta_1^1 + \alpha_{10}^2 + \alpha_{11}^2 + \alpha_{20}^2 + \alpha_{21}^2 + 6\alpha_{10}^3 + 6\alpha_{11}^3 + 2\alpha_{30}^3 + 2\alpha_{31}^3 + 4\beta_{30}^3 + 4\beta_{31}^3 + 20\alpha_1^4 + 24\alpha_2^4 + 4\beta_1^1 + 24\beta_2^4 + 8\alpha_{10}^5 + 8\alpha_{11}^5 + 8\beta_{10}^5 + 8\beta_{11}^5 + 4\alpha_{10}^6 + 4\alpha_{11}^6 + 4\alpha_{20}^6 + 4\alpha_{21}^6 \quad . \tag{F.12}$$